

SEMMELWEIS EGYETEM
DOKTORI ISKOLA

Ph.D. értekezések

2865.

MÜLLER KINGA

Funkcionális Idegtudományok
című program

Programvezető: Dr. Sperlággh Beáta, c. egyetemi tanár
Témavezető: Dr. Hájos Norbert, tudományos tanácsadó

STRUCTURAL BASIS OF PEPTIDERGIC CONTROL OF AMYGDALA FUNCTIONS

PhD thesis

Kinga Müller

János Szentágothai Doctoral School of Neurosciences
Semmelweis University



Supervisor:

Norbert Hájos, DSc

Official reviewers:

Ferenc Mátyás, Ph.D

Gergely Zachar, Ph.D

Head of the Complex Examination Committee:

Alán Alpár, DSc

Members of the Complex Examination Committee:

Lucia Wittner, Ph.D

Tibor Zelles, Ph.D

Budapest,

2023

Table of content

List of abbreviations	3
1. Introduction	4
1.1. From structure to function in amygdala nuclei	4
1.2. Excitatory and inhibitory neurons of the amygdala	7
1.2.1. Neurons in the BLA	7
1.2.1.1. Principal neurons	8
1.2.1.2. Inhibitory interneurons	8
1.2.1.2.1. Perisomatic inhibitory cells	9
1.2.1.2.2. Dendritic inhibitory cells	11
1.2.1.2.3. Interneuron selective interneurons (ISIs) expressing VIP	12
1.2.2. Neurons of CeA	14
1.2.2.1.1. Principal neurons in the CeA	14
1.2.2.2. Axonal projections of CeA neurons	16
1.2.3. Neuromodulation of fear acquisition	18
1.2.3.1. The fear conditioning paradigm	18
1.2.3.2. Neuropeptides of the BLA contribute to fear learning	20
1.2.3.3. PAG-DRN dopaminergic neurons modulate the CeA	21
2. Aims	23
3. Materials and methods	24
3.1. Materials and methods	24
3.1.1. Experimental animals	24
3.1.2. Slice preparation for electrophysiology	25
3.1.3. Whole-cell recordings	26
3.1.4. Virus or tracer injections and optogenetic experiments	26
3.1.5. Post hoc identification of labelled neurons	29
3.1.6. Section preparation for anatomy	30
3.1.7. Immunostaining and imaging with confocal microscope	31
3.1.8. Reconstruction of labelled neurons	32
3.1.9. Human tissue processing	32
3.1.10. Statistical analysis	33
3.2. Personal contribution to the results	34
5. Results	35
5.1. Interneurons and projecting inhibitory cells expressing SST in the BLA	35

5.1.1. Electrophysiological features of SST ⁺ GABAergic cells	35
5.1.2. Determining the ratio of SST ⁺ GABAergic neuron types in the LA and BA	39
5.2. NPY ⁺ inhibitory neurons in the BLA	40
5.2.1. Characterization of NPY ⁺ INs	40
5.2.2. Assessing the ratio of the three inhibitory cell types expressing NPY	43
5.3. CCK ⁺ inhibitory neurons in the BLA	46
5.3.1. Targeting GABAergic neurons that express CCK	46
5.3.2. Targeted neurons in Cck-Cre;Dlx5/6-Flp mice express functional CB ₁ R	47
5.3.3. Subsets of targeted CCK ⁺ INs express NPY or PV	49
5.3.4. Targeted CCK ⁺ INs are morphologically diverse	50
5.4. Characterization of VIP ⁺ neurons projecting to the CeA	53
5.4.1. Verification of the specificity of Vip-IRES-Cre mice	53
5.4.2. Dopamine content of VIP ⁺ neurons in the dorsal tegmentum	54
5.4.3. VIP ⁺ cells in the dorsal tegmentum and their projection areas	56
5.4.4. VIP ⁺ neurons occur in the human PAG and CeA	59
5.4.5. Membrane properties of dorsal tegmental VIP ⁺ neurons and their action on the postsynaptic neurons in the CeA and BNST	61
5.4.6. Input regions of the CeA and BNST identified by retrograde tracing	64
6. Discussion	66
6.1. Diversity of SST ⁺ and NPY ⁺ neurons in the lateral and basal amygdala	66
6.2. Various types of GABAergic INs can be labelled in CCK-Cre;Dlx5/6-Flpe animals	68
6.3. Extended amygdala projecting VIP ⁺ neurons in the dorsal tegmentum	69
7. Conclusion	72
8. Summary	73
9. Összefoglalás	74
10. References	75
11. Bibliography of the candidate's publications	92
12. Acknowledgements	93
13. Tables	94

List of abbreviations

AAV - adenoassociated virus

AP - anteroposterior

BA - basal nucleus of amygdala

BC - basket cell

BLA - basolateral amygdala

BNST - bed nucleus of stria terminalis

CCK - cholecystokinin

CCKBC - cholecystokinin-expressing basket cell

CeA - central amygdala

CeC - central nucleus of the central amygdala

CeL - lateral nucleus of the central amygdala

CeM - medial nucleus of the central amygdala

CRF - corticotrophin-releasing factor

DV - dorsoventral

GABA - γ -aminobutyric acid

IN - interneuron

IPSC - inhibitory postsynaptic current

IPSP - inhibitory postsynaptic potential

LA - lateral nucleus of amygdala

ML - mediolateral

NGF - neurogliaform cell

NPY - neuropeptide-Y

PC - principal cell

PKC δ - protein kinase C δ

PTSD - post-traumatic stress disorder

PV - parvalbumin

PVBC - parvalbumin-expressing basket cell

SST - somatostatin

TH - tyrosine hydroxylase

VIP - vasoactive intestinal polypeptide

vIPAG-DRN - ventrolateral periaqueductal grey - dorsal raphe nucleus

1. Introduction

1.1. From structure to function in amygdala nuclei

The amygdaloid complex is in the medial part of the temporal lobe of the brain. It was first described by the anatomist Burdach, and he named it amygdala after the characteristic almond-like shape in humans (Burdach, 1819).

The amygdala has a critical role in recognizing emotions and threatening environment, cognitive processes that help execute the best behavioural reaction. Interestingly, the amygdala activates during one's reading facial expressions, like fear or calmness (Adolphs et al., 1998). This is an effective strategy to become aware of the mental state of others and avoid threat if needed (Baxter & Croxson, 2012). What is the neuronal background underlying these important functions related to survival?

The amygdala has 13 nuclei (*Figure 1*), but only a few are highlighted here because they will be important later for placing the results into context. The separation of the amygdala nuclei or subdivisions is based on their diverse connectivity (Sah et al., 2003) and cytoarchitecture (McDonald, 1982a), implying that they can be involved in different neuronal functions. The basolateral amygdala (BLA) nuclei, bordered laterally by the external capsule and medially by the internal capsule, comprise of the lateral, basal and basomedial (or accessory basal) nuclei (LA, BA, BMA). A part of my thesis has been conducted in the LA and BA. Although several researchers refer to the LA and BA as a unit, these two nuclei play distinct roles in various amygdala functions, including association of threatening stimuli with neutral stimuli and long-term consolidation of memory traces (Janak & Tye, 2015; Manassero et al., 2018); and may differ in their inhibitory circuits (Lucas et al., 2016; Polepalli et al., 2020). The second part of this thesis focuses on the central amygdala (CeA) which is located medially to the BLA and thus to the internal capsule. CeA has four divisions, the capsular subdivisions (CeC), lateral subdivision (CeL), intermediate subdivision, and medial subdivision (CeM) (Sah et al., 2003) and has a role in expression of fear behaviour (Li et al., 2013) as well as in controlling food intake (Kim et al., 2017).

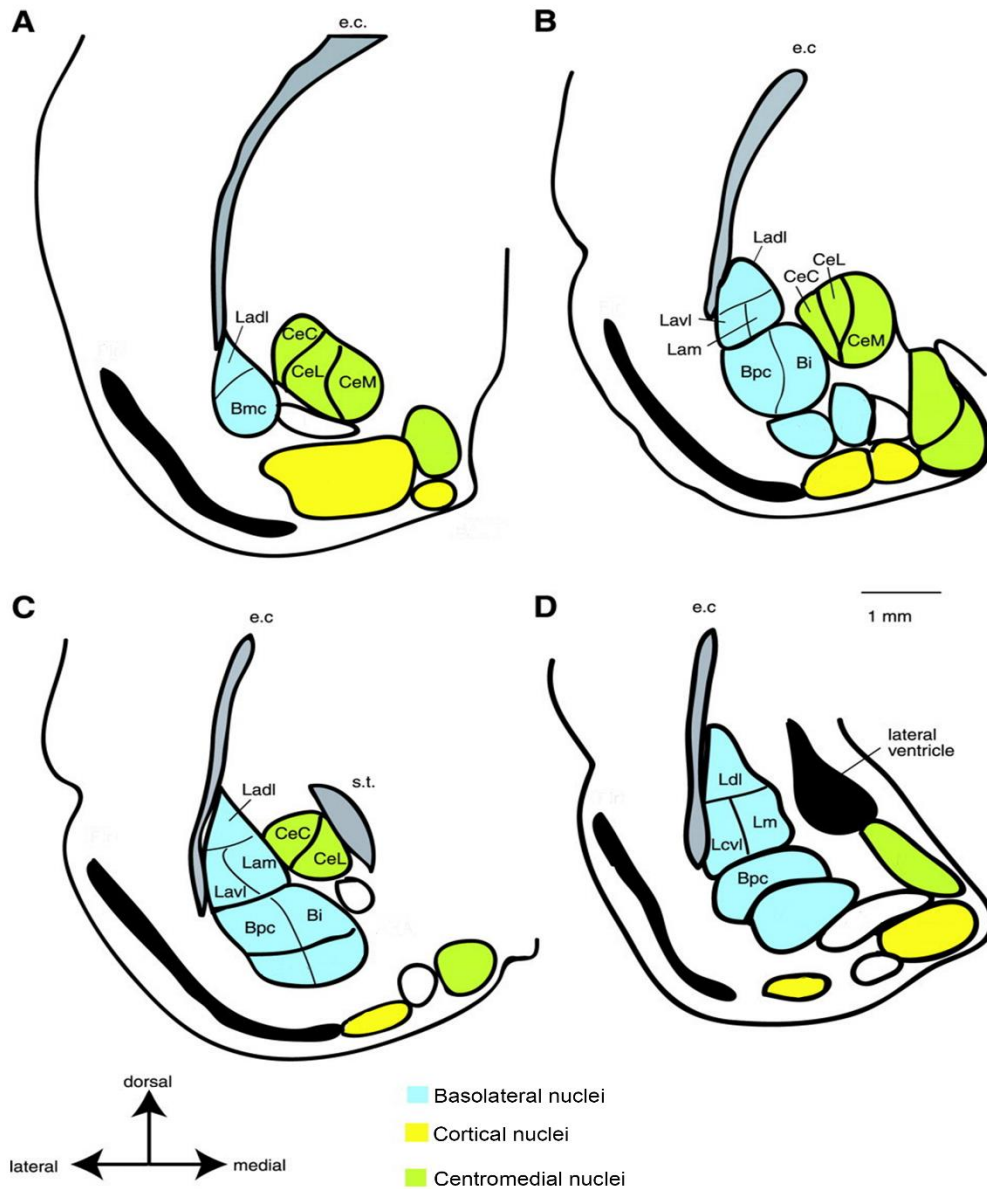


Figure 1. The amygdala nuclei are shown at different distances from the Bregma. The basolateral amygdala (blue) and cortical nuclei (yellow) have cortical origin, while the centromedial nuclei (green) are related to striatal structures. The two nuclei of basolateral nucleus are referred to as the lateral and basal nuclei in the main text. Bmc, basal nucleus magnocellular subdivision; Bi, basal nucleus intermediate subdivision; Bpc, basal nucleus parvocellular subdivision; CeC, CeA capsular subdivision; CeL, CeA lateral subdivision; CeM, CeA medial subdivision e.c., external capsule; Ladi, lateral amygdala dorsolateral subdivision; Lam, lateral amygdalomedial subdivision; Lavi, lateral amygdala ventrolateral subdivision; s.t., stria terminalis. Image is adopted and modified from (Sah et al., 2003).

The amygdala is a heterogeneous region based on embryological, functional, and connectivity data. The origin of the LA and BA is similar to cortical structures, while the CeA is rather a striatal area (Larry W. Swanson & Gorica D. Petrovich, 1998). In addition, the spatiotemporal pattern of gene expression also supports their different developmental

origin (Alvarez-Bolado et al., 1995). This early disunity in their development determines various morphological and neurochemical differences between the BLA and CeA. For instance, they differ in the neurotransmitter content of their projection neurons, as the BLA principal neurons (PC) release glutamate (DeFeudis et al., 1969) while the CeA neurons use GABA (gamma-aminobutyric acid) as a neurotransmitter (Sun & Cassell, 1993).

To understand the functional organization of amygdala circuits, those experiments that aimed to uncover the neural operation under threatening situations contributed the most. According to the classical view, the sensory information about threat arrives in the LA from cortical and thalamic regions, then after processing, the information reaches the lateral subdivision of CeL via the BLA (Duvarci & Pare, 2014). The CeL directs the information to the CeM that projects to downstream regions, like to the midbrain, brainstem and hypothalamus (Huber et al., 2005). Then these regions execute adequate defensive responses to the threatening situation.

De Olmos, Heimer and Alheid introduced the concept of the extended amygdala (Alheid, 2003; De Olmos & Heimer, 1999), proposing that the CeA and bed nucleus of stria terminals (BNST) form together a functional unit. Therefore, both the CeA (especially its lateral nucleus) and BNST (predominantly its anterolateral part or oval nucleus) participate in generating defensive responses (Gungor & Paré, 2016). In addition to their related developmental origin, the BNST and CeA have cell types with similar neuropeptide content and project to overlapping output regions, including autonomic areas (Alheid, 2003). The role of the BNST in fear related functions is not negligible, since the CeL and oval nucleus of BNST mutually innervate each other and both can inhibit the CeM directly (Gungor & Paré, 2016). Thus, the activation of the BNST can silence the output of CeA similarly to the effect of CeL (Gungor & Paré, 2016).

Obviously, the deep knowledge of the circuit organizations of the extended amygdala and the function of each nucleus is crucial to understand their role played in defensive behaviour, but these networks are also regulated by ascending neuromodulatory systems. One of such neuromodulatory systems uses dopamine as the main neurotransmitter and has a profound impact on these two regions of the extended amygdala. The dopaminergic input source of the extended amygdala and BLA is mainly the ventral tegmental area (Poulin et al., 2018). However, it has been reported that the

CeL and the oval nucleus of BNST are innervated mainly, if not exclusively by another group of dopaminergic cells. These dopaminergic neurons are located in the ventrolateral part of the periaqueductal grey (vlPAG) and the dorsal raphe nucleus (DRN), regions that are called the dorsocaudal extent of the ventral tegmental area (Hasue & Shammah-Lagnado, 2002a; Poulin et al., 2018). One of the most numerous neuron types in the vlPAG-DRN contains the neurotransmitter serotonin, but they do not express tyrosine hydroxylase (TH), the rate-limiting enzyme for dopamine synthesis, an enzyme which can be used to visualize dopaminergic neurons (Fu et al., 2010). Furthermore, a portion of dopaminergic neurons in this area also express vasoactive intestinal polypeptide (VIP). Dougalis and their colleagues investigated the relationship between the TH- and VIP-expression: they found in the TH-GFP mice that all VIP-immunostained neurons express GFP and about half of the GFP neurons showed VIP immunoreactivity (Dougalis et al., 2012). Recently, several studies investigated the function of TH⁺ neurons in vlPAG-DRN (Cho et al., 2017; Grössl et al., 2018; Matthews et al., 2016; Yu et al., 2021) but it is not clear whether the subpopulation of TH⁺ neurons expressing VIP has the same or different role in neural functions than dopaminergic neurons lacking VIP.

In summary, to understand the functions of the amygdala at the network level, we need to reveal neuron types in both the BLA and CeA, including the neuropeptide-expressing neurons as well as to uncover the extra-amygdalar peptidergic projections.

1.2. Excitatory and inhibitory neurons of the amygdala

1.2.1. Neurons in the BLA

The BLA is a cortical structure, however, it is non-layered. Similar types of neurons are located here as in the neocortex (Sah et al., 2003), even the ratio between the excitatory PCs and the inhibitory neurons was suggested to be comparable. Around 25% of all neurons are interneurons (IN) in monkey amygdala (McDonald & Augustine, 1993) and 20% in the mouse amygdala (Vereczki et al., 2021). According to the definition, INs arborize locally, while PCs have extrinsic projections as well (McDonald A J, 1991). Around the BLA there are cell islands of GABAergic neurons called intercalated cell masses. These inhibitory neurons are not part of the BLA but instead form a functional unity, controlling the circuit operation both in the BLA and CeA. Intercalated cells have

small somata and short spiny dendrites, and project to the BLA and CeA (Asede et al., 2015; Busti et al., 2011; Millhouse, 1986).

Revealing how the PCs and INs are connected within the circuits is crucial to understand how the amygdala functions during different cognitive processing.

1.2.1.1. Principal neurons

The most evident difference between the two basolateral amygdala nuclei, namely the LA and BA, is the size of the somata of the PCs: they are 10-15 μm and 15-20 μm in diameter in the LA and BA, respectively (McDonald, 1982b). In other aspects like the dendritic arborization and spine density, the PCs in the LA and BA are similar. In addition, amygdalar PCs have similar single-cell properties like those found in the hippocampus or neocortex, including the burst activity evoked by intracellularly injected depolarizing currents, voltage responses upon injected hyperpolarizing currents and the properties of the afterhyperpolarization of their action potentials (Washburn & Moises, 1992). The lack of layers in the BLA is due to the absence of somata arranged next to each other forming a lamina which is a characteristic feature of other cortical structures. These excitatory cells have spines all along the dendrites. The dendrites stay within the borders of the nucleus where the soma is located, which is a feature that helps to define the nuclei of the amygdala (McDonald, 1984). The axons of BLA PCs project many brain regions. Their primary target is the medial prefrontal cortex including the anterior cingulate, prelimbic, infralimbic and M2 premotor cortices. In addition, BLA PCs innervate the BNST, hippocampus, parasubiculum, nucleus accumbens, caudate putamen, paraventricular thalamus, substantia innominata and entorhinal cortex (Hintiryan et al., 2021).

1.2.1.2. Inhibitory interneurons

The classification of GABAergic INs is based on either morphological, electrophysiological features and/or neurochemical content (Defelipe et al., 2013). There are three major IN categories in the cortical structures: i) perisomatic inhibitory cells, which target preferentially the somata, proximal dendrites or axon initial segments of PCs; ii) dendritic inhibitory cells, which predominantly innervate the dendrites of PCs and iii) interneuron-selective interneurons that target specifically other GABAergic cells and largely, if not completely, avoid PCs.

1.2.1.2.1. Perisomatic inhibitory cells

There are 3 types of INs that preferentially form synaptic contacts on the perisomatic region of the PCs in the BLA (*Figure 2*). The following INs prefer to inhibit the perisomatic region: CCK and cannabinoid receptor type 1 (CB₁)-expressing basket cells (BCs), parvalbumin (PV)⁺ BCs (PVBCs) and axo-axonic cells (*Figure 3*). These INs are crucial in the hippocampal and neocortical functions, as well as for those in the BLA (Freund & Katona, 2007; Hájos, 2021; Vereczki et al., 2016).

The PV-containing axo-axonic cells have the shortest dendritic and axonal arbours among the perisomatic region-targeting INs. A characteristic morphological feature of axo-axonic cells is that the axon terminals (boutons) are closely paced to each other along the axons, forming so-called cartridges. Axon terminals in each cartridge contact an axon initial segment. These boutons mostly cover the action potential initiation zone on the axon initial segments, a section, which is 20-40 µm apart from the soma (Veres et al., 2014). This zone of axon initial segments is where the density of voltage-gated Na⁺ channels is the highest along an axon, ensuring action potential generation at the highest likelihood (Lorincz & Nusser, 2010; Veres et al., 2014). Therefore, axo-axonic cells by positioning strategically their output synapses at this action potential initiation zone can veto the spiking of the PCs with a high efficacy (Veres et al., 2014). The Ca²⁺ binding protein calbindin is a good marker to distinguish the PVBCs from the PV⁺ axo-axonic cells because the latter is lacking calbindin in the BLA (Bienvenu et al., 2012; Vereczki et al., 2016). The firing of axo-axonic cells shows a fast-spiking phenotype with a modest accommodation (Barsy et al., 2017).

The PVBCs morphologically resemble to CCK/CB₁BCs, though PVBCs have more axonal varicosities. Both BCs have evenly expanded and extensive dendritic arborization (Vereczki et al., 2016). PVBCs, similarly to axo-axonic cells show fast-spiking firing patterns (Barsy et al., 2017). CCK/CB₁BCs exhibit a slower firing rate compared to the other two cell types, and have a regular spiking firing pattern with accommodation (Barsy et al., 2017). The position of BC synapses on the somata and proximal dendrites ensures the effective control of the postsynaptic cell's activity (Veres et al., 2017).

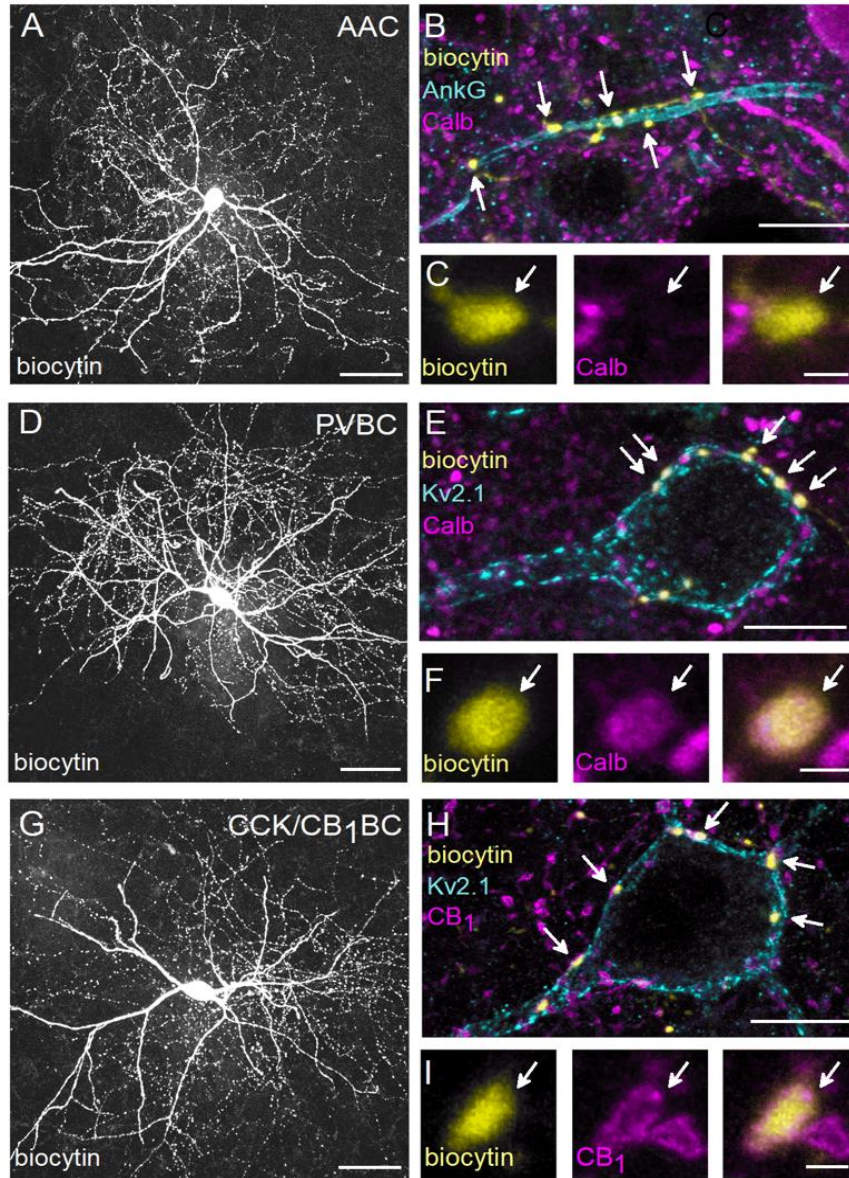


Figure 2. Examples of perisomatic region targeting INs in basal amygdala. ‘Neurochemical content and postsynaptic targets of INs innervating the perisomatic region of principal cells in the BA. Maximum z intensity projection images taken of an *in vitro* biocytin-filled axo-axonic cell (AAC) (A), PVBC (D), or CCK/CB₁BC (G). B, Varicosities of the axo-axonic cell in (A) contact with an axon initial segment visualized by ankyrin G staining and lack calbindin (Calb) immunoreactivity (C). E, The biocytin-containing boutons of the same cell as in (D) form close contacts with the Kv2.1-labelled perisomatic region of a PC and express calbindin (Calb) (F). H, The boutons of the IN in (G) form close appositions with the Kv2.1-immunostained membranes of a PC and express CB₁ (I). AAC, axo-axonic cell; PVBC, parvalbumin-containing basket cell; CCK/CB₁BC, cholecystokinin and CB₁ cannabinoid receptor-expressing basket cell. Scale bars, 50µm in (A, D, G), 10µm in (B, E, H); 1µm in (C, F, I).’ Figure is adopted and modified from (Vereczki et al., 2016).

The connections between the BCs and axo-axonic cells in the BA were also described by our research group using paired recordings. PVBCs and CCKBCs are mutually interconnected with their own type through electrical and chemical synapses with a high probability, and they both innervate axo-axonic cells. PVBCs do not innervate

CCKBCs and vice versa. Axo-axonic cells do not contact BCs (Andrási et al., 2017) as they exclusively target PCs (Vereczki et al., 2016).

The two types of BCs provide inhibitory inputs on the PCs with a similar magnitude (Veres et al., 2017). Despite BCs giving rise to contacts outside of the perisomatic region, i.e., onto the distal dendrites of PCs, these terminals do not contribute substantially to the control of PC spiking (Vereczki et al., 2016; Veres et al., 2017). The main difference between the BC types was revealed in their excitatory inputs using paired recordings: PCs give rise to more synaptic contacts onto single PVBCs than on CCK/CB₁BCs as it was found in the amygdala (Andrási et al., 2017) and earlier in the hippocampus (Gulyás et al., 1999; Mátyás et al., 2004).

1.2.1.2.2. Dendritic inhibitory cells

In contrast to the perisomatic inhibitory cells, which effectively control the spiking of their postsynaptic partners, INs targeting preferentially the PC dendrites were shown to be effective in suppressing the generation of dendritic calcium spikes (Miles et al., 1996). There are two main types of dendrite-targeting INs in the BLA: SST-expressing INs targeting the distal part of the dendrites of PCs and the neurogliaform cells (NGF cells) (*Figure 3*).

The first description of SST⁺ cells in the LA distinguished 3 groups based on morphological features (Gray, 1983). These groups were separated by different soma shapes and dendritic arborizations. This early paper already implied that among SST⁺ neurons there should be cells projecting outside of the amygdala in addition to the local axonal arborization (Gray, 1983). Further studies found that most of SST⁺ neurons (70%) express NPY in the amygdala (McDonald, 1989) and all of them were GABAergic. Regardless of the NPY content, another study discerned two classes of SST⁺ INs in the BLA based on their firing characteristics (Guthman et al., 2020). The maximum firing rate, the hyperpolarization induced sag and action potential halfwidth were used for the classification of SST⁺ neurons in this study. In addition, the authors also investigated the source of their input. Class I which had a fast-spiking firing pattern received direct excitation from the lateral entorhinal cortex. Class II showed a non-fast spiking phenotype and was avoided by the entorhinal terminals (Guthman et al., 2020). It has to be noted that SST⁺ neurons identified with immunostaining typically fall into the class II. In contrast, if Sst-IRES-Cre mice are crossed with reporter mice as Guthman et al., did,

PVBCs are also partially visualized in offsprings (our unpublished observations) which may explain finding neurons with fast-spiking features among SST⁺ INs (class I). Recently it has been revealed that a part of the SST⁺ neurons called long-range nonpyramidal neurons (LRNP) project into basal forebrain and the entorhinal cortex (McDonald & Zaric, 2015). As it was shown that morphological and electrophysiological categorization of SST inhibitory cells are not congruent, we aimed to clarify their single cell features in the BLA.

NGF cells in cortical structures have characteristic firing patterns displaying large afterhyperpolarizations (Mańko et al., 2012; Tamás et al., 2003). In the neocortex, NGF cells evoke slow inhibitory postsynaptic current (IPSC) via activating both GABA_A and GABA_B receptors (Tamás et al., 2003). In contrast, NGF cells evoke slow IPSC predominantly via GABA_A receptors in the BLA (Mańko et al., 2012). Interestingly, NGF cells may efficiently coordinate both the firing of neurons within their axonal clouds, but also themselves, providing an autaptic inhibition. Moreover, GABA can spill over from the synaptic cleft of NGF cells reaching the extrasynaptic GABA receptors (Mańko et al., 2012). This type of communication between neurons is called volume transmission (Oláh et al., 2009; Tamás et al., 2003). It has been shown previously that there are NGF cells in the BLA containing NPY and SST, but whether they express nitric oxide synthase (NOS) like in the hippocampus, is unknown (Mańko et al., 2012; Mcdonald, 1989; Mcdonald et al., 1993). Moreover, neither the exact ratio of these neurons nor their features are known in the BLA. Although the majority of the NPY⁺ neurons in the BLA are GABAergic, this neuropeptide can be expressed in a subset of PCs as well (Mcdonald & Pearson, 1989), an observation which provides a constrain on the use of transgenic mice like Npy-Cre in revealing the features of NPY⁺ INs.

1.2.1.2.3. Interneuron selective interneurons (ISIs) expressing VIP

VIP-expressing INs are the third major source of synaptic inhibition in the BLA, as in the neocortex or hippocampus (Acsády et al., 1996; Hájos et al., 1996; Kepecs & Fishell, 2014; Rhomberg et al., 2018). VIP⁺ INs often express calretinin and rarely CCK, but their ratios vary in different subnuclei of the BLA (Rhomberg et al., 2018). VIP⁺ INs release GABA as their major neurotransmitter. In line with their name, VIP⁺ ISIs innervate other types of INs: PV⁺ INs, SST⁺ INs, CCK⁺ BCs, and other VIP⁺/calretinin-expressing ISIs receive GABA_A mediated inhibition from them (Krabbe et al., 2019;

Rhomberg et al., 2018). Interestingly, NGF cells are largely avoided by inputs from VIP⁺ ISIs in the BLA (Rhomberg et al., 2018), as well as in other cortical areas (Abs et al., 2018; Kannan et al., 2022), Activity of VIP⁺ INs during fear learning disinhibit PCs, which may help in forming associative memory (*Figure 3, Figure 4*) (Krabbe et al., 2019; Rhomberg et al., 2018).

In summary, all types of GABAergic cells present in other cortical networks have been identified in BLA circuits as well. A notable difference between the BLA and other cortical structures is in the ratio of the different types of INs (Hájos, 2021). For instance, VIP⁺ INs in the BLA are more abundant than in the neocortex, whereas PV⁺ INs are more dominant in the neocortex than in the BLA (Vereczki et al., 2021; Xu et al., 2010). How these differences in the proportion of distinct IN types translate to the differences on circuit operation is not yet fully understood.

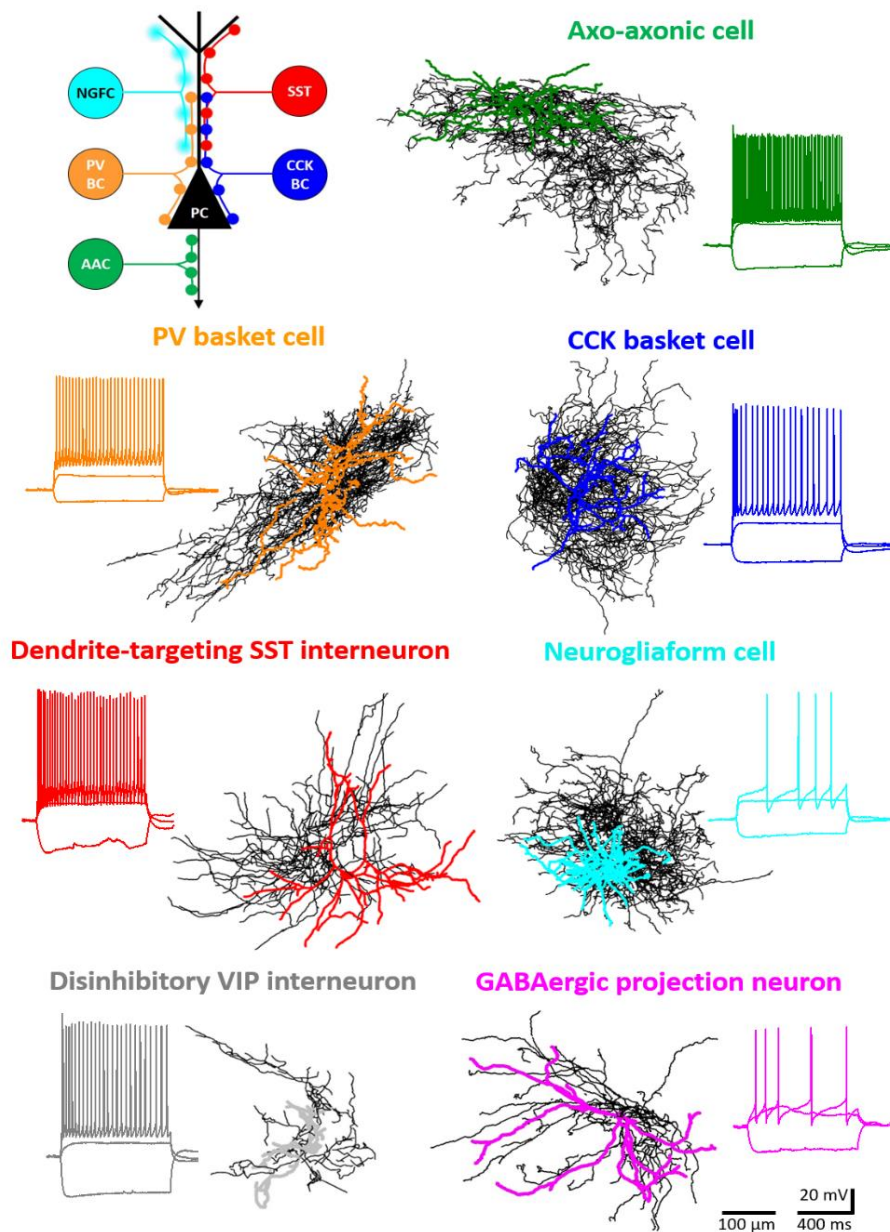


Figure 3. ‘Major inhibitory cell types in the basolateral amygdala (BLA). Intracellularly labelled GABAergic cells were sampled in slice preparations and reconstructed (dendrites in colour, axons in black). Voltage responses to depolarizing and hyperpolarizing step current injections are shown for each example cell. Schematic (upper left panel) shows the different membrane domains of principal cells (PC) innervated by distinct IN types. NGFC, neurogliaform cells expressing NPY; SST, dendrite-innervating INs expressing somatostatin; PVBC, parvalbumin-containing basket cells; CCKBC, cholecystokinin-expressing basket cells; AAC, axo-axonic cells.’ Figure is adopted from (Hájos, 2021).

1.2.2. Neurons of CeA

1.2.2.1.1. Principal neurons in the CeA

The BLA transmits the processed fear related information to the CeA which has a crucial role in the execution of defensive behaviour (Pitkänen et al., 1997). The PCs in

the CeA, being a striatal structure, are the GABAergic medium spiny neurons which emit axons locally and project also to external areas, controlling defensive circuit operation in downstream regions (Sun & Cassell, 1993). CeA neurons are highly interconnected via their local axon collaterals (Fadok et al., 2017; Hunt et al., 2017). The striatal origin of the CeA makes it unreasonable to continue the logic of morphological categorization that was used for BLA cortical inhibitory circuits. Instead of the IN classification based on the targeted membrane region of the postsynaptic neurons, the neurons in the CeA will be introduced through their neuropeptide content, the morphological and the electrophysiological features.

Many neuropeptide expressing cells are distributed through the CeA subdivisions (Cassell et al., 1986). VIP⁺ and CCK⁺ neurons in the CeA are only sparsely present (Cassell et al., 1986). In a study, McCullough and colleagues investigated the colocalization of neuropeptides with *in situ* hybridizations in the CeA (Fryxell et al., 2010). In the CeL, they found the highest expression of mRNA of corticotrophin-releasing factor (CRF) and SST (McCullough et al., 2018). The CeL and CeM shared a similar amount of tachykinin2, which is an important neuropeptide that controls fear memory processes (Andero et al., 2016). In the CeM they found neurotensin in the largest number among the other CeA subdivisions. The CeC contained the highest level of mRNA of protein kinase C δ (PKC δ) and dopamine receptor type 2 (McCullough et al., 2018). In the CeL, the genes of SST, CRF, neurotensin and tachykinin2 were co-expressed in a significant ratio, in contrast to that found in the CeM where they co-occurred minimally (McCullough et al., 2018).

In general, the morphological and electrophysiological features of neuropeptide-expressing neurons are not subdivision specific in the CeA (Martina et al., 1999). Still, there are some morphological properties of neurons characteristic to subdivisions, like most of the CeM neurons have oval somata, collateralized axons and few non ramifying dendrites decorated sparsely with spines (Martina et al., 1999). The medium spiny neurons in the CeL have smaller cell bodies, dendrites bearing many spines and emit several branches (Martina et al., 1999). With some exceptions, the dendrites of CeA neurons remain in the same subdivision as their cell bodies (Chieng et al., 2006). Interestingly, there are authors who imply that CeA neurons can be interconnected via gap junctions (Chieng et al., 2006), in addition to synaptic coupling.

As for the electrophysiological properties, the late-firing neurons are the most common type in the CeA, they make up 100%, 95% and 56% of CeC, CeM and CeL neurons, respectively (Chieng et al., 2006; Martina et al., 1999). In the CeM these types can display burst activity with a low firing threshold, but this region also contains regular-spiking neurons. In addition, neurons in the CeL show an additional type of firing characterised by single spikes (Chieng et al., 2006; Martina et al., 1999).

These various cell types in the CeA show specific local connectivity. For instance, in spite of the local axon collaterals of PKC δ^+ neurons in the CeL, they contact other neuron types with a low probability, while the other neurons target PKC δ^+ and PKC δ^- neurons with a higher chance (Hunt et al., 2017). In addition, a higher connectivity between different types of CeL neurons was found compared to that observed between neurons their own kind (Hou et al., 2016). Moreover, CeL neurons give rise to larger postsynaptic responses on those neurons which belong to different types in comparison to that recorded between the same type (Hou et al., 2016). Local connections investigated in Sst-IRES-Cre mice found the connection rate was higher between SST $^+$ neurons compared to PKC δ^+ neuron pairs (Hunt et al., 2017). SST $^+$ and PKC δ^+ neurons mutually inhibit each other and both types project to CeM neurons (Ciocchi et al., 2010).

1.2.2.2. Axonal projections of CeA neurons

The CeA is one of the centres for the regulation of autonomic functions. It is heavily connected to BNST, parabrachial nucleus, PAG, hypothalamus, basal forebrain, nucleus tractus solitarius, dorsal motor nucleus of the nervus vagus, and locus coeruleus in the brainstem (Fadok et al., 2018).

The CRF $^+$, neurotensin $^+$ and SST $^+$ neurons project into the parabrachial nucleus from the CeL. Interestingly, the abundance of a neuron type in a subdivision does not correlate with the main source of the long-range projection (Cassell et al., 1986). For example, CRF $^+$ and SST $^+$ neurons are present in the CeM, yet the CRF $^+$ and SST-containing efferents in the medulla originate mainly from the CeL (Veening et al., 1984). Another unique feature of CeA is that cells expressing the same neuropeptide have different morphology in the CeM and CeL (Cassell et al., 1986). For example, the CRF $^+$ neurons in the CeM are large and have spine-free dendrites, while in the CeL they are smaller, and their dendrites are decorated with spines (Cassell et al., 1986).

The function of three main cell types ($\text{PKC}\delta^+$, SST^+ and CRF^+) has been linked to fear acquisition (Figure 4, Fadok et al., 2018). Neurons that were found to be inhibited during the presentation of the conditioned signal upon fear acquisition were named as ‘Fear off’ or ‘CeL off’ neurons and were found to express $\text{PKC}\delta$, while ‘CeL on’ neurons are excited by the conditioned stimulus and express SST . ‘CeL on’ neurons project into the PAG and induce freezing if activated. In contrast to this, the ‘CeL off’ neurons can indirectly control the PAG function and thus, the defensive behaviour. The third type, CRF^+ neurons can inhibit the SST^+ ‘CeL on’ neurons, leading to reduced fear reactions. ‘CeL off’ and CeM neurons are reciprocally connected and the balance which neuron type activity will dominate usually depends on the context and stimuli, determining the behavioural outcome (Fadok et al., 2018).

As described in the first chapter, there is a reciprocal connection between the CeA and BNST. Since similar neuron types ($\text{PKC}\delta$, SST , CRF) are present both in the CeL and the oval nucleus of the BNST, that are often being activated under similar challenges, it is safe to assume that these two main parts of the extended amygdala act together controlling their downstream targets.

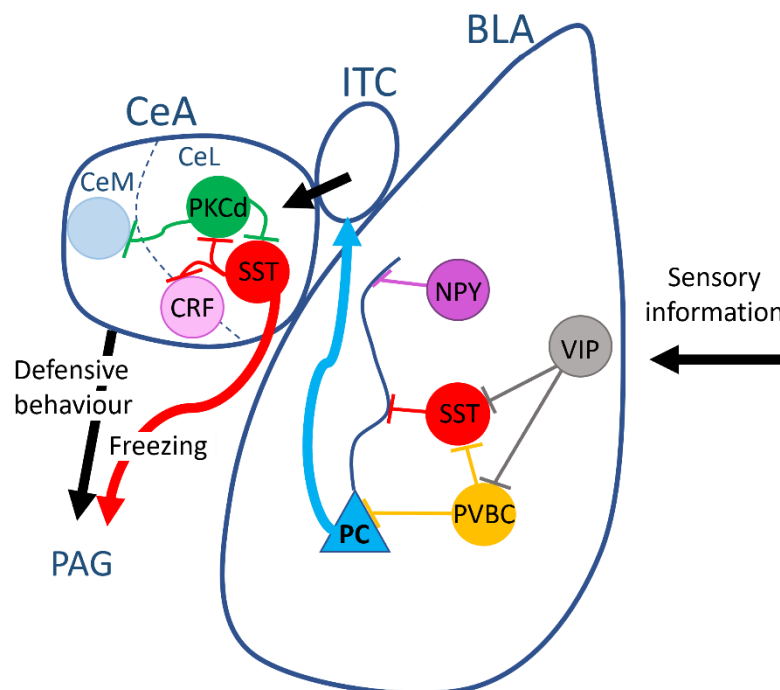


Figure 4. Fear related pathways of amygdala nuclei with the emphasis on GABAergic circuits. The sensory information carrying the fear related conditioned stimulus or unconditioned stimulus arrives to the BLA from external sources. VIP^+ neurons receive extra-amygdalar inputs and inhibit other INs, especially SST^+ and PV^+ GABAergic neurons. PV^+ INs can inhibit PCs or the SST^+ INs. Dendrite targeting SST^+ and NPY^+

cells are involved in the fear memory formation by controlling the plasticity at dendritic spines. BLA PCs project to the CeA through the ITC. In the CeA the distinct types of CeL cells can mutually inhibit each other. The CeL has 'fear on' (SST⁺) and 'fear off' (PKC δ ⁺) neurons which are activated or inhibited by the fear related inputs, respectively. CRF⁺ neurons of CeL control the other types of cells. The main output region of the CeL is the CeM. CeA output regulates the circuit operation in the PAG, leading to proper fear response. SST⁺ cells of CeL can directly evoke freezing, while the PKC δ ⁺ neurons indirectly induce defensive behaviour by disinhibiting the CeM.

1.2.3. Neuromodulation of fear acquisition

1.2.3.1. The fear conditioning paradigm

To understand the cellular and circuit mechanisms underlying associative learning and memory acquisition, a commonly used behavioural paradigm is fear conditioning. With the help of this paradigm, studies revealed that many brain areas are involved in fear memory acquisition, consolidation, and recall. The BLA, CeA, prefrontal cortex, hippocampus, thalamus and PAG are those brain regions where local circuits interconnected with remote areas support learning and memory in this model (Tovote et al., 2015).

The aim of fear conditioning or Pavlovian aversive conditioning is to achieve an association in individuals between a neutral cue (tone or light signal) and a fearful or noxious stimulus (e.g. mild foot shock, (Fendt & Fanselow, 1999)). The initially neutral cue is called conditional stimulus, while the latter is the unconditional stimulus (Fendt & Fanselow, 1999). If the conditioned and unconditioned stimulus are presented together several times, then the association between the cue and the noxious stimulus goes under consolidation, therefore the cue itself without the presentation of the noxious stimulus will evoke the fear reaction (Fendt & Fanselow, 1999). The experimenter records the freezing of the rodents (they are motionless to reach 'invisibility' from the predators) which is one of the responses to threatening stimuli (Fendt & Fanselow, 1999). The other measurable response of the animals are the elevated respiration, heart rate or vocalisation (Fendt & Fanselow, 1999). These responses all serve the survival of the animals and to learn threats to enable them to avoid next time. Therefore, fear state itself is beneficial, because it helps us to avoid danger and cope with challenges. However, persistent fear without the presence of a threat is detrimental and this is the definition of anxiety (Tovote

et al., 2015). This unreasonable state of alarm is in the background of post-traumatic stress disorder (PTSD, Shalev et al., 2017).

Fear acquisition produces two types of, though not independent, memories based on the conditioned stimulation: contextual memory and cue-dependent memory. The hippocampus mediates primarily the threat associated context dependent fear acquisition, whereas the amygdala is responsible for the cue-dependent memory formation (Phillips & LeDoux, 1992). Importantly, the healthy brain has a system to overwrite the fear related engram (Herry et al., 2010). This is called extinction learning, which is dependent on the developmental state and previous experiences (Herry et al., 2010). Extinction is a new learning process that overwrites a previously formed fear memory, such that the conditioned stimulus which predicted danger to the animal becomes a signal for safety. The infralimbic cortex is one of the key brain areas which control extinction learning (Herry et al., 2010).

The hub position of the amygdala nuclei in the circuit supports the integration of different sensory information and the generation of fear memory (Comeras et al., 2019; Pape & Pare, 2010). The processed sensory inputs of the conditioned and unconditioned stimuli arrive into the BLA which, after further processing, forwards them to the CeA and BNST, the regions which control the autonomic centres, regulating the execution of fear responses (Comeras et al., 2019).

The olfactory, auditory, visual, noxious, or somatosensory information is carried into the LA via different afferents. It is widely assumed that the conditioned and unconditioned stimulus converge in the LA where synaptic plasticity is accompanied with learning (McKernan & Shinnick-Gallagher, 1997; Rogan et al., 1997). Recent data however shows the association of the conditioned and unconditioned stimulus can occur already in the thalamus (Barsy et al., 2020). The processed sensory information from the LA is conveyed via the intercalated cell mass to the CeA (Hagihara et al., 2021) and from there to the autonomic centres including the PAG (*Figure 4*). The intercalated cell mass has more subnuclei around the BLA and it has an important relay function between the LA and CeA mediated by inhibitory neurons (Ehrlich et al., 2009; Paré, 2003).

The execution of defensive behaviour is dependent on the PAG. Its dorsal parts are responsible for active defence in the fear response, including the escape (Carrive, 1993), while the ventral parts participate in the passive defence, like the execution of

freezing (Carrive, 1993). The PAG is a part of the ascending pain pathway, which terminates in the prefrontal cortex or insular cortex (Price, 2000). The pain evoked by mild foot shock represents the unconditioned stimulus arriving in the LA from the PAG via the thalamus (Barys et al., 2020). The unconditioned stimulus can be a teaching signal coming from the PAG neurons expressing μ -opioid receptors or dopamine (Grössl et al., 2018; McNally & Cole, 2006). These signals are interpreted as prediction error because these types of PAG neurons are activated by unexpected, but not expected stimuli (McNally et al., 2011).

1.2.3.2. Neuropeptides of the BLA contribute to fear learning

The neuropeptide expressing inhibitory cell in the BLA and CeA are crucial in fear memory formation and extinction. For instance, unexpected unconditioned stimulus can activate BLA VIP⁺ INs, and these neurons are important in the gating of fear learning by disinhibiting of PCs via the selective inhibition of other INs, especially SST⁺ or PV⁺ neurons in the BLA (Krabbe et al., 2019; Rhomberg et al., 2018). Interestingly, VIP⁺ and PV⁺ neurons not only share their input pattern but also one of their function, which is the inhibition of SST⁺ neurons (Krabbe et al., 2019). In addition to the VIP⁺ IN selective INs, there are VIP⁺ INs in the BLA, as in the other cortical areas (Acsády et al., 1996; Hájos et al., 1996; Katona et al., 1999), that express CCK and CB₁ cannabinoid receptors (Rhomberg et al., 2018). These VIP⁺ INs inhibit the perisomatic region of the PCs (Rhomberg et al., 2018). The function of these CCK and CB₁R-expressing VIP neurons in the fear modulation has not been elucidated (Krabbe et al., 2019).

SST⁺ INs, with the help of PV INs can coordinate the activity of BLA PCs during fear learning. Optogenetic activation of SST⁺ inhibitory neurons during the tone period suppressed the PC activation via dendritic inhibition. The inhibition of SST⁺ inhibitory neuron activity during tone leads to less freezing during the subsequent memory recall, indicative for evidence of impaired learning. In contrast, light stimulation of PV⁺ INs during tone presentation can directly inhibit SST⁺ inhibitory cells, leading to disinhibition of PCs. As a consequence, mice show enhanced freezing behaviour during fear memory recall, which was interpreted as a sign of enhanced learning (Wolff et al., 2014).

It is worth to mention the role of NPY and its receptors in the BLA in the fear learning, too. An experiment where Y1 or Y2 types of NPY receptors were knocked out,

confirmed their crucial role in the execution of proper fear response and extinction learning (Verma et al., 2012). As the normal level of this neuropeptide in the BLA regulates the adequate fear reaction and it promotes extinction, it is widely believed that NPY has an anxiolytic role (Comeras et al., 2019).

All these above examples emphasize the importance of the distinct kinds of neuropeptide-expressing inhibitory neurons in fear related behaviours linked to the amygdala. As our knowledge about INs expressing different neuropeptides are still in infancy, we also set out to investigate these GABAergic cells in the circuits of the BLA.

1.2.3.3. PAG-DRN dopaminergic neurons modulate the CeA

As it was mentioned in the first part of this thesis, the vast majority of the dopaminergic input of the CeA arrives from the vPAG-DRN (Hasue & Shammah-Lagnado, 2002). In the CeL, DRN dopaminergic axons terminate on their postsynaptic partners which express PKC δ or SST and dopamine receptor D1 (Grössl et al., 2018). Recently, the function of this population of dopaminergic neurons has been investigated by many research groups. For instance, Matthews and colleagues revealed that photostimulation of DRN dopaminergic somata using ChR2-expression specifically in these neurons increased social preference in mice (Matthews et al., 2016). Others found that these neurons are active during the awake state and promote wakefulness (Cho et al., 2017). The inhibition of CeA-projecting DRN dopaminergic neurons also causes impaired fear learning. This is a reciprocal circuit because CeL sends a reinforcement signal to the PAG during fear conditioning (Grössl et al., 2018). In addition to the fear learning, CeA-projecting dopaminergic neurons can participate in the modulation of pain perception as well. It was shown that the optogenetic stimulation of vPAG-DRN TH⁺ neurons enhance antinociception, the block of noxious senses, especially the thermal and mechanical modalities of perception (Taylor et al., 2019). Later it has been revealed that the reaction to the pain is sex dependent. The antinociception for the optogenetic activation of TH⁺ neurons increased in male mice, while in female mice the locomotion was enhanced as a response (Yu et al., 2021).

Interestingly, around half of the dopaminergic neurons express VIP in the vPAG-DRN (Dougalis et al., 2012; Zhao et al., 2022). It raises the question why this population of neuromodulatory system requires a neuropeptide as well. What can be the unique

function of VIP⁺ neurons independent of their dopamine content, if there is any? In the last part of this thesis, we investigated this question in detail.

2. Aims

The main goals of our studies were to determine the features of the neuropeptide-expressing neurons in the amygdala and to reveal the impact of a neuropeptidergic input on the amygdala functions. Therefore, we focused on four main topics with the following specific questions:

- I. To unfold the nature of the somatostatin (SST)-expressing GABAergic neurons in the BLA circuits.
 - What are the electrophysiological and morphological properties of the distinct SST⁺ inhibitory neurons in the BLA?
 - How many SST⁺ GABAergic neurons are in the LA and BA?
- II. To determine the properties of neuropeptide Y (NPY)-containing neurogliaform (NGF) cells in the BLA.
 - How do the electrophysiological features differ between the various NPY⁺ inhibitory neurons in the BLA?
 - What is the number of NPY⁺ GABAergic cells of the LA and BA?
- III. To probe a new strategy for the investigation of cholecystokinin (CCK)-expressing inhibitory neurons.
 - What are the electrophysiological properties of the GABAergic neurons that express CCK neuropeptide?
 - What is the distribution pattern of the diverse CCK-expressing neurons in the BLA?
- IV. To unravel the characteristics of the vasoactive intestinal polypeptide (VIP)-expressing inputs of the CeA.
 - What are the output features of the VIP⁺ neurons located in the vIPAG-DRN region?

3. Materials and methods

3.1. Materials and methods

In this part, the materials and methods related to the four main chapters of the results are separated as

- Section 1 which relates to the chapters of ‘5.1. Interneurons and projecting inhibitory cells expressing SST in the BLA’ and ‘5.2. NPY⁺ inhibitory neurons in the BLA’
- Section 2 is linked to the ‘5.3. CCK⁺ inhibitory neurons in the BLA’
- Section 3 coupled with the ‘5.4. Characterization of VIP⁺ neurons projecting to the CeA’

3.1.1. Experimental animals

All procedures involving animals were performed according to methods approved by the Hungarian legislation (1998 XXVIII, section 243/1998, renewed in 40/2013) and institutional guidelines. All procedures were in compliance with the European convention for the protection of vertebrate animals used for experimental and other scientific purposes (ETS number 123). Every effort was taken to minimise animal suffering and the number of animals used. For this study, the following mouse lines were obtained from The Jackson Laboratory or from Mutant Mouse Resource & Research Center (MMRRC) (*Table 1*). Transgenic mice have C57Bl/6 background. Adult (P60-90) males and females were used for electrophysiological recordings. Mice were housed in same-sex groupings (2-4 per cage). Housing was in a temperature- and humidity-controlled vivarium under a 12 h light/dark cycle (lights on 06:00 h).

Section 1: To study the ratio or morphology of the SST⁺ or NPY⁺ neurons, Sst-IRES-Cre (Ssttm2.1(cre)Zjh, Jax stock #013044) and Npy-Cre;Dlx5/6-Flp (BAC-Npy-Cre mice (strain # RRID:MMRRC_034810-UCD) x Dlx5/6-Flpe (Tg(mI56i-flpe)39Fsh, JAX stock #010815)) mice were used (*Table 1*). In addition to these mouse lines, in electrophysiological studies Npy-Cre x Ai14 (Gt(ROSA)26Sor_tm14(CAG/LSL_tdTomato)Hze) mice were used. Both males and

females were used for electrophysiological recordings, whereas only the right hemisphere of the male mice was used to estimate the proportion of distinct IN types in the BLA in each case.

Section 2: To study CCK-expressing GABAergic neurons, Cck-IRES-Cre (Ccktm1.1(cre)Zjh/J, JAX stock #012706) and Dlx5/6-Flpe (Tg(mI56i-flpe)39Fsh/J, JAX stock #010815) mice were obtained from The Jackson Laboratory. Homozygous Cck-Cre and homozygous Dlx5/6-Flpe mice were bred to produce Cck-Cre;Dlx5/6-Flp (CCK IN) mice.

Section 3: To study VIP-expressing neurons, Vip-IRES-Cre and Ai14 reporter (Gt(ROSA)26Sor_tm14(CAG/LSL_tdTomato)Hze; RRID:IMSR_JAX:007914), mouse lines were crossed and their offspring, the Vip-Cre::tdTomato were used in the electrophysiological experiments as well as Vip-IRES-Cre//Gt(ROSA)26Sor_CAG/LSL_ZsGreen1 (Vip-IRES-Cre_ZsGreen1), VGAT-IRES-Cre//Gt(ROSA)26Sor_CAG/LSL_ZsGreen1 (Vgat-IRES-Cre_ZsGreen1). In anatomical studies, we used Vip-IRES-Cre mice.

3.1.2. Slice preparation for electrophysiology

After 4-6 weeks following injection of viral vectors mice were deeply anaesthetized with isoflurane, the brain was quickly removed and placed into ice cold solution containing the following (in mM): 252 sucrose, 2.5 KCl, 26 NaHCO₃, 0.5 CaCl₂, 5 MgCl₂, 1.25 NaH₂PO₄, 10 glucose, bubbled with 95% O₂/5% CO₂ (carbogen gas). Depending on the project, either BLA containing horizontal or CeA, BNST or PAG containing coronal, 200 µm thick brain sections were prepared with a vibratome (VT1200S, Leica Microsystems) and kept in an interface-type holding chamber containing ACSF at 36°C that gradually cooled down to room temperature. ACSF contained the following (in mM): 126 NaCl, 2.5 KCl, 1.25 NaH₂PO₄, 2 MgCl₂, 2 CaCl₂, 26 NaHCO₃, and 10 glucose, bubbled with carbogen gas. After at least a 60-min-long incubation, slices were transferred to a submerged-type recording chamber and perfused with 32-34°C ACSF with a flow rate of 1.5-2 ml/min.

3.1.3. Whole-cell recordings

Recordings were performed under visual guidance using differential interference contrast microscopy (via a model FN-1 Nikon or BX61W Olympus upright microscope) using a 40x water dipping objective. Fluorescent protein expression in neurons was visualised with the aid of a mercury arc lamp and a CCD camera (Andor Technology). Patch pipettes (5-7 M Ω) for whole-cell recordings were pulled from borosilicate capillaries with inner filament (thin-walled, OD 1.5) using a P1000 pipette puller (Sutter Instrument). In whole-cell recordings, the patch pipette contained a K-gluconate based intrapipette solution as follows (in mM): 115 K-gluconate, 4 NaCl, 2 Mg-ATP, 20 HEPES, 0.1 EGTA, 0.3 GTP (sodium salt), and 10 phosphocreatine adjusted to pH 7.3 using KOH, with an osmolarity of 290 mOsm/L. The pipette also contained 0.2% biocytin. Recordings were performed with a Multiclamp 700B amplifier (Molecular Devices), low-pass filtered at 3 kHz, digitised at 10 kHz, recorded with an in-house data acquisition and stimulus software (Stimulog, courtesy of Zoltán Nusser, Institute of Experimental Medicine) or Clampex 10.4 (Molecular Devices), and were analysed with EVAN 1.3 (courtesy of Istvan Mody, Department of Neurology and Physiology, University of California, Los Angeles), Clampfit 10.4 (Molecular Devices), and OriginPro 2018 (OriginLab). For firing pattern analysis, neurons were recorded in current-clamp mode at a holding potential of -65 mV or neurons in the PAG of -70 mV. Voltage responses were tested with a series of hyperpolarizing and depolarizing square pulses of current with 800 ms duration and amplitudes between -100 and +100 pA at 10 pA step intervals, then up to 300 pA at 50 pA step intervals, and finally up to 600 pA at 100 pA step intervals.

3.1.4. Virus or tracer injections and optogenetic experiments

Anaesthesia was induced and maintained with ketamine/xylazine cocktail applied intraperitoneally 125 mg/kg for ketamine and 10 mg/kg for xylazine and mice were secured in a stereotaxic frame (David Kopf Instruments) during the virus injections (*Table 1*).

Section 1: To label SST⁺ or NPY⁺ neurons in the BLA four injections per animal were aimed unilaterally at the following coordinates: 1.5 mm to bregma (AP), 3.2 mm lateral to the midline (ML), 4.0 mm deep from the cortical surface (DV); 1.5 mm AP, 3.2

mm ML, 5.0 mm DV; 2.1 mm AP, 3.2 mm ML, 4.0 mm DV; and 2.1 mm AP, 3.2 mm ML, 5.0 mm DV. Adeno-associated virus (AAV)- based constructs engineered to transfect Cre⁺ and Cre⁺/Flp⁺ neurons with AAV2/5-EF1a-DIO-EYFP-WPRE-hGH and AAVdj-hSyn-C(on)/F(on)-EYFP-WPRE, respectively. They were obtained from the University of Pennsylvania Vector Core and the University of North Carolina Vector Core, respectively. The virus titers were 3-6x10¹² vg/ml. At each site, 350 nl (total of 1400 nl/hemisphere) of AAV2/5-EF1a-DIO-EYFP-WPRE-hGH (flow rate: 50 nl/min) was unilaterally injected into the right BLA of 9- to 12-week-old homozygous Sst-IRES-Cre mice. To visualize SST⁺ projection neurons in the amygdalar region, 300 nl of AAVretro-EF1a-mCherry-IRES-Flpo obtained from Addgene (titer, 7x10¹² vg/ml) was unilaterally injected into the basal forebrain (0.25 mm AP, 1.3 mm ML, 4.4 mm DV) or entorhinal cortex (4.25 mm AP, 3.25 mm ML, 3.5 mm DV) of Sst-IRES-Cre mice, followed by the injection of AAVdj-hSyn-C(on)/F(on)-EYFP-WPRE into the BLA at two AP coordinates as above (total of 400 nl/amygdala). In the case of 3 Npy-Cre;Dlx5/6-Flp mice, AAVdj-hSyn-C(on)/F(on)-EYFP-WPRE (total of 1400 nl/hemisphere) was injected into the amygdala using the same coordinates as above. Despite the fact that the same amount of AAVdj was injected into Npy-Cre;Dlx5/6-Flp mice, the spread of the viral infection was smaller as in case of AAV2/5 injection and only the LA was fully infected. Therefore, three additional Npy-Cre;Dlx5/6-Flp mice were injected with ML coordinates modified from 3.2 to 2.8 mm, which resulted in full infection of the BA.

Section 2: Cck-Cre;Dlx5/6-Flp mice were injected bilaterally into the BLA (-1.4 to 1.5 mm AP, 3.22 to 3.3 mm ML, -4.4 to -4.85 mm DV). Viruses were injected in a volume of 400-500 nl per hemisphere over 10 min. The AAV-based INTRSECT (INTRonic Recombinase Sites Enabling Combinatorial Targeting) related constructs engineered to transfect Cre⁺/Flp⁺ cells with ChR2 (AAVdj-hSyn-Con/Fon-hChR2(H134R)-EYFP-WPRE) in *ex vivo* experiments were obtained from the University of North Carolina Vector Core or directly from the Deisseroth laboratory. The virus titers were 3– 6 x 10¹² vg/ml.

Section 3: To evaluate the light evoked transmitter release from the axons of the VIP⁺ neurons in the extended amygdala, AAV5-EF1a-DIO-ChR2-mCherry (UNC, Lot#AV4314J) viruses were injected bilaterally to the vIPAG of Vip-IRES-Cre mice (-4.7 mm and -5 mm AP, 0.8 mm ML, -2.6 mm DV; 10° angle, 400 nl bilaterally). AAV5-EF1-

DIO-EYFP virus (Addgene 27056) was used to visualise antero-retrogradely the collateralization of VIP⁺ neurons in the whole brain, thus we inject this AAV into the BNST (0.25 mm AP, 2 mm ML, 3.5 mm DV, 18.5° angle) of Vip-IRES-Cre mice. In this case EYFP-expression was allowed for 6 weeks. To visualise the VIP⁺ neurons in the PAG we injected AAV1-CAG-FLEX-tdTomato (Addgene 28306-AAV1) or AAV1-Cre(on)-GFP (courtesy by Peer Wulff) in the PAG. For the retrograde labelling of the CeA or BNST projecting neurons we used cholera toxin β subunit injected into the CeA (-1.6 mm AP, 2.6 mm ML, -4.1 mm DV, with iontophoresis for 10 mins with 5 μ A, 2-2 sec on and off) and fluorogold into the BNST (same coordinates as above, with iontophoresis for 5 mins with 2 μ A, 2-2 sec on and off) unilaterally.

The injection cannula was slowly withdrawn 5 min after injection. Fluorescent protein expression was allowed for 4-5 weeks, before the animals were killed.

Whole-field blue light (447 nm) laser illumination (Roithner Laser Technik, Vienna, Austria) was applied for 100 ms using a Digital Mirror Device based pattern illuminator (Mightex Polygon 400, Mightex Systems) to activate all neurons that expressed ChR2. In the case of activating ChR2-expressing VIP⁺ terminals 5 x 5 ms long light pulses were applied at 10 Hz every 20 sec, using a pattern illuminator. The recorded neurons were clamped at a holding potential of -65 mV. Series resistance was in the range of 15–25 M Ω . For peak and area analysis, five consecutive traces were averaged.

All drug effects from different projects were evaluated after a 10-min wash-in of bath-applied gabazine (5 μ M, Sigma), CGP 5699A (1 μ M, courtesy of Istvan Mody), CP 55,940 (2 μ M, Tocris), NBQX (5 μ M, Tocris) or APV (50 μ M, Tocris), or after 20-min wash-in of bath-applied AM251 (2 μ M, Tocris). During the recording in CCK-expressing GABAergic neurons in the BLA the peak amplitude for the fast and slow components was determined at distinct time points (n = 23 cells). The area of these two components was calculated only for those events in which the fast component was blocked by gabazine (n = 10 cells): the remaining slow component was subtracted from the original trace resulting in the area for the fast component. For firing pattern analyses, EYFP⁺ neurons in Cck-Cre;Dlx5/6-Flp mice were recorded in current clamp mode at a holding potential of -65 mV. After the recordings, slices were fixed overnight in 4% PFA in PB 0.1 M.

3.1.5. Post hoc identification of labelled neurons

Biocytin content of recorded neurons was visualised using Cy3-conjugated streptavidin in slices prepared from Npy-Cre;Dlx5/6-Flp and Cck-Cre;Dlx5/6-Flp mice. Alexa488-conjugated streptavidin was used to reveal the biocytin loaded neurons in slices prepared from Npy-Cre x Ai14 mice and Vip-IRES-Cre, while Alexa647-conjugated streptavidin in AAV-injected Sst-IRES-Cre mice. After the visualisation of recorded neurons, confocal images of the filled cells were obtained using a confocal microscope (Nikon model C2) under a Plan-Apochromat VC 20 objective (NA 0.75, z step size: 1 mm; xy: 0.31mm/pixel).

Slices (not resectioned) were immunostained with antibodies based on the firing pattern characteristics and features of the dendritic and axonal arbours of the recorded neurons (*Table 1, Table 2, Table 3*). Incubation of antibodies was performed for 7-8 d at 4°C.

Section 1: The presence of nNOS and PV in SST⁺ inhibitory cells was revealed with goat anti-nNOS and rabbit anti-PV using DyL405-conjugated donkey anti-goat first and subsequently using donkey anti-rabbit in 2 cases, where no nNOS immunoreactivity was seen in the soma of tested neurons. To visualise the Kv2.1 type of voltage-gated potassium channels in slices, mouse anti-Kv2.1 antibody was used, which was developed by Cy3-conjugated donkey anti-mouse antibody. The neurochemical content of biocytin-filled NPY⁺ INs was tested with the use of the following primary antibodies: rabbit anti-PV, guinea pig anti-SST, goat anti-nNOS, chicken anti-calbindin, guinea pig anti-calbindin, or rabbit anti-CB₁. The following secondary antibodies were used to visualise these primary antibodies: DyL405-conjugated donkey anti-rabbit, DyL405-conjugated donkey anti-guinea pig, DyL405-conjugated donkey anti-chicken, DyL405-conjugated donkey anti-goat, Alexa647-conjugated donkey anti-rabbit, Cy5-conjugated donkey anti-goat, or Cy5-conjugated donkey anti-guinea pig. To reveal the axon initial segments, rabbit anti-Ankyrin G was used after antigen retrieval (Veres et al., 2014). This antibody was visualised with an Alexa647-conjugated donkey anti-rabbit.

Section 2: Putative CCKBCs were immunostained with goat anti-CB₁R antibody and visualised using DyL405-conjugated donkey anti-goat antibody. Only those cells (five of seven) expressing CB₁R in their axonal terminals were categorised as CCKBCs. Putative fast-spiking cells were immunostained with rabbit anti-PV visualised with A647-conjugated donkey anti-rabbit, and chicken anti-calbindin visualised with DyL405-

conjugated donkey anti-chicken. Confocal images (see below) were taken to assess calbindin and PV coexpression at axonal terminals. Those cells (three of nine) coexpressing calbindin and PV at their axonal boutons were categorised as PVBCs, whereas those cells (six of nine) which expressed PV, but not calbindin, at their axon terminals were considered axo-axonic cell. To further confirm the latter classification, *in vitro* slices containing both PVBCs and axo-axonic cells were resectioned into 30 μm -thick sections, pepsin digested as described previously (Veres et al., 2014) and immunostained using a mouse anti-ankyrin G antibody visualized with an Alexa Fluor 488-conjugated donkey anti-mouse antibody. Those cells which showed cartridges of axonal terminals in close apposition to ankyrin G⁺ profiles were confirmed as axo-axonic cells.

Section 3: Slices in experiments using optogenetics experiments where the transmitter release from VIP⁺ terminals was evaluated in the CeA or BNST were immunostained with the primary antibodies: rabbit anti-SST, rat anti-RFP, mouse anti-PKC δ and with the following secondaries: DyL405-conjugated anti-rabbit, Cy3-conjugated anti-rat, A647-conjugated anti-mouse.

For the quantification of the input on axon initial segments, the images were subsequently deconvolved with Huygens software (SVI) and analysed using the “Cell counter” and “SNT” plugins in the ImageJ software.

All antibodies used in this study are listed in *Table 2*, *Table 3*.

3.1.6. Section preparation for anatomy

After being anaesthetised with ketamine/xylazine, adult tracer- or viral-injected or non-injected transgenic mice (P56-P70) were transcardially perfused with 0.9% NaCl for 1-2 minutes followed by a fixative solution containing 4% PFA in 0.1 M PB, pH 7.4, for 30 min. Coronal sections (50-100 μm thick) were prepared from the tissue blocks containing the entire amygdalar or midbrain region using a Leica VT1000S vibratome (Leica Microsystems). Sections were stored in a cryoprotectant antifreeze solution consisting of glycerol, ethylene glycol, distilled H₂O, and PBS (3:3:3:1 volume ratio) at -20°C until further processing (Watson et al., 1986).

3.1.7. Immunostaining and imaging with confocal microscope

To estimate the ratios of inhibitory cell types, sections prepared from AAV-injected Cre mouse lines or transgenic mice were incubated in a mixture of primary antibodies, followed by a mixture of secondary antibodies listed in *Table 3*. The sections were rinsed in PBS and blocked for 2 h in a solution containing 0.2% Triton X-100, 10% normal goat serum, and 2% bovine serum albumin.

Section 1: To reveal the neurotransmitter characteristics of axons in the contralateral amygdala on injection of viral vectors into the amygdala region of NPY-Cre mice, immunostaining using a mixture of goat anti-GFP and rabbit anti-VGluT1 was performed. To visualise these antibodies, a mixture of Alexa488-conjugated anti-goat and Cy3-conjugated anti-rabbit was used.

Section 2: To reveal the immunoreactivity for different markers, sections containing the BLA of Cck-Cre;Dlx5/6-Flp mice were further processed for immunostaining with the following antibody mixtures (*Table 2*, *Table 3*): rabbit anti-CaMKII and guinea pig anti-PV, rabbit anti-NPY (courtesy of Prof. Günther Sperk) and guinea pig anti-nNOS, rabbit anti-NPY and guinea pig anti-PV, or rabbit anti-PV and guinea pig anti-calbindin. To visualise these antibodies, Cy3-conjugated donkey anti-rabbit antibody and Cy5-conjugated donkey anti-guinea pig were used. In addition, we incubated different sections in rat anti-SOM or in rabbit anti-CB₁R, which stains only the CB₁R-expressing GABAergic axon terminals. The localization of these antigens was visualised with Cy3-conjugated donkey anti-rat or DyL405-conjugated goat anti-rabbit. Those CCK GABAergic neurons that showed EYFP immunoreactivity in both the cytoplasm and cell membrane were considered EYFP⁺ and could be clearly distinguished from those EYFP⁻ neurons that soma and proximal dendrites were surrounded by axonal varicosities expressing EYFP.

Section 3: For the investigation of vIPAG-DRN VIP⁺ neurons, the retrograde tracing of CeA and BNST were visualised with goat anti-cholera toxin β subunit and guinea pig anti-fluorogold visualised by Cy3-conjugated anti-goat, A488-conjugated anti-guinea pig secondary antibodies. The following antibodies were used as well: rabbit anti-VIP, mouse anti-TH, rat anti-RFP or chicken anti-GFP. For the visualization Cy3-conjugated anti-rabbit, Cy3-conjugated anti-rat, A488-conjugated anti-chicken, A647-conjugated anti-mouse were applied.

After several washings, the sections were mounted and coverslipped with Vectashield (Vector Laboratories) in each case. A confocal microscope (model C2, Nikon Instruments Europe BV) was used to obtain images of soma (under a Plan-Apochromat 20x objective (N.A. 0.75, z step size: 1 μm , xy: 0.62 $\mu\text{m}/\text{pixel}$)) and axon terminals (under a Plan-Apochromat VC 60x objective (N.A. 1.4, z step size: 0.5 μm , xy: 0.21 $\mu\text{m}/\text{pixel}$)).

Multichannel confocal images of the BLA, CeA and PAG were obtained using a Nikon A1R or C2 microscope, apochromatic lens (CFI Plan Apo VC 20x NA 0.75 and 60x NA 1.40) (z stacks, 1 μm step size). The image analysis was performed using NeuroLucida Explorer. To follow the labelled axons of virally labelled tracings through different slices we used 3DHISTECH Panoramic MIDI II slide scanner (with a Zeiss, Plan-Apochromat 10x objective (N.A. 0.3, resolution: 650 nm)).

3.1.8. Reconstruction of labelled neurons

The dendritic and axonal arbours of the intracellularly filled neurons were reconstructed with NeuroLucida 10.53 software, using confocal stacks acquired from the cell. The drawings of each neuron were analysed with NeuroLucida Explorer, and the values were corrected for shrinkage and flattening of the tissue (correction factor in the z axis: 1.7; no correction in the x and y axis). Branched structure analysis was used to study the dendritic length and number of nodes. Sholl analysis was used to estimate the complexity of the dendritic arbour by determining the number of processes crossing concentric spheres centred on the cell soma with 50 μm increments in their radius. Close apposition of a labelled bouton onto its target was defined as no apparent gap between the two profiles in 3D view.

3.1.9. Human tissue processing

Brain tissue samples used for analysis were collected and perfused by the members of the Human Brain Research Laboratory (ELRN Institute of Experimental Medicine). The ethics committee at the Regional and Institutional Committee of Science and Research Ethics of Scientific Council of Health (ETT TUKEB 15032/2019/EKU) validated this experiments. Cause of deaths were not related with neurological problems of the studied control subject (SKO19). The perfusion started no later than 3 hours and 15 mins after

the death. Before the perfusion, brains were washed for 30 mins with a solution containing anticoagulant (5 ml heparin) solved in 1.5 L physiological saline. For the fixative solution 4% paraformaldehyde and 0.05% glutaraldehyde were solved in phosphate buffer (PB, pH 7.4) (4–5 L in 1.5–2 h). From the whole perfused brain, we used only amygdala and midbrain blocks or 50 μm thick sections. After the sectioning, they were put in 30% sucrose solution and were frozen three 3 times over liquid nitrogen to help the penetration of the antibodies. Before the immunostaining, sections were washed with PBS and endogen peroxidase activation were blocked with 1% H_2O_2 solution. Then VIP, TH, NeuN immunostaining were made as mentioned above with the exception of the rinse of cupric sulphate (CuSO_4) solution to reduce the autofluorescence (Schnell et al., 1999). After immunostaining sections were dipped in distilled H_2O than rinsed in CuSO_4 solution (CuSO_4 solved in distilled water and ammonium acetate buffer (50 mM $\text{CH}_3\text{COONH}_4$, pH 5.0) for 30 mins, after dipped into distilled H_2O again. Human sections were mounted, and images were taken as described above.

3.1.10. Statistical analysis

Data are presented as mean \pm SEM, if not indicated otherwise. Statistical significance ($p < 0.05$) was assessed by t-test for comparison of data with a normal distribution, whereas Kruskal–Wallis ANOVA, Dunn’s test, Mann-Whitey (MW) U test, and Kolmogorov–Smirnov test were used for datasets with a non-normal distribution.

Group effects in electrophysiological experiments were analysed using paired t-test. For scatter plots, each symbol represents the mean of five consecutive events.

3.2. Personal contribution to the results

In SST⁺ electrophysiological investigation, I recorded about half of the cells, and I analysed all of the recordings. On the anatomy part, I participated in the reconstruction of the filled neurons, and I quantified the GFP and/or NOS labelled SST⁺ neurons of BLA.

In the case of NPY⁺ neurons I recorded around half of the cells, and I analysed all of them.

The anatomical part of the CCK-Cre;Dlx5/6-Flp experiment was done by me, I quantified the CB₁ content of EYFP labelled boutons and determined the neurochemical content of EYFP labelled somata.

From the VIP⁺ study, the recordings, and analyses in the optogenetic and electrophysiologic parts were done by my colleagues. I made all the viral or retrograde tracings and anatomical quantifications of dopaminergic neurons in vIPAG-DRN. I made the immunohistochemical staining on mice and human tissues.

5. Results

5.1. Interneurons and projecting inhibitory cells expressing SST in the BLA

5.1.1. Electrophysiological features of SST⁺ GABAergic cells

In the mouse BLA, SST is present in a significant number of GABAergic cells; however, their postsynaptic targets, morphologic appearance, and single-cell features are mostly unexplored. Therefore, we first examined the postsynaptic target distribution of SST-expressing axon terminals. We labelled SST-expressing inhibitory cells in Sst-IRES-Cre mice using a viral vector, and then the sections containing the amygdala region were immunostained for a voltage gated potassium channel Kv2.1, which visualises the perisomatic region of amygdalar PCs (Vereczki et al., 2016). By counting the number of EYFP-expressing boutons that formed close appositions with the Kv2.1-immunoreactive somata, we observed that a very few of SST-expressing boutons target this membrane compartment of PCs either in the LA or BA (LA: 1%, n = 667 boutons; BA: 1.8%, n = 1388 boutons, n = 2 mice). These results suggest that SST-containing boutons preferentially innervate the dendrites of neurons in mice similarly to that found in rats (Muller et al., 2007). To reveal the targets of SST-expressing axon endings and their occurrence along the dendritic tree of PCs, we intracellularly labelled single PCs in the LA and BA in acute slices that were prepared from mice where EYFP was expressed in SST-containing GABAergic cells. Using double immunostaining, we found that EYFP-expressing boutons that formed close appositions with the intracellularly labelled PCs were evenly distributed along their dendritic trees (*Figure 5A, B*). LA (n = 8) and BA (n = 9) PCs were similarly covered by EYFP⁺ axon terminals (p=0.28, Kolmogorov–Smirnov test); therefore, these results were pooled (*Figure 5B*). With a closer inspection, we observed that EYFP-expressing boutons overall targeted dendritic shaft more frequently than spines (*Figure 5B*). In LA, 137 and 814 boutons contacted spines and dendritic shaft, respectively (n = 8 PCs, 12,176 μm total dendritic length), whereas 131 boutons formed close appositions with spines and 411 boutons with shafts of BA PCs (n = 9, 13,816 μm total dendritic length). The ratio of boutons contacting shafts versus

spines in the LA (6.3 ± 1.1 %) and BA (4.3 ± 0.8 %) was similar ($p = 0.16$, Mann-Whitney U test). The distribution of EYFP-expressing boutons targeting the dendritic shaft or spines along the dendritic trees was not significantly different either ($p=0.16$ in the LA, and $p=0.08$ in the BA). Thus, our results confirmed that the vast majority of SST-containing axon terminals target the dendritic compartment of amygdalar PCs (Muller et al., 2007; Wolff et al., 2014); consequently, these GABAergic cells are in a position to play a role in dendritic inhibition. In the next set of investigations, our goal was to characterise the GABAergic cells giving rise to SST-containing boutons in the two examined amygdalar nuclei. Previous studies showed that SST is expressed at least in two types of GABAergic cells. One type innervates primarily the dendrites of PCs, whereas the other type, the somata of which are present often in the external capsule, projects to remote areas, including the basal forebrain and entorhinal cortex (McDonald et al., 2012; McDonald & Zaric, 2015). Yet, none of these inhibitory cell types has been examined in detail. To record from SST-expressing GABAergic projection cells, we applied an intersectional strategy by injecting retroAAV-mCherry-Flpo viruses into the basal forebrain or entorhinal cortex of Sst-IRES-Cre mice, and AAV-C(on)/F(on)-EYFP into the amygdala region. This approach revealed retrogradely labelled SST⁺ cells in the BLA (as well as in surrounding areas) in green, some of which were recorded and filled with biocytin in acute slices (*Figure 5C*). We sampled 28 and 16 GABAergic cells that projected to the basal forebrain or the entorhinal cortex, respectively. We included only those neurons in the analysis that had axon collaterals in the LA and/or BA (12 and 8 SST⁺ projection cells targeting the basal forebrain and entorhinal cortex, respectively); that is, these GABAergic projection cells were in the position to participate in amygdala function as well. As neither the features of dendritic arbours nor the single-cell electrophysiological characteristics were found to be different in inhibitory cells projecting to the basal forebrain or entorhinal cortex ($p>0.05$), we pooled the two datasets. Previous findings indicated that SST⁺ GABAergic projection neurons often express nNOS (He et al., 2016; Sik et al., 1994); therefore, we tested the presence of this enzyme in the sampled neurons using immunostaining. Accordingly, the vast majority of SST⁺ GABAergic projection neurons indeed showed immunoreactivity for nNOS (78%, $n = 18$ tested cells). In each group of SST⁺ GABAergic projection cells, i.e., targeting the basal forebrain or the entorhinal cortex, 2 neurons lacking immunoreactivity for nNOS were

found. These observations, therefore, imply that the presence of nNOS in SST⁺ inhibitory cells may be a good tool to separate projection cells from those that are local INs. Next, we aimed to compare the properties of these SST⁺ projection cells with SST⁺ INs. To this end, we randomly sampled green cells in acute slices that were prepared from the amygdala region of Sst-IRES-Cre mice after viral labelling (*Figure 5C*). A total of 31 EYFP⁺ neurons were recorded with sufficiently labelled dendritic and/or axonal arbours (17 in the LA and 14 in the BA). Of these green neurons, two were fast-spiking INs (one of them showed immunopositivity for PV, whereas in the other case, the PV immunoreactivity could not be unequivocally determined) and one NGF cell. These three neurons were excluded from further analyses. Using immunostaining, we tested the expression of nNOS in remaining EYFP⁺ neurons and found that this enzyme was present only in a minority of randomly sampled SST⁺ inhibitory cells (15%, n = 28; 2 in the LA and 2 in the BA; *Figure 5D*). As our results show that nNOS is often present in SST⁺ GABAergic projection cells, we excluded these four SST⁺/nNOS⁺ inhibitory cells from further comparisons because they might have been randomly sampled projection neurons. Thus, the restricted group of SST⁺ INs was composed of 13 and 11 cells in the LA and BA, respectively. As the single cell features of SST⁺ INs located in the LA and BA were similar (p>0.05), the results were pooled and compared with those obtained for SST⁺ GABAergic projection cells. We found that all but one parameter of firing investigated were similar in the two types of SST⁺ inhibitory cells (*Figure 5C, E; Table 5*). During the inspection of intracellularly labelled SST⁺ inhibitory cells, we noticed that projection cells often emitted elongated dendrites and had only a few axon collaterals in slices, whereas local INs had rather multipolar dendritic trees and dense axonal arborisation (*Figure 5C, E*). As the dendritic tree may be less impacted by slicing than axons, we compared only the features of dendrites in the two groups of SST⁺ inhibitory cells (*Figure 5F*). We found no difference in any parameters for SST⁺ INs in the LA (n = 8) and BA (n = 7; p>0.05); therefore, the two datasets were pooled and compared with those obtained for SST⁺ projection cells (n = 10). Although no difference was found in the total dendritic length between SST⁺ projection cells (2467±434 μm, n = 10) and INs (2695±234 μm, n = 15, p = 0.62), the structure of their dendritic trees was clearly different. Sholl analysis revealed that the dendritic branches of SST⁺ projection neurons were longer and less ramified (*Figure 5F*), which was also reflected in the total number of nodes (11.8±1.8, n

= 10 SST⁺ projection cells; 19.6±2.7, n = 15 SST⁺ INs; p = 0.043). These results show that the two groups of SST⁺ inhibitory cells display distinct dendritic morphology.

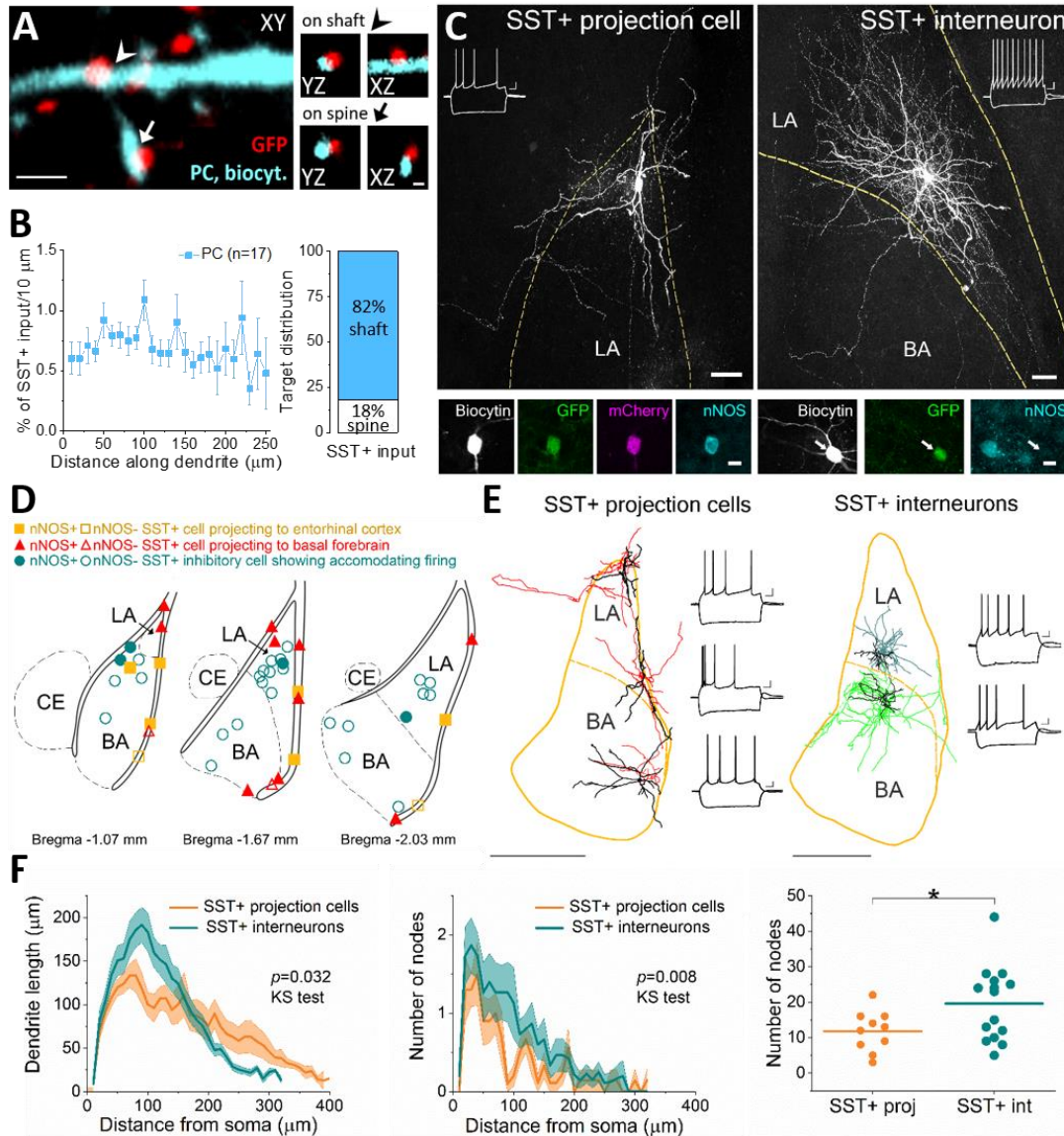


Figure 5. Characterization of GABAergic cells expressing SST in Sst-IRES-Cre mice. **A**, GFP⁺ boutons labelled in the LA and BA using a viral strategy in Sst-IRES-Cre mice form close appositions with a dendritic shaft (arrowhead) and spine (arrow) of an intracellularly labelled amygdalar principal cell (PC). Scale bars: large images, 4 μ m; small images, 1 μ m. **B**, Left, SST⁺ inputs evenly covered the dendritic tree of PCs (8 LA and 9 BA PCs). Right, The majority of SST⁺ boutons (n = 1493) target dendritic shafts of amygdalar PCs. **C**, Two examples of biocytin filled SST⁺ GABAergic cells recorded in acute slices. SST⁺ projection cells were labelled using an intersectional strategy by injecting retroAAV-mCherry-Flpo into the basal forebrain or entorhinal cortex and AAV-C(on)/F(on)-EYFP into the amygdala region. SST⁺ INs were visualised on injection of AAV-DIO-EYFP into the BLA. Both SST⁺ projection cells and INs showed accommodation in their spiking and displayed a sag in their voltage responses on negative step current injection (insets). In SST⁺ projection cells, nNOS was typically present, whereas SST⁺ INs were mostly immunonegative for this enzyme. Scale bars: large images, 50 μ m; small images, 10 μ m. **D**, Distribution of SST⁺ inhibitory cells recorded in amygdalar slices. Each symbol represents the location of the cell body. **E**, Neurolucida reconstruction of three SST⁺ inhibitory cells projecting to the basal forebrain and two SST⁺

INs (black represents dendrites; colour represents axons) and the corresponding voltage responses on intracellular step current injections. Scale bar, 500 μm . The elongated and less ramified dendrites of projection cells, and more branched axons of INs, and also the similar voltage responses of both types of SST⁺ inhibitory cells on step current injections ($x = 100 \text{ ms}$, $y=10\text{mV}$). **F**, Comparison of the structure of the dendritic trees of SST⁺ projection cells ($n = 10$) and INs ($n = 15$) using Sholl analysis. Dendritic length (left) and the number of nodes (centre) as a function of distance from the soma are significantly different. Solid line indicates mean. Dashed line indicates SEM. Whereas the total dendritic length is comparable for the two SST⁺ inhibitory cell types, the total number of nodes is significantly higher for SST⁺ INs (* $p = 0.043$). Dots represent number of nodes for individual neurons. Lines indicate the mean.

5.1.2. Determining the ratio of SST⁺ GABAergic neuron types in the LA and BA

In the next set of experiments, we attempted to estimate the ratio of SST⁺ GABAergic cells by labelling them in Sst-IRES-Cre mice using a viral vector (*Figure 6A-E; Table 4*). We found that the ratio of SST⁺ inhibitory cells differed significantly in the two amygdalar nuclei (*Table 4*). As two INs with a fast-spiking phenotype were found among randomly sampled SST⁺ inhibitory cells, we checked the colocalization of PV and SST in the population of GABAergic cells: we found a negligible presence of this Ca²⁺ binding protein in SST⁺ inhibitory cells (LA: 1.3%, $n = 77$; BA: 1.6%, $n = 185$, $n = 3$ mice). Finally, we assessed the ratio of SST⁺ INs and SST⁺ GABAergic cells with long-range projections in virus-labelled cells in Sst-IRES-Cre mice using immunostaining against nNOS (*Figure 6D*). We observed that a considerable fraction of GFP-expressing SST⁺ neurons showed immunolabelling for nNOS⁺ (LA: 41.6%; BA: 25%), a ratio that was significantly different in the LA and BA ($p=0.043$; *Figure 6E; Table 4*). These data indicate, in line with observations obtained in other cortical areas, that dendrite-targeting SST⁺ INs are more abundant than GABAergic projection cells expressing SST.

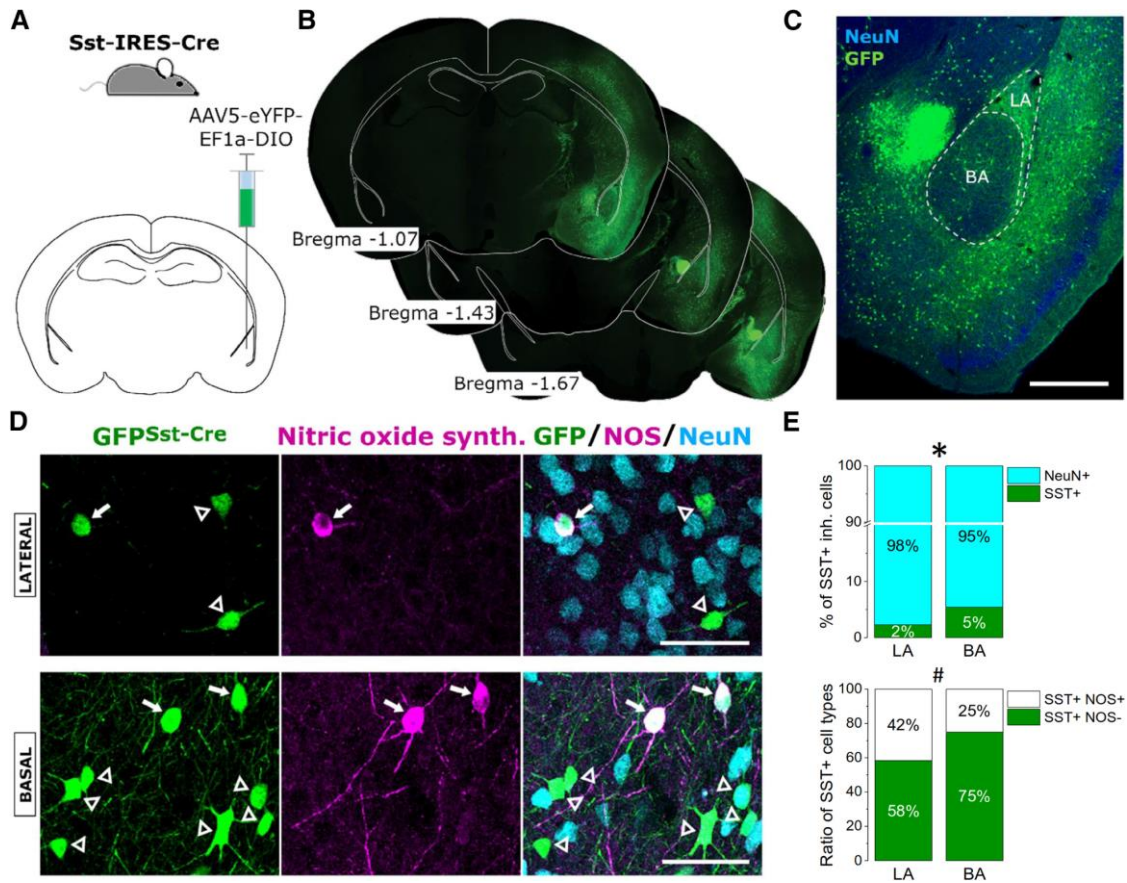


Figure 6. SST-expressing GABAergic cells in the LA and BA. **A**, Schematic of the strategy for targeting SST-expressing GABAergic cells in the amygdala. **B**, Representative images of GFP expression after virus transfection taken at the corresponding anterior-posterior coordinates (in mm) relative to bregma. **C**, Representative example of the amygdalar region taken at a higher magnification. Scale bar, 500 μ m. **D**, In the majority of GFP-labelled neurons in Sst-IRES-Cre mice, no immunoreactivity for NOS (open arrowheads) was observed, yet there were a number of virus labelled neurons that showed immunopositivity for this enzyme (arrows) in both nuclei. Scale bars, 50 μ m. **E**, Both the percentage of SST⁺ GABAergic cells (top) and the percentage of SST⁺ inhibitory cells that express NOS (bottom) were different between the two nuclei. * $p=0.0018$. # $p = 0.043$ compared with *t*-tests.

5.2. NPY⁺ inhibitory neurons in the BLA

5.2.1. Characterization of NPY⁺ INs

In the subsequent investigation, we aimed to estimate the fraction of distinct types of GABAergic cells that express NPY in the two amygdalar nuclei. As NPY has been shown to be a characteristic marker for the vast majority, if not for all NGF cells in cortical regions (Armstrong et al., 2012; Mańko et al., 2012; Paul et al., 2017) as well as a fraction of SST⁺ inhibitory cells (McDonald & Zaric, 2015), we used Npy-Cre mice to label these

GABAergic neurons in the amygdala by injecting viruses carrying EYFP. We found that the vast majority of labelled neurons in Npy-Cre mice had indeed morphologic features typical for GABAergic neurons, but there were some labelled neurons with clear PC appearance. In line with this later notion, there was a considerable axonal projection in the contralateral BA in unilaterally injected Npy-Cre mice, axon collaterals that were decorated with boutons immunoreactive for VGluT1, a type of vesicular glutamate transporter expressed in amygdalar PCs (Andrási et al., 2017). In addition, PCs could be recorded, although infrequently, in the offsprings of Npy-Cre x Ai14 mice (see below). Thus, to ensure that we study only NPY⁺ GABAergic neurons in the amygdala, double-transgenic mice were generated by crossing Npy-Cre mice with Dlx5/6-Flpe mice that express Flp recombinase in the majority of GABAergic neurons in cortical structures (Miyoshi & Fishell, 2011). Then, we injected INTRSECT viruses into the amygdalar region of Npy-Cre;Dlx5/6-Flp mice to transfect those GABAergic neurons with EYFP content that express both Cre and Flp recombinases. This approach resulted in no labelling in PCs assessed by the lack of axonal projection in the contralateral BA and by sampling no PCs in acute slice preparations. To reveal the cell types that express NPY in the LA and BA, we performed whole-cell recordings in EYFP-expressing neurons in acute amygdalar slices that were prepared from AAV-injected Npy-Cre;Dlx5/6-Flp mice or offspring of Npy-Cre x Ai14 mice. Based on the single-cell electrophysiological features, including the action potential half-width (measured at half the amplitude between the threshold and the peak voltage), maximum spiking rate, accommodation ratio, membrane time constant, and sag amplitude, three main GABAergic cell groups could be identified among randomly sampled neurons expressing reporter proteins (*Figure 7, table 6*). The largest number of recorded neurons (52%) were NGF cells showing a typical late-spiking phenotype (*Figure 7A, D*). The single-cell properties of these neurons could be characterised by wide action potentials, moderate spike rate with accommodation, fast membrane time constant, and no or minimal sag in their voltage responses on negative current injections (*Figure 7E; Table 6*). Labelled INs in this group displayed characteristic morphologic features of NGF cells, including short smooth dendrites that often ramified and dense local axonal arborisation (*Figure 7A*). Many of these INs showed weak immunoreactivity for nNOS (22 of 25 tested), but none for PV (0 of 9 tested), calbindin (0 of 25 tested), or SST (0 of 4 tested) (*Figure 7A*). Surprisingly,

the second largest group of INs (33%) showed a fast-spiking phenotype (*Figure 7B, D*). These INs had narrow spikes, the highest firing rate, no accommodation in spiking, fast membrane time constant, and no sag (*Figure 7E; Table 6*). Spine-free dendrites and axon arborisation of the INs in this category resembled the appearance typical for PVBCs and axo-axonic cells (Vereczki et al., 2016). Immunostaining revealed that many of these NPY⁺ INs were indeed immunoreactive for PV (5 of 7 tested) and for calbindin (3 of 6 tested) (*Figure 7B*). Of 6 fast-spiking INs tested, we observed SST immunoreactivity in 1 case. In addition, where only a part of the axon could be revealed, labelled boutons of this fast-spiking NPY⁺ IN formed close appositions with axon initial segments visualised by Ankyrin G staining, confirming that some of the axo-axonic cell can express NPY. The third group of recorded neurons (15%) had relatively narrow spikes, showed accommodation in spiking, and had a relatively slow membrane time constant and a sag in their voltage responses on negative current injections (*Figure 7E; Table 6*). Morphologic characteristics of these GABAergic cells were similar to those typical for SST⁺ INs, including sparsely spiny dendrites and elongated soma, as suggested by previous studies (McDonald & Zaric, 2015). Indeed, all but one of the NPY⁺ GABAergic cells in this group showed strong immunopositivity for SST (6 of 7 tested) (*Figure 7C*). We have also recorded from an NPY⁺ IN, which showed clear immunoreactivity for CB₁ on its axon terminals and displayed a typical firing pattern of CCKBCs. In addition to inhibitory cells, some PCs were also recorded in offspring of Npy-Cre x Ai14 mice (n = 3), but not in AAV-injected Npy-Cre;Dlx5/6-Flp mice. These results obtained in acute slices combined with immunocytochemical data suggest that the ratio of NGF cells, PV⁺ fast-spiking INs, and SST⁺ inhibitory cells visualised in Npy-Cre;Dlx5/6-Flp mice by a viral vector can be assessed by their PV or SST content at the population level.

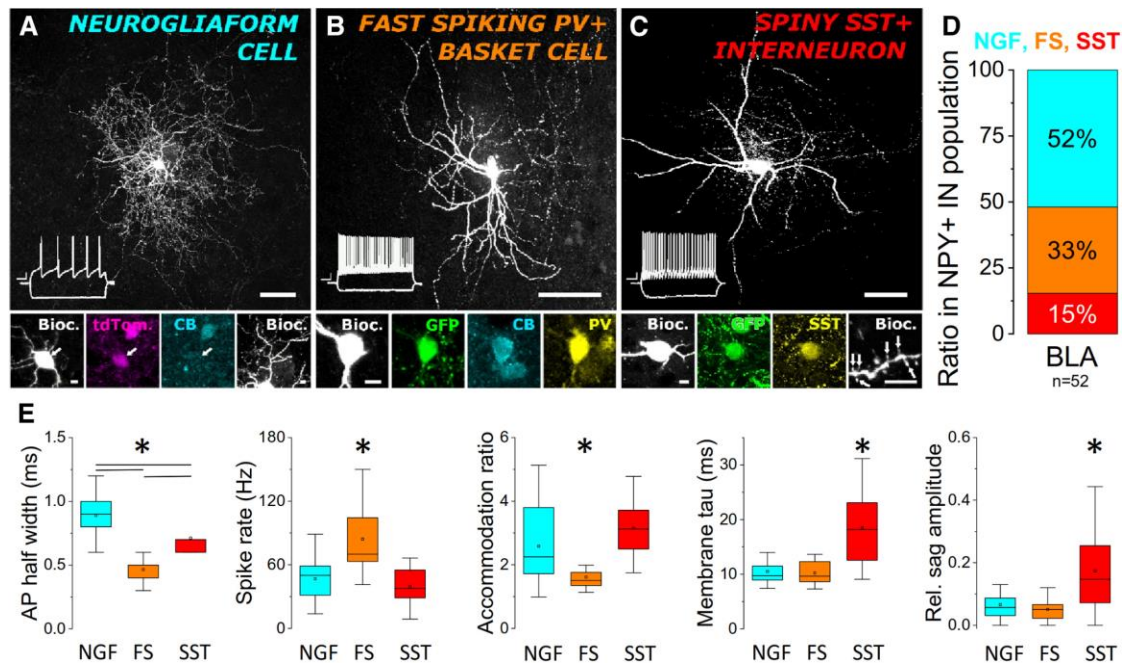


Figure 7. Three distinct inhibitory cell types express NPY in the amygdala. **A**, In amygdalar slices prepared from offspring of virus-injected *Npy-Cre;Dlx5/6-Flp* mice or *Npy-Cre x Ai14* mice, the majority of recorded neurons had neurogliaform cell (NGF) morphology: a dense local axon arborization; short, frequently ramified dendrites (see bottom right small image below), a late-spiking phenotype (inset) and lacked calbindin (CB) content. **B**, Another large group of NPY^+ INs showed a fast-spiking phenotype (inset) and was immunoreactive for PV, and often for calbindin, which is typical for PV^+ basket cells. **C**, Inhibitory cells in the smallest group of NPY^+ neurons had sparsely spiny dendrites (white arrows point to spines in the bottom right small image) and showed immunopositivity for SST. Firing of these INs showed accommodation and sag in their voltage responses upon negative step current injection (inset). Scale bars: large images, $50\ \mu\text{m}$; small images, $5\ \mu\text{m}$. Scale bars of the firing patterns: $x = 100\ \text{ms}$, $y = 10\ \text{mV}$. Bioc., biocytin. **D**, Ratio of the morphologically, neurochemically, and electrophysiologically different NPY^+ inhibitory cell types sampled *in vitro*, with biocytin labelling. BLA here refers to LA and BA. **E**, Single-cell properties of the three distinct GABAergic cell types expressing NPY in the amygdala. *Significant difference. For data, see *Table 6*.

5.2.2. Assessing the ratio of the three inhibitory cell types expressing NPY

Before performing estimation about PV or SST content at the population level in *Npy-Cre;Dlx5/6-Flp* mice, we first determined the fraction of all NPY^+ inhibitory cells in the LA and BA (*Figure 8E; Table 4*). The ratio of NPY^+ inhibitory cells was significantly different in the two amygdalar nuclei (*Table 4*). To reveal the ratio of NPY^+ inhibitory cells that express PV, SST, or none of these markers, we tested the neurochemical content of GFP^+ cells using immunostaining (*Figure 8D, F*). We observed that a significant fraction ($\sim 25\%$) of these neurons was immunoreactive for PV (*Figure 8D, E; Table 4*).

In addition, a similarly large portion (~27%) of EYFP-expressing GABAergic neurons showed immunoreactivity against SST (*Figure 8F, G; Table 4*). Thus, based on the immunostaining, approximately half of the NPY⁺ GABAergic neurons (~45% in both amygdalar nuclei) was not immunoreactive either for PV or for SST, a group of neurons that should correspond to NGF cells according to the results of the previous *in vitro* experiments (*Figure 7*). Although there is almost no overlap between PV and SST immunoreactivity in amygdalar inhibitory cells, it would be more accurate to estimate the ratio of NPY⁺ neurons lacking PV and SST immunoreactivity in the same immunostained sections. Moreover, calbindin, which was absent in *in vitro* labelled NGF cells but is present in a large number of various types of GABAergic cells in the BLA (McDonald & Mascagni, 2001a), may visualise additional inhibitory cell types, refining the ratio of NGF cells even more. Therefore, we performed immunostaining against PV, SST, and calbindin in amygdalar sections of Npy-Cre;Dlx5/6-Flp mice in which EYFP expression visualised NPY⁺ GABAergic cells. Using this approach, we found that NGF cells may represent ~45% of NPY⁺ GABAergic cells expressing EYFP but lacking immunoreactivity for PV, SST, and calbindin (four sections/mouse, 3 mice) (*Figure 8G; Table 4*). As we found NPY⁺ neurons composed 3.8% and 8.1% of all neurons in LA and BA, respectively (*Figure 8E*). Thus, based on the observations that almost half of all NPY⁺ GABAergic cells are NGF cells, we calculated that these INs make up 1.8% and 3.5% of all neurons in the LA and BA, respectively.

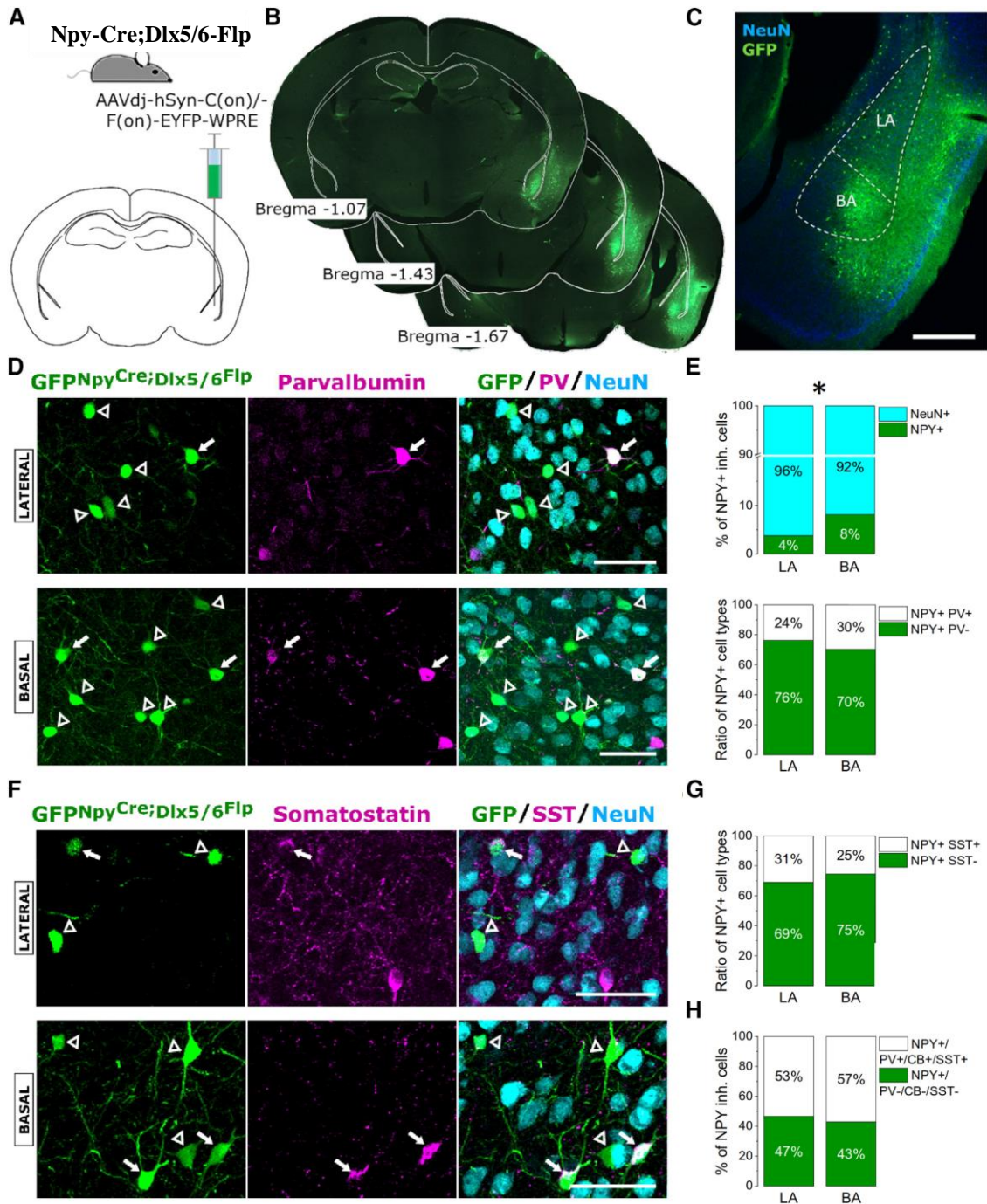


Figure 8. NPY-expressing GABAergic cells in the LA and BA. **A**, Schematic of the strategy for targeting NPY-expressing INs in the amygdala. **B**, Representative images of GFP-expression after virus transfection taken at the corresponding anterior-posterior coordinates (in mm) relative to bregma. **C**, Representative example of the amygdalar region taken at a higher magnification. Scale bar, 500 μ m. **D**, In Npy-Cre;Dlx5/6-Flp mice, a notable portion of GFP-labelled GABAergic cells expresses PV (arrows) in both nuclei. Open arrowheads indicate GFP⁺ neurons lacking PV immunoreactivity. Scale bar, 50 μ m. **E**, The ratio of NPY⁺ GABAergic cells in the LA and BA was significantly different (top, * $p < 0.001$), but the ratio of NPY⁺ inhibitory cells containing PV did not differ (bottom). **F**, Another portion of NPY⁺ GABAergic cells showed immunoreactivity for SST (arrows) in both nuclei. Open arrowheads indicate GFP⁺ neurons lacking SST immunoreactivity. Scale bar, 50 μ m. **G**, The proportion of NPY⁺ and SST⁺ inhibitory cells was comparable in the LA and BA. **H**, Almost half of the virus-labelled neurons in Npy-Cre;Dlx5/6-Flp mice

should represent the population of NGF cells both in the LA and BA, assessed by lack of immunoreactivity in GFP-labelled INs for PV, calbindin, and SST.

5.3. CCK⁺ inhibitory neurons in the BLA

5.3.1. Targeting GABAergic neurons that express CCK

Next, we aimed to investigate the properties of INs containing CCK. However, our previous results clearly showed that CCK is also present in subpopulations of PCs in the BLA (Rovira-Esteban et al., 2017), thus to separate these two types of CCK⁺ neuron types, we turned to the intersectional strategy as above. To assess the selectivity of the intersectional targeting approach using Cck-Cre;Dlx5/6-Flp mice, we performed *ex vivo* electrophysiological recordings in these mice that were transfected with the INTRSECT-ChR2 virus in their BLA (n = 4 mice, *Figure 9AóC*). Whole-cell recordings in EYFP-negative, likely PCs (n = 23), which were postsynaptic to EYFP-expressing neurons in BLA containing brain slices, revealed that blue light illumination evoked outward currents, but with substantial variance both in the peak amplitude and decaying phase (*Figure 9D, G*). Further inspection of these responses indicated that in some cases, the light-evoked currents clearly had fast and slow components, recognized by distinct peaks (*Figure 9E*). The two outward components had significantly different peak amplitude (fast component: 201.6 ± 27.8 pA, slow component: 63.6 ± 10.7 pA, n = 23 neurons, t = 4.55, p < 0.001; *Figure 9G*), but they carried similar charge (fast component: 18.4 ± 6.2 pC, slow component: 8.4 ± 2.2 pC, n = 10 neurons, p = 0.1; *Figure 9J*). We then performed pharmacological manipulations showing that the fast component was blocked by the GABA_A receptor antagonist, gabazine (peak amplitude in control: 202.3 ± 50.3 pA; in gabazine: 2.0 ± 0.5 pA, n = 10 neurons, t = 3.99, p = 0.003; *Figure 9F,H*). Conversely, the remaining slow outward current was eliminated by the GABA_B receptor antagonist, CGP 5699A (peak amplitude in gabazine: 47.9 ± 20.4 pA, in CGP 5699A: 1.2 ± 0.8 pA, n = 4 neurons, t = 2.38, p = 0.04; *Figure 9F,I*). No inward (i.e., excitatory synaptic current) was evident in any recordings, even in the presence of both GABA receptor antagonists; indicating that photostimulation exclusively evoked inhibitory,

GABA receptor-mediated synaptic currents in BLA neurons, consistent with the selective targeting of INs, and not PCs, in this region.

5.3.2. Targeted neurons in Cck-Cre;Dlx5/6-Flp mice express functional CB₁R

Based on earlier reports that CCKBCs in the BLA express CB₁R, we next asked whether the targeted BLA INs were CB₁R-positive (Katona et al., 2001; McDonald & Mascagni, 2001; Rovira-Esteban et al., 2017; Vereczki et al., 2016; Veres et al., 2017). To test the responsiveness of the targeted cells to CB₁R activation, we generated light-evoked postsynaptic currents (PSCs) in EYFP-negative cells followed by bath application of the CB₁R agonist, CP 55,940. The application of the agonist reduced the peak amplitude of light-evoked events by 50% (control: 209.8 ± 88.4 pA, in CP: 112.6 ± 47.6 pA, peak ratio: CP/ctr: $51.3 \pm 5.4\%$, $n = 5$ neurons from 3 mice, $t = 2.35$, $p = 0.039$; *Figure 9K,L*). We verified that the CP 55,940-induced reduction was CB₁R mediated by abolishing the effect via preincubation with the CB₁R antagonist, AM251 (peak amplitude in AM251: 261.8 ± 70.2 pA, in AM251 + CP 55,940: 259.5 ± 78.4 pA, peak ratio: AM251 + CP 55,940/AM251: $96.7 \pm 8.9\%$, $n = 4$ neurons from 2 mice, $p = 0.89$; *Figure 9M,N*). These data demonstrate that a significant component of synaptic currents in BLA neurons evoked by light illumination in slices stems from signalling through the CB₁R. Consistent with these findings, immunostaining BLA sections containing transfected processes revealed that ~40% of EYFP-expressing axonal varicosities were positive for CB₁R (*Figure 9OóR*). These results indicate that a significant proportion of the targeted cells exhibit a defining feature of CCKBCs.

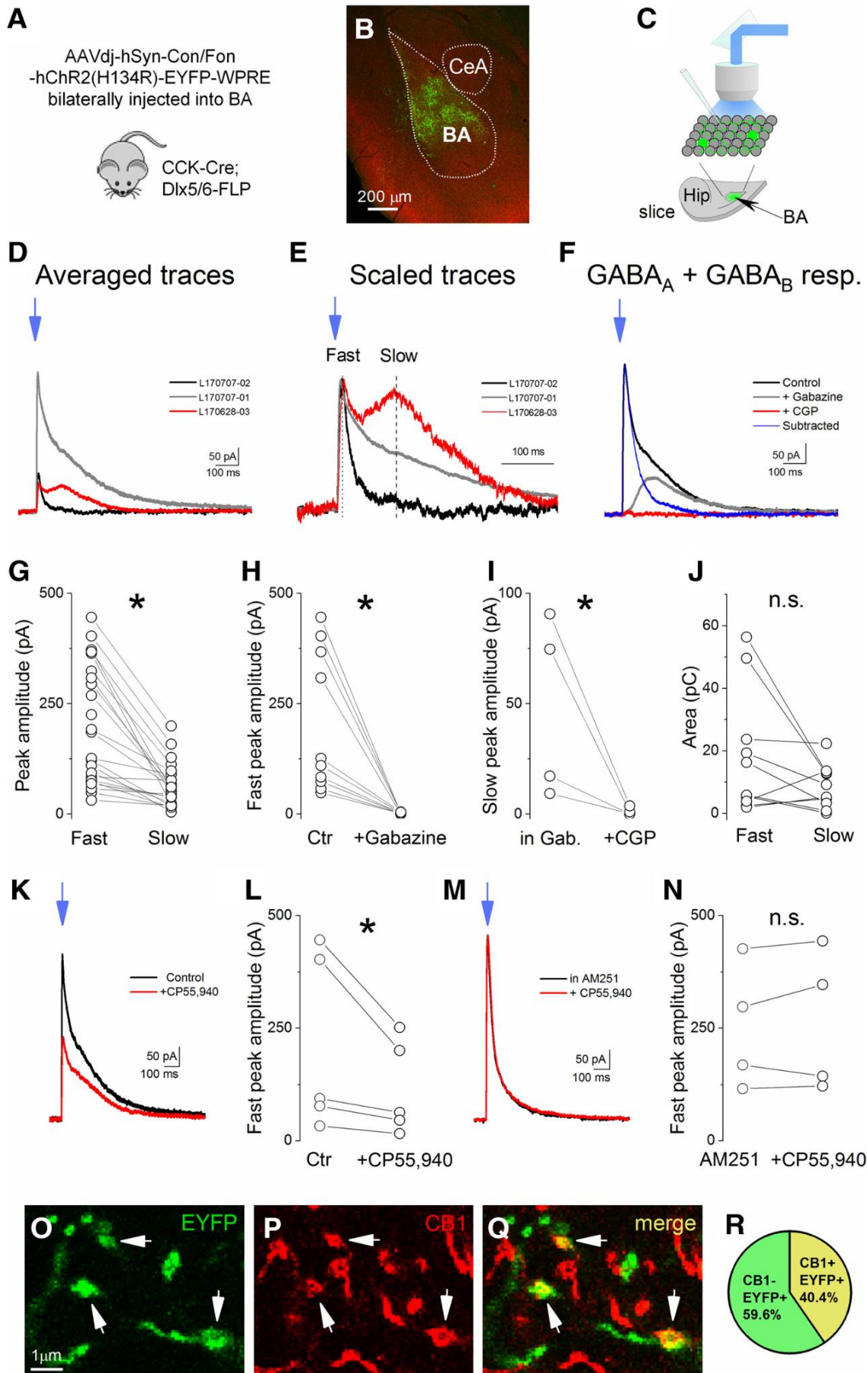


Figure 9. Photostimulation of GABAergic cells in the BA. **A**, Schematic drawing showing the intersectional viral strategy used to target CCK INs in CCK-Cre;Dlx5/6-FLP double-transgenic mice. **B**, Example of INTRSECT AAVdj-hSyn-Con/Fon-hChR2(H134R)-EYFP-WPRE (INTRSECT-ChR2) expression in the BLA (BA= basolateral amygdala, CeA = central amygdala). **C**, Schematic drawing represents a horizontal slice with viral expression shown in green (Hip = hippocampus). Whole-cell patch clamp recordings were performed in non-green cells, likely in PCs in slices prepared from double-transgenic mice injected with AAV containing INTRSECT-ChR2. **D, E**, Averaged traces of five consecutive PSCs obtained in three different neurons evoked by light illumination (blue arrow). High variability both in peak amplitude (D) and decaying phase (D, E) is typical for events evoked in different neurons. The traces in E are peak scaled. Dashed lines show where the peak amplitude for fast and slow components of evoked currents was measured. **F**, Traces from an experiment measuring the antagonist-sensitivity of light-evoked responses. Gabazine (5 μ M) wash-in eliminated the fast GABA_A-mediated component, while CGP 5699A (1 μ M) blocked the remaining slow GABA_B-mediated component. Importantly, no inward, i.e., EPSC, could be observed in the presence of the GABA receptor antagonists, indicating that the applied intersectional strategy allowed us to excite selectively GABAergic cells. **G**, Peak amplitude of the fast components in evoked responses measured in the same neurons was significantly larger than the peak amplitude of the slow components. **H**, The fast components were blocked by bath application of gabazine (*paired t-test). **I**, The slow components were eliminated by CGP 5699A wash-in. **J**, The area, i.e., the charge of the fast and slow components evoked in the same neurons, was not different. GABA_A receptor-mediated fast responses were isolated by subtracting the responses recorded in the presence of gabazine from the control traces and their area was measured. Example traces (subtracted) are shown in F. The area of the GABA_B receptor-mediated slow components were determined on the traces recorded in the presence of gabazine. **K**, Averaged traces taken from an example experiment indicate that the light-evoked PSCs are smaller on wash-in of a CB₁R agonist, CP 55,940 (2 μ M). **L**, In all experiments tested, bath application of CP 55,940 significantly reduced the peak amplitude of the fast component. **M**, Averaged traces taken from an experiment showing that, in the presence of the CB₁R antagonist, AM251 (2 μ M), bath application of CP 55,940 (2 μ M) did not cause a reduction in the peak amplitude. **N**, Preincubation of the slices in AM251 prevented the CP 55,940-induced reduction of the peak amplitude of light-evoked postsynaptic responses. **O–Q**, A portion of EYFP-expressing axon terminals is immunoreactive for CB₁ (arrows). **R**, Approximately 40% of EYFP-expressing axonal varicosities were immunopositive for CB₁R (156 EYFP⁺ varicosities were tested in two mice); *p<0.05 fast versus slow, +gabazine versus control (Ctr), +CGP versus in gabazine (Gab), +CP versus Ctr. N.s., non-significant.

5.3.3. Subsets of targeted CCK⁺ INs express NPY or PV

While our findings indicate that a substantial proportion of the targeted CCK GABAergic neurons had properties of CCK/CB₁R-expressing BCs, two observations led us to wonder whether other IN populations were also infected. First, light-evoked responses were not fully blocked by CB₁R agonist, in contrast to earlier recordings obtained in the BLA (Vogel et al., 2016) and second, they displayed a prominent GABA_B receptor-mediated component in the light-evoked outward current that is uncharacteristic of BCs (Rovira-Esteban et al., 2017; Veres et al., 2017; Vogel et al., 2016). This led us to perform immunolabelling for presence of various IN neurochemical markers in EYFP-expressing cells. We found that ~29% of EYFP cells expressed NPY (19 NPY⁺ out of 65 EYFP⁺ neurons) and ~17% expressed PV (14 PV⁺ out of 82 EYFP⁺ neurons; *Figure 10Aó C*), whereas none of them expressed SST (0 out of 33 EYFP⁺ neurons) or nNOS (0 out of

41 EYFP⁺ neurons). Of note, PV and NPY only rarely coexpressed in the same neurons (1 PV⁺ neuron coexpressed NPY out of 174 PV⁺ neurons, while one NPY⁺ neuron contained PV out of 96 NPY⁺ neurons), consistent with prior studies (Mańko et al., 2012). We also detected calbindin in some of PV/EYFP-expressing neurons (three of seven; *Figure 10B*). Previous studies have established that calbindin content of PV⁺ INs identify the neuron as a BC (McDonald & Betette, 2001), as distinguished from PV⁺ INs lacking this Ca²⁺-binding protein, which are axo-axonic cell (Andrási et al., 2017; Bienvenu et al., 2012; Vereczki et al., 2016). Finally, in line with our *in-situ* hybridization and electrophysiological data, none of the EYFP-expressing cells examined (n = 51) were immunopositive for a glutamatergic neuronal maker, CaMKII (*Figure 10D*).

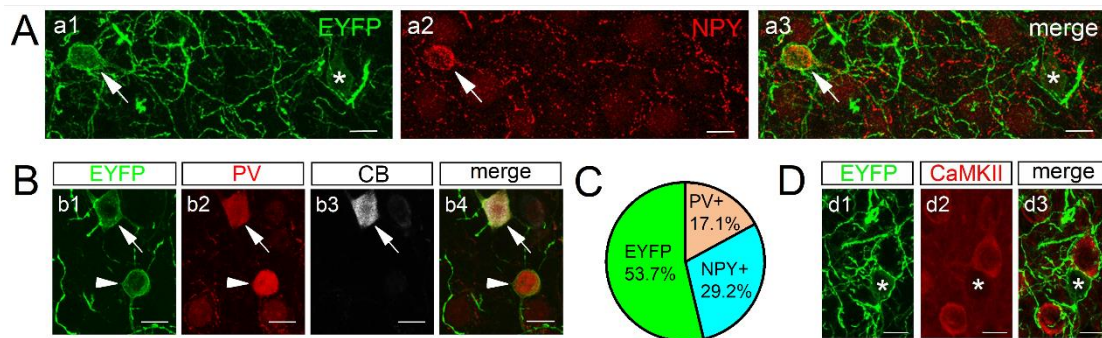


Figure 10. GABAergic cells labelled with intersectional viral strategy represent different populations of INs in *Cck-Cre;Dlx5/6-Flp* mice. **A**, Example of EYFP-expressing cells (panel a1) that either are (panel a2, arrow) or are not (panel a3, asterisk) also immunopositive for NPY (scale bar = 10 μ m). **B**, Example of two EYFP-expressing cells (panel b1, arrow and arrowhead) that both contain PV (panel b2), but only one of which is also immunopositive for calbindin (CB, panel b3, arrow; scale bar = 10 μ m). **C**, Pie chart showing the ratio of EYFP-expressing neurons that contain PV or NPY. Note a large proportion of cells does not express either PV or NPY. **D**, Example of EYFP-expressing cell (panel d1, asterisk) and non-overlapping cells immunopositive for CaMKII (panels d2, d3; scale bar = 10 μ m).

5.3.4. Targeted CCK⁺ INs are morphologically diverse

Our immunolabelling results suggest that, in addition to CCK/CB₁R-expressing BCs, three IN subtypes: PVBCs, PV⁺ axo-axonic cell and NPY⁺, likely NGF cells, were targeted in *Cck-Cre;Dlx5/6-Flp* mice using intersectional strategy. To substantiate this, we intracellularly labelled and immunostained EYFP⁺ neurons obtained from our slice preparations to allow for a direct comparison between the firing properties and neurochemical phenotype of each cell (*Figure 11A*). Of 33 EYFP⁺ cells labelled, all had dendritic and axonal morphologic features consistent with INs and not PCs. Examination

of these cells based on the action potential width at half maximum, 50% decay time of the afterhyperpolarization and maximum firing rate led us to classify three main subcategories which, in turn, corresponded well to differences in their respective immunocytochemical features (*Figure 11B*). One group was characterised by a fast-spiking phenotype (i.e., narrow action potential and high, >100-Hz firing-rate; *Figure 11C*). Within this group, both PVBCs (n = 3; *Figure 11D*) and PV⁺ axo-axonic cells (n = 5; *Figure 11E*) were identifiable; the former showed immunoreactivity for calbindin and avoided the axon initial segments visualised by Ankyrin G staining, while the latter lacked calbindin and their axonal varicosities formed close appositions with axon initial segments. A second group discharged action potentials with an intermediate half width and at the lowest rate. The cells in this group had axonal varicosities immunopositive for CB₁R, identifying them as CCK/CB₁-expressing BCs (n = 5; *Figure 11F*). The third last group had the widest action potentials and longest afterhyperpolarization and were identifiable as NGF cells based on previously published results (Armstrong et al., 2012; Mańko et al., 2012; Tamás et al., 2003); n = 20, *Figure 11G*). Indeed, quantification revealed the majority (~60%) of the *in vitro* recorded and labelled cells fell into the latter, NGF cell, subclass, with roughly equal (~9–15%) proportions in the other classes (*Figure 11H*).

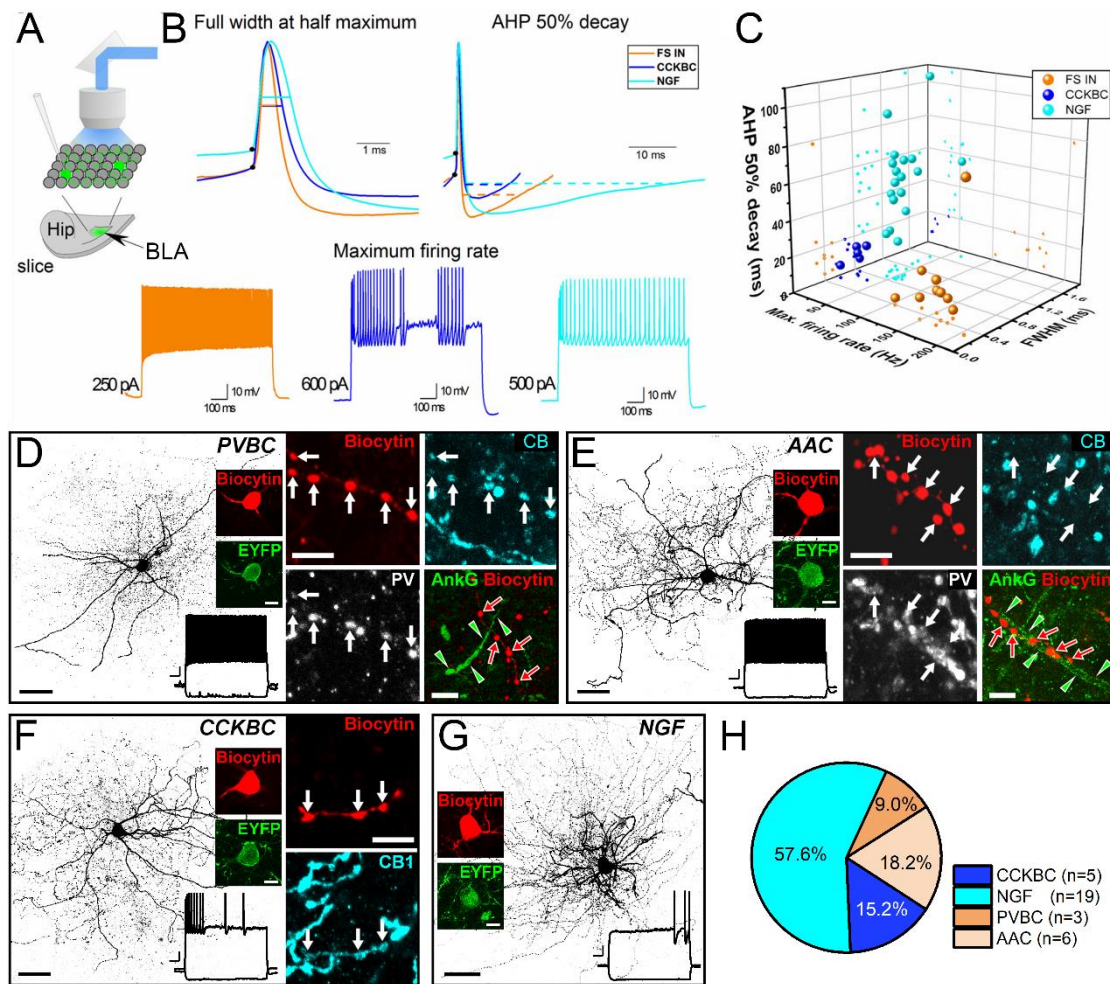


Figure 11. Action potential features distinguish GABAergic cell types labelled with intersectional viral strategy in *Cck-Cre;Dlx5/6-Flp* ($n = 4$) mice. **A**, Schematic drawing depicts a horizontal slice with viral expression shown in green (Hip = hippocampus). Whole-cell patch clamp recordings were performed in INTRSECT-ChR2-transfected GABAergic cells (green circles) visualised by blue light illumination. **B**, Traces exemplifying differences in the full width at action potential half maximum (FWHM), 50% decay of afterhyperpolarization (AHP) and maximum firing rate for the three electrophysiologically distinct IN groups: fast-spiking INs (FS INs) in orange, CCK⁺ basket cells (CCKBCs) in blue, and NGF cells in cyan. **C**, 3D plots showing the separation of 33 intracellularly labelled EYFP⁺ INs based on the three action potential parameters. **D–G**, Examples of four distinct types of EYFP-expressing INs intracellularly filled by whole-cell recording *in vitro*. In each case, a maximal intensity projection of a 3D confocal image of the labelled INs is shown together with its firing pattern and the EYFP-expression at the soma level. **D**, An example for a PV⁺ basket cell (PVBC) identified based on its firing pattern, calbindin (CB) and PV positivity in its axonal boutons (white arrows in insets) and forming no close appositions (red arrows) with ankyrin G (AnkG)-labelled axon initial segments (delimited by green arrowheads). **E**, An example for a PV axo-axonic cell (AAC) identified based on its firing pattern, PV positivity and calbindin negativity in its axonal boutons (white arrows in insets) and forming close appositions by its axonal boutons (red arrows) with an AnkG-labelled axon initial segment (marked by green arrowheads). **F**, An example for a CCKBC identified based on its firing pattern and on the CB₁ content in its axonal boutons (white arrows in insets). **G**, An example of a NGF based on its dendritic and axonal morphology and characteristic firing pattern. **H**, Pie chart showing the ratio of identified IN types in a group of EYFP-expressing neurons in the BLA that were randomly sampled in slice preparations. For D–G depictions of maximal intensity projections of intracellularly filled cells, scale bar = 40 μ m, insets = 5 μ m; firing pattern scale bar x-axis = 100 ms, y-axis = 10 mV.

Previous chapters presented our findings about the neuropeptide-expressing inhibitory neurons in the BLA. The last chapter will show the properties of dorsal tegmental VIP⁺ neurons connected with extended amygdala.

5.4. Characterization of VIP⁺ neurons projecting to the CeA

5.4.1. Verification of the specificity of Vip-IRES-Cre mice

At the beginning of the following investigations, we investigated the specificity of the transgenic mice, Vip-IRES-Cre line used in the subsequent studies. In virus injected Vip-IRES-Cre mice, VIP immunostaining was applied. This approach allowed us to test the overlap between the genetically and immunocytochemically labelled VIP⁺ neurons (*Figure 12A*). As we have not found differences between the sexes, ($p > 0.05$, Mann-Whitney test), we pooled data. From all the virally labelled neurons the immunostaining marked 80.2% (male: 7.3 ± 9.2 immunolabelled, 22.3 ± 19 virus-labelled and 104.3 ± 20.9 immuno- and virus-labelled neurons in 4 mice; female: 10.4 ± 2.6 immunolabelled, 21.4 ± 6.1 virus-labelled and 117.2 ± 52.2 immuno- and virus-labelled neurons in 5 female mice, *Figure 12B*), whereas 92% (93% in male and 91.1% in female, *Figure 12C*) of immunolabelled neurons were also visualized with viral vectors.

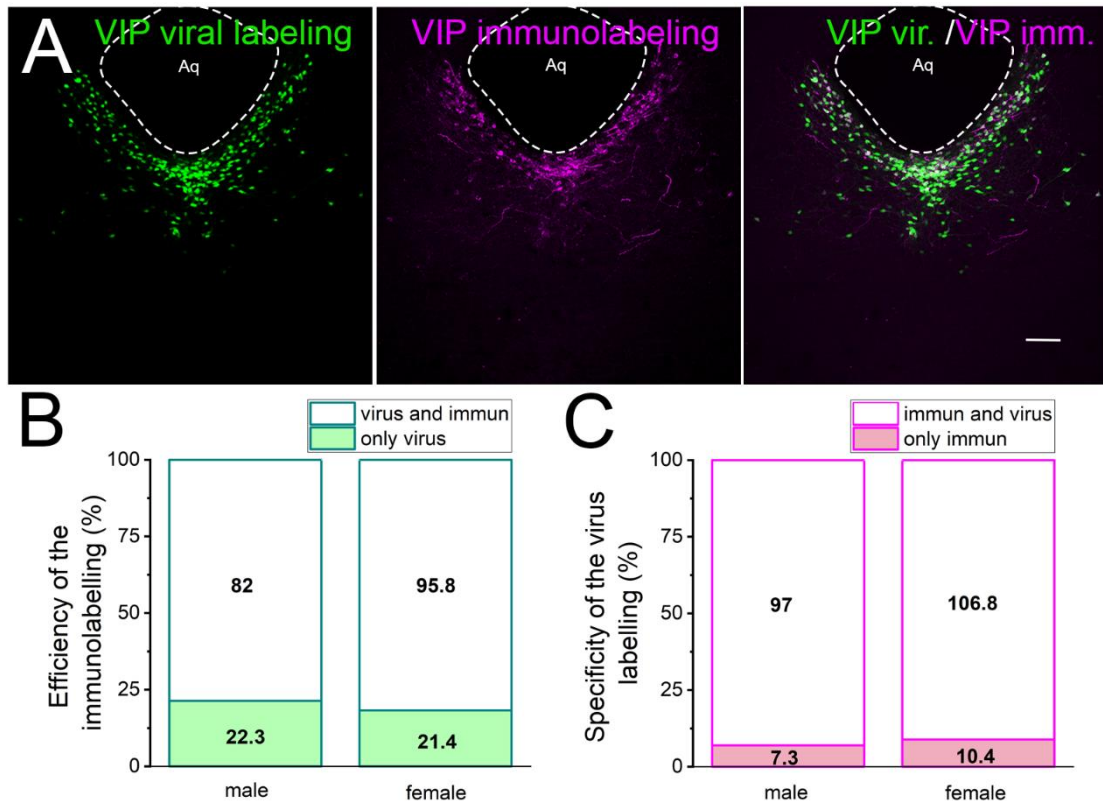


Figure 12. Specificity and efficiency of labelling the VIP⁺ neuron. **A**, The confocal images show the GFP containing viral labelling (green) and immunolabelling (magenta) in the PAG/DRN region (upper row). Scale bar = 100 μ m, Aq, Aqueduct. **B**, The graphs present the virus labelled neuron numbers in male (n = 4) and female (n = 5) mice. **C**, The graphs depict the immunolabelled neuron numbers in male (n = 4) and female (n = 5) mice.

5.4.2. Dopamine content of VIP⁺ neurons in the dorsal tegmentum

As previous studies suggested that VIP⁺ neurons in the dorsal tegmentum are dopaminergic (Dougalis et al., 2012; Poulin et al., 2014; Zhao et al., 2022) we aimed to confirm these results by investigating the presence of VIP in dopaminergic neurons. Firstly, we quantified the dopamine marker, tyrosine hydroxylase (TH) and VIP coexpression in vPAG-DRN (i.e., in dorsal tegmentum) neurons in male (n = 5) and female mice (n = 5, *Figure 13A*). We used viral and immunocytochemical visualisation of the VIP neurons to reach complete labelling. The quantifications were made at 3 different antero-posterior levels of the PAG region from each animal. We found that 26.2% \pm 1.9 of the VIP neurons in males and 28.8% \pm 2.3 in females expressed TH, without any significant differences between sexes (p = 0.409, two sample *t*-test). 25.9%

± 3.3 of the TH neurons in males and $29.2\% \pm 1.0$ in females coexpressed VIP ($p = 0.367$, two sample t -test). We counted 254.4 ± 22.2 and 248.8 ± 21 VIP⁺/TH⁻ neurons in male and female animals (without sex difference, $p=0.914$, two sample t -test), respectively. We found no difference between sexes in the VIP⁺/TH⁺ neuron numbers (90 ± 14.4 labelled cells in males, and 98.4 ± 5.2 cells in females, $p=0.599$, two sample t -test), nor in the VIP⁻/TH⁺ neuron numbers (253.4 ± 14.7 labelled cells in males, 239.4 ± 11.8 cells in females, $p = 0.48$, two sample t -test). These results clearly suggest that a large fraction (more than 20 %) of VIP⁺ neurons are indeed dopaminergic.

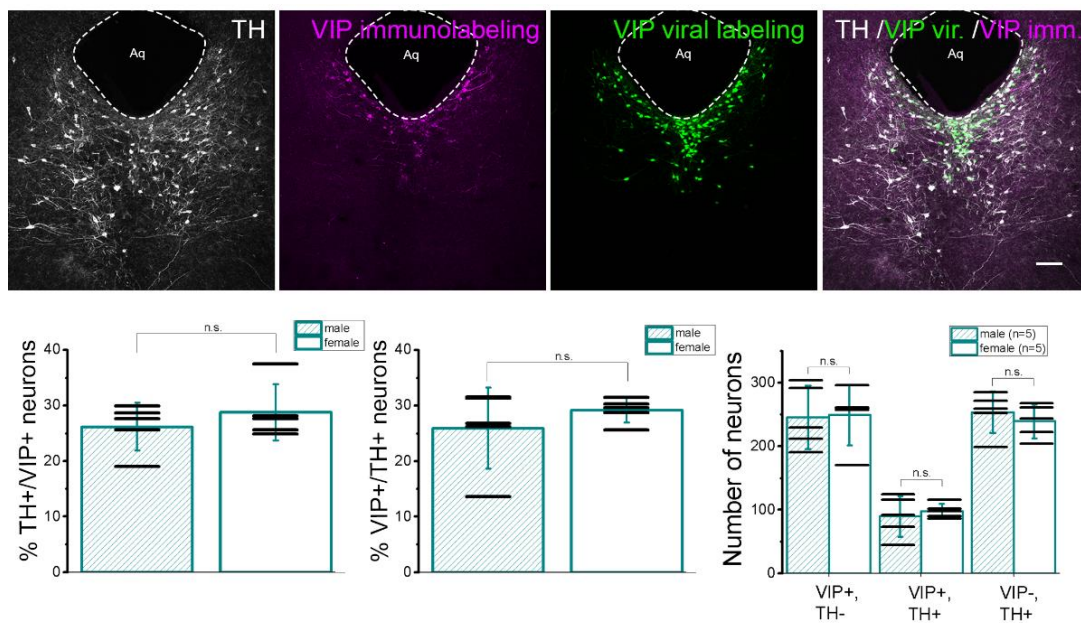


Figure 13. One-fourth of VIP⁺ neurons contain tyrosine hydroxylase (TH), which is the rate-limiting enzyme of dopamine synthesis. The confocal images show that the estimated number of VIP⁺ neurons in the PAG-DRN visualised by viral (green) or immunolabelling (magenta) together with the TH (white), scale bar = $100 \mu m$. The ratio of VIP⁺ neurons expressing TH (plot on left), the ratio of dopaminergic neurons expressing VIP (plot in the middle) and the number of neurons expressing VIP, TH, and both (plot on right) compared between male and female mice are shown. N.s. no significant difference, $p = 0.005$, Aq, aqueduct.

5.4.3. VIP⁺ cells in the dorsal tegmentum and their projection areas

The location of VIP-expressing cells in vIPAG-DRN has been described earlier (Paspalas et al., 2000), however, their anatomical and physiological features are still elusive. As shown (*Figure 13*), a subpopulation of this cell type expresses TH, the marker of dopaminergic phenotype (Dougalis et al., 2012). In this midbrain region, the function, and the properties of TH⁺ neurons were studied, though these investigations have not distinguished subgroups of dopaminergic neurons expressing or lacking VIP. Therefore, we aimed to reveal the characteristics, including firing and morphological features of VIP⁺ neurons in the dorsal tegmentum.

As a first step, we used Vip-Cre::tdTomato mice to explore the localization of the somata of VIP⁺ neurons in the v/vIPAG and DRN. We found that these neurons are close to the wall of the 4th ventricle but extend even more ventral into the DRN (*Figure 14A*). We observed that TdTomato labelled VIP⁺ neurons distributed along the anteroposterior axis -3.88 mm to -4.84 mm to bregma and they were most abundant between -4.48 mm to -4.72 mm. Then, we visualised the axons of VIP⁺ neurons by injecting AAV-CAG-FLEX-tdTomato into the vIPAG-DRN of Vip-IRES-Cre mice. Axon terminals from vIPAG-DRN VIP⁺ neurons were found to be restricted to the dorsolateral (or oval part) of the BNST and the lateral nucleus of the CeA (*Figure 14B*), the two nuclei, which are a part of the extended amygdala. Importantly, we did not observe axon terminals in any other brain regions.

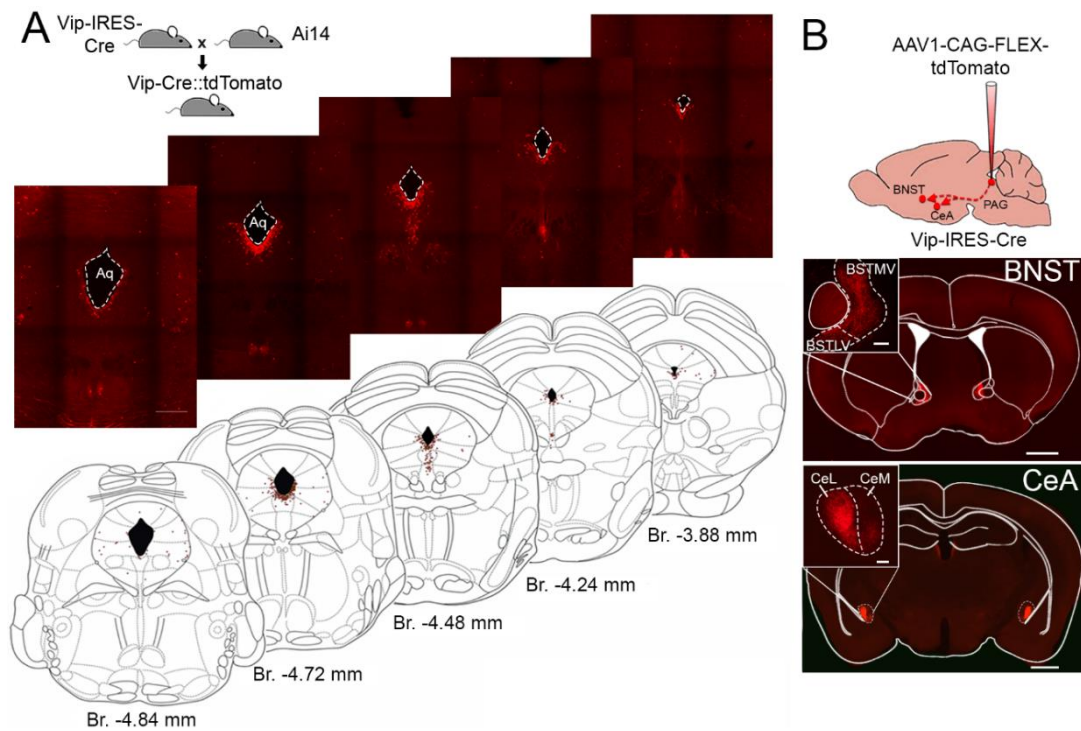


Figure 14. VIP⁺ neurons in the vIPAG-DRN project exclusively into the CeA and BNST **A**, VIP⁺ neurons in vIPAG-DRN are visualised in Vip-Cre::tdTomato mice, the offspring of Vip-IRES-Cre and reporter (Ai14) mice. TdTomato-expressing VIP⁺ neurons surround the 4th ventricle ventrally and laterally, i.e., they are within the ventrolateral PAG and penetrate the DRN, too. Maps of the soma distribution of VIP⁺ neurons (red dots) are shown below. They are distributed along the anteroposterior axis from -3.88 mm to -4.84 mm to bregma. Scale bar = 500 μ m. **B**, The AAV1-CAG-FLEX-tdTomato labelled vIPAG-DRN VIP⁺ neurons restricted their axons to the BNST and lateral division of the CeA. Scale bar = 500 μ m, insets = 100 μ m.

To explore whether the same VIP⁺ neurons project to both the BNST and CeA, or individual neurons innervate either the BNST or CeA, we injected retrograde tracers fluorogold and cholera toxin β subunit into the BNST and CeA, respectively. In the vIPAG and DRN we found both single and dual labelled VIP⁺ neurons, indicating that there is a population of VIP⁺ neurons which innervate both nuclei (Figure 16).

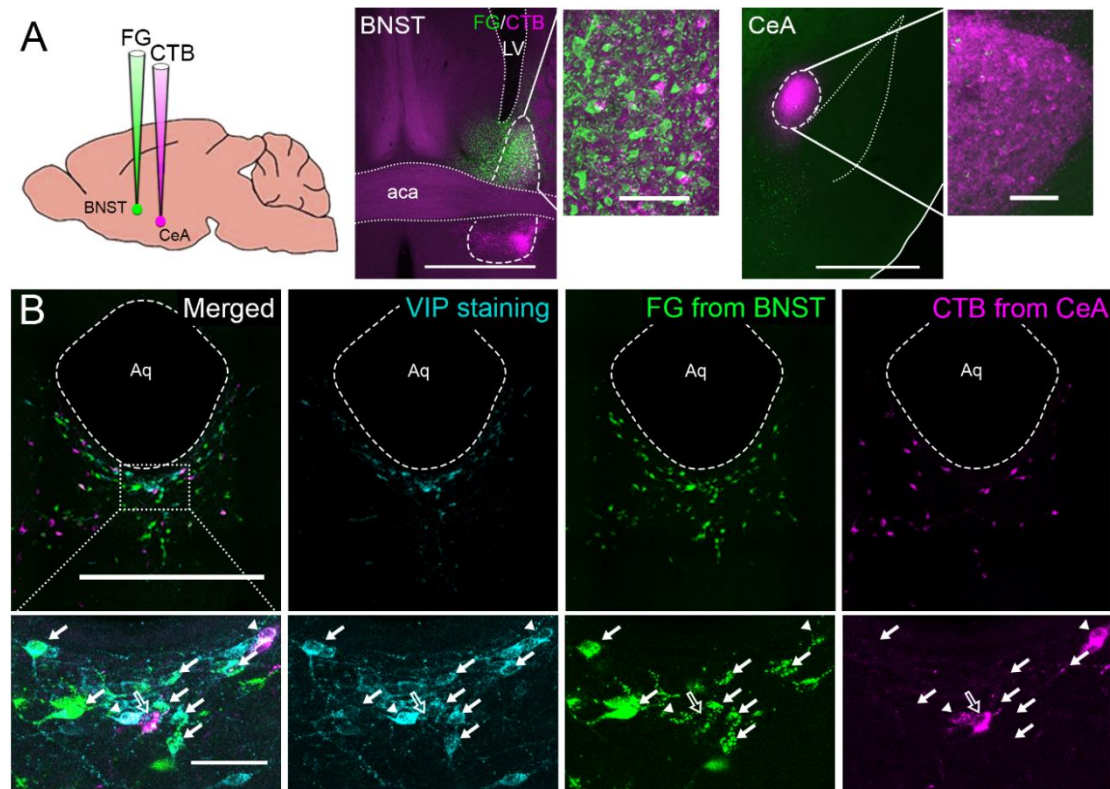


Figure 15. vIPAG-DRN VIP⁺ neurons express the retrograde tracers injected in the CeA or BNST. **A**, A schematic figure depicts the retrograde labelling strategy and the injection sites. Oval nucleus of BNST was targeted with fluorogold (FG, in green) and CeA with CTB (cholera toxin subunit β , in magenta). Scale bar = 1000 μm , insets = 500 μm . Aca, anterior part of the anterior commissure; LV, lateral ventricle. **B**, VIP, cholera toxin β subunit or fluorogold labelled somata around the ventricle in the PAG-DRN. Scale bar = 500 μm . **C**, The colocalization of the VIP and fluorogold (arrow); fluorogold and cholera toxin β subunit (empty arrow); fluorogold, cholera toxin β subunit and VIP (arrowhead). Scale bar = 50 μm .

To strengthen these results, i.e. that VIP⁺ neurons in the vIPAG-DRN collateralise and therefore they could control the function of the BNST and CeA simultaneously and extend this by showing that they can even project to the contralateral hemisphere, we performed antero-retrograde neuronal tracing in *Vip-IRES-Cre* mouse ($n = 2$, *Figure 16*). We injected the AAV5-EF1-DIO-EYFP virus into the BNST unilaterally. BNST projecting vIPAG-DRN VIP⁺ neurons took the viruses up at their axon terminals, transport them back to the somata and expressed the EYFP in their whole arborisation. We observed that in addition to the soma-dendritic labelling within the vIPAG-DRN there were many EYFP⁺ axons in the contralateral BNST, as well as in the CeA in both hemispheres. Thus, our results confirmed that there are VIP⁺ cells that are able to control these two nuclei of the extended amygdala bilaterally and therefore, simultaneously.

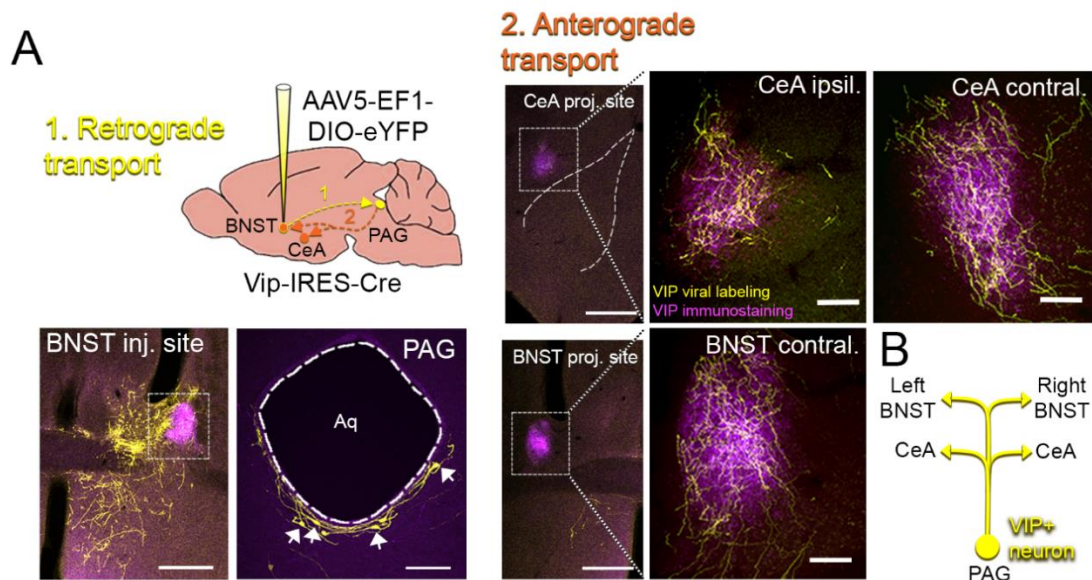


Figure 16. **A**, A schematic figure indicates the retro-antegrade labelling strategy. 6 weeks after the AAV5-EF1-DIO-EYFP unilateral virus injection into the right BNST (injection site, bottom left) resulted in retrogradely labelled somata of EYFP-expressing VIP⁺ neurons in the PAG (arrows) and anterogradely labelled axons in the ipsilateral (ipsil.) and contralateral (contral.) CeA as well as in the contralateral (contral.) BNST. Confocal images of virally labelled VIP⁺ axons are depicted in yellow and immunolabelled VIP⁺ axons in purple to visualise the target area within the nuclei. Scale bar = 500 μ m, insets = 100 μ m, Aq = aqueduct. **B**, Summary drawing summarizes the tracing results, showing that there are VIP⁺ neurons in the vIPAG-DRN that are able to control the CeA and BNST in both sides simultaneously.

5.4.4. VIP⁺ neurons occur in the human PAG and CeA

So far, we used mice to study VIP⁺ neurons, but as a further step, we tested the hypothesis whether these cells are present in humans as well. To this end, we made immunohistochemistry in post-mortem brain sections. In most cases, the VIP⁺ and TH⁺ labelling was colocalized in the human PAG (82.6% of VIP⁺ neurons were TH⁺, *Figure 17A*). In addition, VIP⁺ axon fibres in the CeA were numerous, especially in the lateral part (*Figure 17B*). These results highlight the relevance of our study obtained in mice suggesting VIP⁺ neurons present in humans may have a similar function as in rodents.

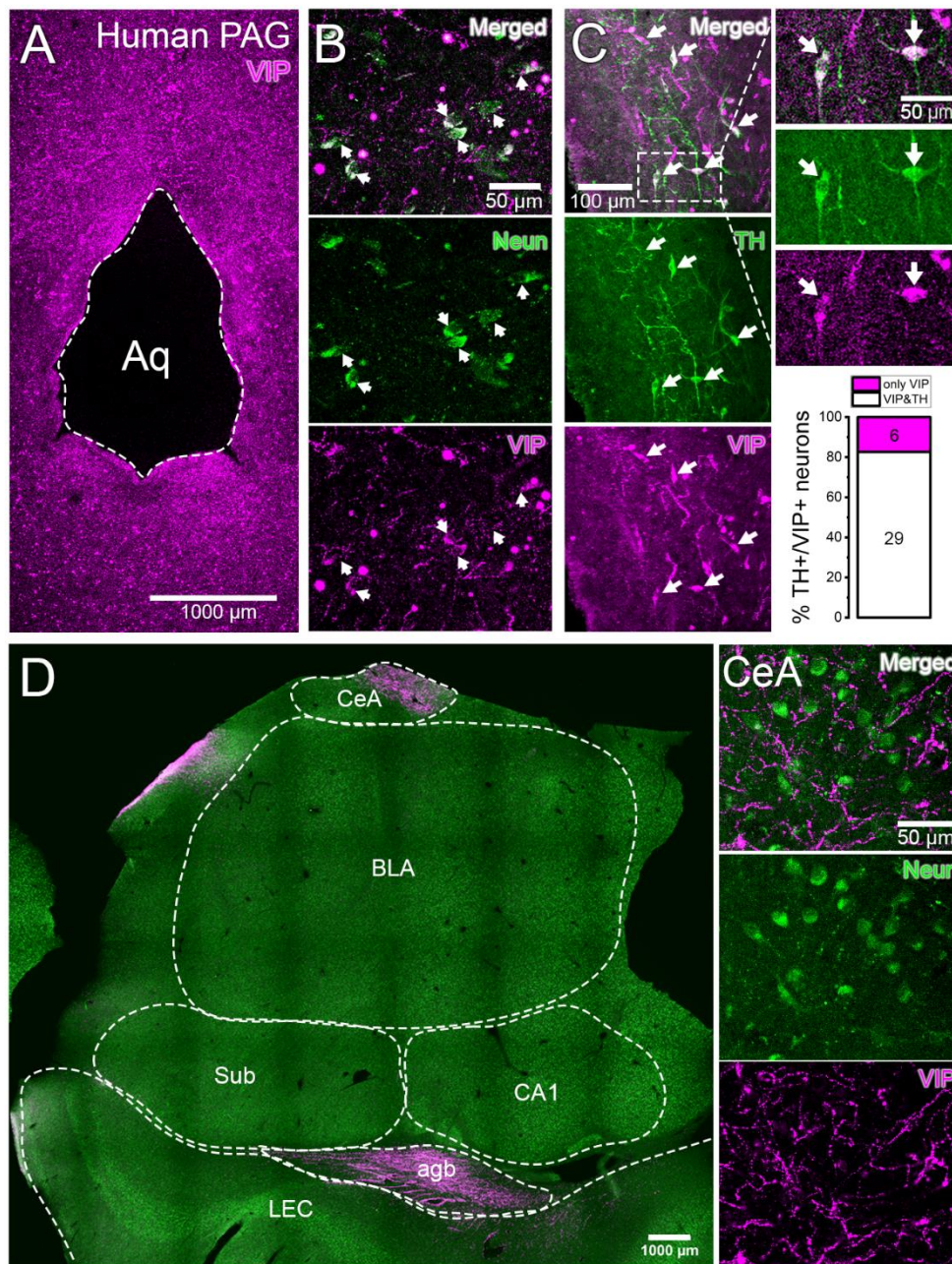


Figure 17. VIP immunolabelling in human PAG and CeA. **A**, A section taken at a low magnification from the human PAG region indicate many VIP immunoreactive somata shown in magenta. **B**, VIP (magenta) immunostaining colocalizes (white arrows) with NeuN (green), indicating that VIP is present in neurons. **C**, VIP⁺ somata express TH (green) shown by white arrows. The part of the image (rectangle) is enlarged showing two VIP⁺ and TH⁺ neurons at higher magnification. The ratio of TH content of VIP⁺ neurons is shown in the graph, averaged number of cells are written inside the column (n = 2 slices of 1 human). **D**, *Left*, A section from a human amygdala is immunostained for VIP (magenta) and NeuN (green). *Right*, an image taken at a higher magnification from the CeA shows numerous axon collaterals immunoreactive for

VIP among NeuN⁺ somata. Agb, angular bundle; CA1, CA1 region of the hippocampus; CeA, central amygdala; BLA, basolateral amygdala; LEC, lateral entorhinal cortex; Sub, subiculum.

5.4.5. Membrane properties of dorsal tegmental VIP⁺ neurons and their action on the postsynaptic neurons in the CeA and BNST

To reveal the membrane characteristics of VIP⁺ neurons, which determine the firing features, we investigated their voltage responses upon intracellularly injected current steps, the membrane properties that were compared to GABAergic neurons also in the PAG/DRN. To this end, whole-cell patch-clamp recordings were made in dorsal tegmental neurons in acute brain slices prepared from *Vip-IRES-Cre::ZsGreen1* and *Vgat-IRES-Cre::ZsGreen1* mouse lines to assess the active and passive membrane properties of VIP⁺ (n = 20) and vesicular GABA transporter-expressing (VGAT⁺, n = 11) neurons, respectively (*Figure 18A,B*). We found that VIP⁺ neurons required larger current steps to evoke the first action potential (AP threshold), their input resistance was lower, and the membrane time constant was shorter than those parameters observed in VGAT⁺ neurons (*Figure 18C*). Further, there was a significant difference between their relative sag amplitude, which is related to the amount of the ‘pacemaker current’, the hyperpolarization activated non-selective cation current through hyperpolarization-activated cyclic nucleotide-gated channels (HCN) expressed by a neuron, but their action potential amplitude was similar. Our electrophysiological data clearly show that vPAG-DRN VIP⁺ neurons have different membrane properties than inhibitory neurons in this region (*Figure 18, Table 7*). Overall, the single-cell membrane features, e.g. spike frequency adaptation or large sag of VIP⁺ neurons were found to be similar to the dopaminergic neurons in the ventral tegmental area and substantia nigra pars compacta (Dufour et al., 2014; Margolis et al., 2006).

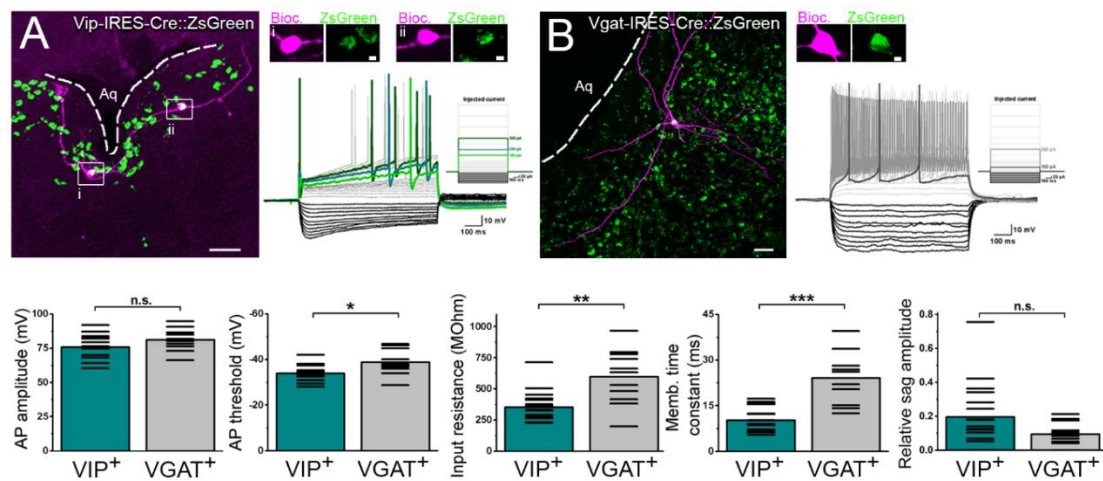


Figure 18. Dorsal tegmental VIP⁺ neurons have different firing properties compared to VGAT⁺ neurons in this area. **A**, PAG containing slices were prepared from *Vip-IRES-Cre::ZsGreen1* mice where ZsGreen1⁺ (green) neurons were recorded and filled with biocytin (magenta). The membrane voltage changes upon hyperpolarizing and depolarizing current step injections are shown from an example VIP⁺ neuron ($n = 20$ from 4 mice). **B**, Similarly, VGAT⁺ neurons ($n = 11$ from 2 mice) were recorded in slices prepared from *Vgat-IRES-Cre::ZsGreen1* mice. Scale bar = $50 \mu\text{m}$, insets = $5 \mu\text{m}$ firing pattern scale bar x-axis = 100 ms, y = 10 mV, Aq = aqueduct. Single-cell membrane properties of the two distinct cell types in the vPAG (the graphs in the bottom). N.s. = No significant difference. * $p < 0.05$. For data, see Table 7.

Next, we aimed to determine the nature of the neurotransmitter molecules released from the axon terminals of VIP⁺ neurons in their target areas. To achieve this goal, we combined optogenetics with slice recordings (*Figure 19A*). AAV5-EF1a-DIO-ChR2-mCherry vectors were injected into the PAG of *Vip-IRES-Cre* mice. After 4-6 weeks following the injection, we prepared acute slices from the regions containing the BNST or CeA. Whole-cell recordings were performed in neurons in these nuclei. To activate the axon terminals of VIP⁺ neurons, which leads to evoke postsynaptic responses in the postsynaptic neurons, whole field illumination was applied using blue light. We found that there was a higher response probability in the CeA than in the BNST (12 out of 22 and 6 out of 25, respectively). As single cell RNA sequencing data showed that *Vglut2* is expressed in VIP⁺ neurons in the midbrain (Poulin et al., 2020), we tested the hypothesis whether dorsal tegmental VIP⁺ neurons can release glutamate from their axon terminals using pharmacology. In line with this idea, bath-application of $10 \mu\text{M}$ NBQX and $50 \mu\text{M}$ APV which are α -amino-3-hydroxy-5-methyl-4-isoxazolepropionic acid (AMPA) and N-methyl-D-aspartate receptor (NMDA) ionotropic glutamate receptor antagonist, respectively, fully eliminated the blue light-evoked responses in CeA and BNST neurons. Consequently, vPAG-DRN neurons can excite neurons in the extended amygdala nuclei

via activation of ionotropic glutamate receptors. During the recordings, cells were filled with biocytin, and then their neurochemical content was identified post hoc using immunostaining (Figure 19B). In spite of the fact that SST and PKC δ are present in a large population of CeA and BNST neurons, we found only a moderate co-localization of these marker in neurons that received postsynaptic inputs from VIP $^+$ axons SST (n = 7 out of 54 recorded cells, 13%) and PKC δ (n = 16 out of 54 recorded cells, 30%). These data indicate that the primary target of dorsal tegmental VIP $^+$ neurons is a population of CeA and BNST neurons that are distinct from those expressing SST and PKC δ .

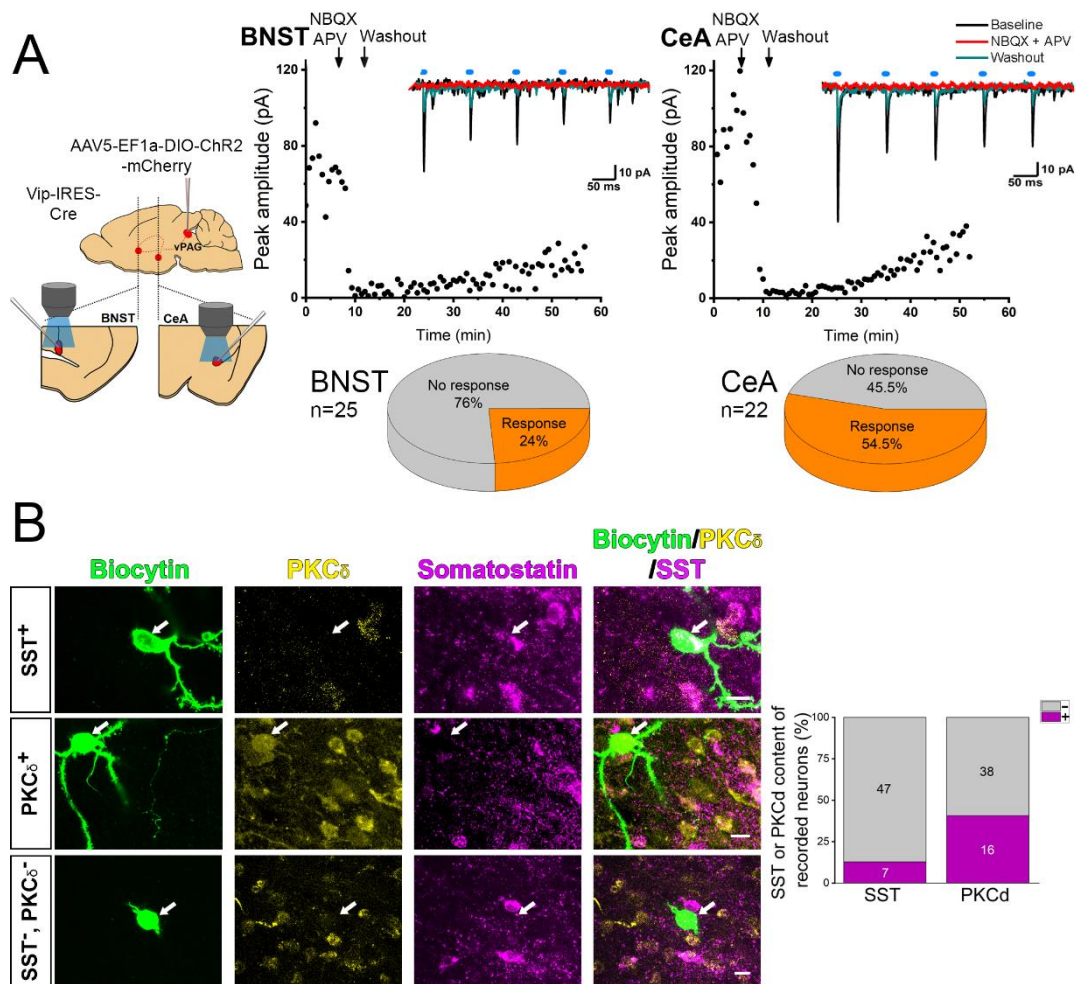


Figure 19. Photostimulation of dorsal tegmental VIP $^+$ terminals in the CeA and BNST. **A**, Schematic figure of the optogenetic experiment. AAV5-EF1a-DIO-ChR2-mCherry vectors were injected into the PAG/DRN of Vip-IRES-Cre mice, then VIP $^+$ axons were excited with blue light (447 nm) during the recording in CeA and BNST neurons. Bath-applied NBQX and APV diminished the evoked postsynaptic responses in neurons in the CeA and BNST, indicating that VIP $^+$ neurons evoke excitatory postsynaptic currents. 24% of recorded BNST neurons and 54.5% of CeA neurons was found to receive a postsynaptic response from VIP $^+$ axons upon light stimulation (n = 4 mice). **B**, Investigating the neurochemical content of filled

postsynaptic cells show that 13% of all recorded neurons ($n = 54$ cells) were immunopositive (purple) for SST and 30% for PKC δ , respectively. Scale bar = 10 μ m.

5.4.6. Input regions of the CeA and BNST identified by retrograde tracing

To reveal the different brain regions projecting to the CeA and BNST we injected retrograde tracers cholera toxin β subunit and fluorogold (*Figure 15A*) followed by identifying brain areas where retrogradely labelled neurons were observed. First, these two extended amygdala nuclei mutually innervated each other, indicated by the presence of labelled somata (*Figure 15A*). Second, the CeA and BNST were innervated by neurons from the same regions (*Figure 20*), with the exception of the retrorubral field (RRF), where we observed neurons retrogradely labelled only from the CeA. These results demonstrate that the CeA and BNST receive projections from almost identical brain regions, an observation which support the view that these extended amygdala nuclei may have a similar function in brain operation.

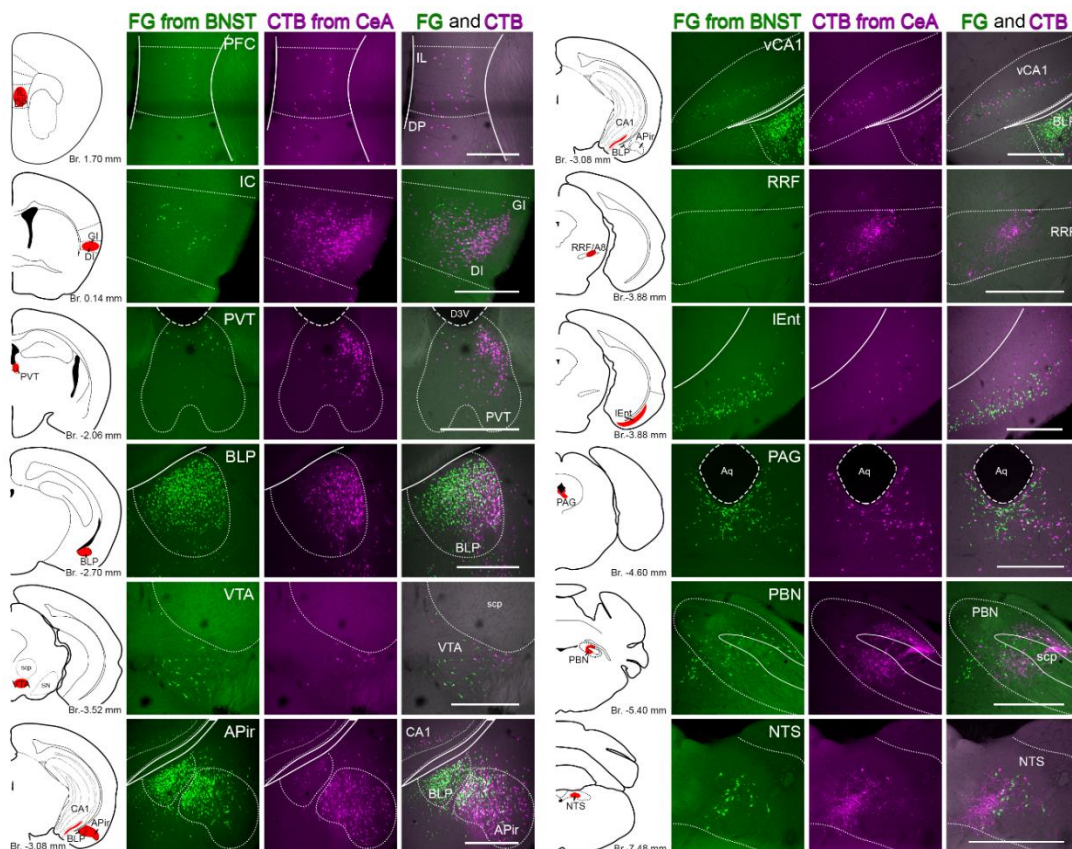


Figure 20. The retrograde tracing study of the CeA and BNST shows common projection sites. The oval nucleus of the BNST was targeted with fluorogold (FG, in green) and the CeA with cholera toxin β subunit (CTB, in magenta), injection strategy depicted in *Figure 15A*. On the schematic atlas figures (Paxinos & Franklin, 2004), the location of the labelled somata is indicated in red. On the corresponding confocal images fluorogold- and cholera toxin β subunit-containing neurons are shown. PFC, prefrontal cortex; IL, infralimbic cortex; DP, dorsal peduncular cortex; IC, insular cortex; GI, granular insular cortex; DI, dysgranular insular cortex; PVT, paraventricular thalamic nucleus; D3V, dorsal 3rd ventricle; BLP, basolateral amygdaloid nucleus, posterior part; VTA, ventral tegmental area; scp, superior cerebellar peduncle; APir, amygdalopiriform transition area; SN, substantia nigra; CA1, cornu ammonis 1 in hippocampus; vCA1, ventral CA1; RRF, retrorubral fields; lEnt, lateral entorhinal cortex; PAG, periaqueductal grey; Aq, aqueduct; PBN, parabrachial nucleus; NTS, nucleus tractus solitarius; Scale bar= 500 μ m.

6. Discussion

In this study, we examined the structural and functional organization of peptidergic neurons in the amygdala. Our main findings are as follows:

I) We described the morphological and electrophysiological features of two types of SST-expressing neurons in the BLA. One type preferentially targets the dendrites of PCs, i.e., they belong to the dendrite targeting IN category and lack nNOS content. The other type of SST⁺ neurons projects to the basal forebrain and/or entorhinal cortex, and often contains nNOS, and can be found preferentially in the capsules surrounding the BLA. The ratio of SST⁺ INs are higher than SST⁺ projecting GABAergic neurons in the BLA.

II) In the BLA, we characterised 3 subtypes of NPY⁺ inhibitory neurons: half of them were late spiking NGF cells, 32% of them were fast-spiking PV⁺ and 15% were spiny SST⁺ INs. We found a double amount of NPY⁺ GABAergic neurons in the BA than in LA.

III) GABAergic neurons expressing CCK were visualized with intersectional viral strategy. We found ~40% of inhibitory INs in Cck-Cre mice expressed CB₁Rs, whereas others had the features of NGF cells or PV-expressing INs.

IV) By studying the peptidergic innervation of the extended amygdala we found that dorsal tegmental VIP⁺ neurons project to the CeA and BNST. The neurotransmitter molecule of VIP⁺ neurons is glutamate as the excitation of the axon terminals of these dorsal tegmental neurons lead to activation of ionotropic glutamate receptors on the postsynaptic targets. In addition, a large fraction of VIP⁺ neurons were found to be dopaminergic both in mice and humans.

6.1. Diversity of SST⁺ and NPY⁺ neurons in the lateral and basal amygdala

In this study we attempted to assess the ratio of distinct inhibitory neuron types expressing neuropeptides in the LA and BA. We took advantage of the fact that, in adult

Sst-IRES-Cre and Npy-Cre mice, viral labelling visualises one or a few GABAergic cell categories that can be separated by immunostaining.

In this study, we provide the first detailed characterization of SST⁺ GABAergic cells in the LA and BA. As in the hippocampus and neocortex (Katona et al., 1999; Wang et al., 2004), SST⁺ inhibitory cells target predominantly the dendritic shaft and, to a lesser extent, the spines of PCs. SST⁺ GABAergic cells that project to the basal forebrain or entorhinal cortex (McDonald et al., 2012; McDonald & Zaric, 2015) were found to be immunopositive for nNOS. This enzyme content in SST⁺ GABAergic cells thus helped us to estimate the ratios of INs and projection neurons expressing SST in the LA and BA. We found a similar ratio for SST⁺ GABAergic projection cells in the amygdala as it was reported in the hippocampus (5%-6%) (Bezaire & Soltesz, 2013). However, this latter study estimated significantly less local SST⁺ INs in the hippocampus (4%-5%), than we found in the amygdala (10%-16%), or others in the neocortex (17%-20%) (Xu et al., 2010). Future studies should clarify the reason of this surprisingly low ratio of SST⁺ INs in the hippocampus.

NPY has been shown to be expressed often in NGF cells (Armstrong et al., 2012; Fuentealba et al., 2010; Mańko et al., 2012; Perrenoud et al., 2013; Tricoire et al., 2010). In neocortical areas, 7%-10% of GABAergic cells were found to express NPY (Xu et al., 2010), whereas ~30% of all inhibitory cells may belong to NGF cell family in the hippocampus (Bezaire & Soltesz, 2013). Thus, the LA and BA, where we estimated 14%-15% of GABAergic cells to be NGF cells, a proportion that take up an intermediate position between these two cortical structures. Our observation that Cre recombinase under the control of Npy gene promoter is expressed in a portion of PV⁺ basket and axo-axonic cells in the two amygdalar nuclei examined is novel, but not surprising, as in the hippocampus NPY immunoreactivity has been reported in some PV⁺ INs (Klausberger et al., 2004). In line with findings in cortical regions (He et al., 2016; Lim et al., 2018) we also observed that many SST⁺ GABAergic cells express NPY. We identified the subtypes of SST⁺ and NPY⁺ INs in the BLA, which may facilitate the future research of fear learning and extinction in healthy and in disorders (e. g. anxiety or PTSD). The exact ratio of these peptidergic IN types in the BLA should further our

understanding about the changes in the fraction of distinct IN types in various pathological conditions.

6.2. Various types of GABAergic INs can be labelled in CCK-Cre;Dlx5/6-Flpe animals

There is a growing appreciation of the critical contribution of INs to the regulation of network activity to support behavioural functions subserved by the BLA, including Pavlovian fear and extinction. However, a description of the subclass of BLA INs expressing the neuropeptide, CCK, has proved elusive. Here, we sought to genetically access BLA CCK INs to define the neurochemical and physiologic phenotype of these cells.

Using an intersectional approach by transfecting Cre⁺/Flp⁺ cells in CCK-Cre;Dlx5/6-Flpe transgenic mice with opsin-containing INTRSECT viruses, we selectively targeted GABAergic INs in the BLA and showed that almost half of these neurons expressed functional CB₁R on their axonal boutons. In line with this anatomical observation, the application of a CB₁R agonist reduced the amplitude of light evoked IPSCs by half in recorded PCs. Taken together, this is strong evidence that a significant portion of the cells targeted by the INTRSECT strategy is CCKBCs, given that prior studies have shown that in the BLA CCKBCs express CB₁R on their boutons that, when activated, markedly suppress inhibitory transmission (Azad, 2004; Barsy et al., 2017; Katona et al., 2001; McDonald & Mascagni, 2001b; Rovira-Esteban et al., 2017; Veres et al., 2017; Vogel et al., 2016). This functional connection between CCK and CB₁R has been of a particular interest to the field given compelling evidence linking endocannabinoid signalling, in the BLA and other regions, to extinction (Patel et al., 2017). One proposal is that endocannabinoids could inhibit CCK release in the BLA (Beinfeld & Connolly, 2001; Chhatwal et al., 2009) and thereby oppose the peptide's pro-fear/anxiety effects to enable extinction (Bowers & Ressler, 2015; Del Boca et al., 2012; Frankland et al., 1997; Harro, 2006).

In addition, we found that the genetically targeted CCK INs could give rise to a prominent GABA_B receptor-mediated component in the light-evoked outward currents that likely does not originate from CCKBCs. Indeed, further examination using a

combination of immunostaining, electrophysiological recordings and morphologic inspection indicated that targeting CCK cells also included PVBCs, PV⁺ axo-axonic cells, and NGF cells. A portion of the latter INs might express NPY (Mańko et al., 2012). Based on available data, we concluded that recombination in these cells reflects the genuine presence of CCK in adult BLA cells at low levels that were not detected by prior studies using other approaches. This conclusion is based on several observations. First, other studies using genetic approaches also support a significant diversity of CCK-expressing INs in the BLA, among which INs with NGF cell morphology and firing characteristics were evident (Jasnow et al., 2009; Veres et al., 2017; Vogel et al., 2016). Second, CCK mRNA was unequivocally detected in axo-axonic cells both in the neocortex (Paul et al., 2017) and hippocampus (Harris et al., 2018) and even in a portion of hippocampal PVBCs (Harris et al., 2018). Third, using a different approach to that used herein, involving crossing offspring of CCK-Cre and Nkx2.1-Flp mice with an Ai65 reporter line, another recent study reported labelling of axo-axonic cells in the neocortex (Paul et al., 2017). Fourth, dense core vesicles are readily observed in axon terminals of both PV-containing basket and axo-axonic cells (Takács et al., 2015), indicating the presence of neuropeptides in these GABAergic cell types that have not been labelled so far in Sst-Cre or VIP-Cre mouse lines. Taken together with these prior observations, our results strongly speak to the importance of applying multiple phenotypic criteria when classifying CCK INs and underscore the limitations of demarcating this population based on a single, neurochemical marker (Harris et al., 2018). The difference in ratio of distinct IN types obtained by immunostaining in perfused tissue (*Figure 9**Figure 10*) and by randomly sampled neurons recorded in *in vitro* slices (*Figure 11*) may reflect the fact that some cell types are better able to tolerate the procedure of slice preparation than others.

6.3. Extended amygdala projecting VIP⁺ neurons in the dorsal tegmentum

Our results confirm the earlier observations about the localization and projection of vIPAG-DRN VIP⁺ neurons (Poulin et al., 2018; Zhao et al., 2022). Interestingly, with viral tracings studies, we found individual VIP⁺ neurons which can project not only to both nuclei of the extended amygdala but both hemispheres, too. Thus, they can control

the function of these regions at the same time. Our results regarding the collateralisation of VIP⁺ neurons extend the previous anatomical data: reconstructed individual vPAG-DRN dopaminergic neurons have axon terminals in CeA and BNST, but it was only shown unilaterally and VIP content was not examined (Lin et al., 2020).

Previous studies have revealed that the midbrain VIP⁺ cells express Vglut2 (Poulin et al., 2018; Zhao et al., 2022) and our electrophysiological recordings combined with optogenetic strengthened that these neurons are excitatory as they activate ionotropic glutamate receptors on their postsynaptic partners. The electrophysiological features of the VIP⁺ neurons show that they are distinct from GABAergic neurons in this area. The specificity of VIP⁺ cells is the I_h current generated by the activation of hyperpolarization-activated cyclic nucleotide-gated channels which are required for producing a sag in voltage responses upon negative current injections (Dougalis et al., 2012). The presence of sag was typically described in dopaminergic neurons in this or other regions (Blythe et al., 2009; Dougalis et al., 2017; Dufour et al., 2014). This difference may suggest a separate function of VIP⁺ neurons from others non-dopaminergic neurons located in the PAG.

We found the coexpression of TH⁺ labelling in VIP⁺ cells was less than 30%, which is different from data that were reported in a recent study in the same region in the PAG (Zhao et al., 2022). The sensitivity of the distinct antibodies can be an explanation for these differences. Probably the genes determine the dopamine are expressed by all VIP neurons, but the level of the expression can vary, allowing the detection of TH levels only in a subset of VIP⁺ neurons.

In our experiments using optogenetics combined with slice physiology, we found that a part of SST⁺ or PKCδ⁺ neurons received monosynaptic responses upon the activation of VIP⁺ axons in the BNST or CeA similarly to that what others noted in the case of the activation of the dopaminergic axons in the CeA (Grössl et al., 2018). At present, it is not clear which extended amygdala neuron types are the primary targets of dorsal tegmental VIP⁺ neurons. The CRF⁺ cells in the CeA can be a good candidates for the main postsynaptic partners of VIP⁺ neurons, because CRF⁺ neurons were described as the target population of VIP⁺ axons in the BNST (Kozicz et al., 1997, 1998). Future studies should determine the exact cell population targeted by vPAG-DRN VIP⁺ neurons.

Using sections from a human brain, we confirmed that VIP⁺ neurons are present in the human PAG. Importantly, these VIP⁺ neurons expressed TH, similarly to that observed in mice. Further, we found VIP⁺ axon collaterals in the human CeA. At present we do not know whether these peptidergic fibres in the CeA originate from the PAG region, but based on our mouse data, this would be an obvious explanation. Overall, our results obtained in human brain tissue support the idea that this peptidergic midbrain-extended amygdala pathway may be present in primates in addition to rodents. Based on the tracing studies, a portion of VIP⁺ neurons can distribute the information to their output regions simultaneously and bilaterally. This noticeable property supports the possible hub position of the vIPAG-DRN VIP⁺ neurons.

In summary, our present study using mice determined the ratio of SST⁺ and NPY⁺ GABAergic neurons in the LA and BA as well as provided a realistic estimate for the proportions of inhibitory cell types expressing CCK. These results will pave the ground for future studies, specifically for those aiming to reveal the changes in amygdala inhibitory circuits in different models of neuropsychiatric diseases, including anxiety, autism spectrum disorder, and schizophrenia. The significance of these investigations is highlighted by the fact that hyperexcitability in the amygdala, arising from the imbalance between excitation and inhibition, typifies many pathologic brain states in humans (Prager et al., 2016; Rosen & Schulkin, 1998; Rosenkranz et al., 2010; Sharp, 2017; Takarae & Sweeney, 2017).

Furthermore, we described that glutamatergic VIP⁺ neurons in the PAG-DRN project exclusively to the CeA and BNST, simultaneously and bilaterally. The VIP⁺ neurons are dopaminergic and exist in rodents and humans as well. VIP⁺ neurons are in the position to modulate the function of the extended amygdala. The function of VIP⁺ neurons is still elusive, but based on the structural features, these neurons may play a role in fear related processes, a hypothesis that will be assessed in future studies.

7. Conclusion

The balance of inhibitory and excitatory inputs arriving on PCs is critical for the proper function of the amygdala. We described three types of neuropeptidergic inhibitory neurons in the basolateral amygdala (BLA) and a neuropeptidergic excitatory input to the extended amygdala. We quantified the proportions of the given inhibitory cell types in the BLA, which may provide a solid ground for future studies aiming to clarify the changes in different pathological operation linked to the amygdala.

The dendrite targeting SST⁺ or NPY⁺ INs are morphologically or electrophysiologically diverse. In Sst-IRES-Cre mice, we separated two types of GABAergic neurons based on nNOS content and morphology. However, their electrophysiological features were found to be similar.

In Npy-Cre mice, both electrophysiological and anatomical features of the 3 subtypes of amygdala INs were distinct. We found that NGF cells have a late spiking firing phenotype and give rise to dense local axons and short dendrites. The next group was the fast-spiking PV⁺ INs with spine-free dendrites, and axons resembling BCs or axo-axonic cells. The last NPY⁺ subgroup was SST⁺ sparsely spiny neurons. The proportion of both SST⁺ and NPY⁺ GABAergic neurons was higher in the BA compared to LA, though the ratio of subgroups of NPY⁺ neurons was not different.

In Cck-Cre;Dlx5/6-Flp mice 40% of virally labelled boutons expressed CB₁ cannabinoid receptor, whereas the other INs expressing CCK belonged to the NGF cells, PV⁺ axo-axonic cells and BCs.

Using Vip-IRES-Cre mice we found that a portion of VIP⁺ neurons in the dorsal tegmentum region expressed the TH, a marker for dopaminergic neurons both in mice and humans. We proved that these VIP⁺ neurons can provide a control in the networks of the CeA and BNST bilaterally by releasing glutamate.

8. Summary

The amygdala nuclei located in the temporal lobe play an important role in the formation of fear behaviour and emotional memory. Uncovering its cell types and their connectivity is pivotal in understanding and treating amygdala-related diseases, e.g., anxiety and PTSD.

Based on their different developmental origin and functional roles, the amygdala can be divided into several nuclei, of which the basolateral, and central amygdala nuclei are the subjects of this thesis. The neuropeptide-expressing inhibitory neurons are abundant in all the mentioned nuclei and have a prolonged effect on their postsynaptic partners compared to the impact of the classical neurotransmitter-releasing neurons. Yet, their morphological features and connectome are still unexplored. Therefore, we examined the properties of inhibitory neurons expressing somatostatin, neuropeptide Y or cholecystinin in these amygdala nuclei.

We separated two subtypes of inhibitory neurons expressing somatostatin, based on morphology and nitric oxide synthase content, although their firing patterns were similar. In addition, we distinguished three different subgroups of neuropeptide Y⁺ cells: neurogliaform cells with slower firing rate and dense axonal cloud were the most abundant cell type; fast-spiking neurons with smooth dendrites and neurons containing somatostatin with spiny dendrites were also identified in this neuropeptide-expressing group. 40% of cholecystinin-containing inhibitory cells could be labelled by immunostaining against type 1 cannabinoid receptors. Surprisingly, some of the genetically labelled cholecystinin expressing inhibitory cells had the properties of neurogliaform cells, fast-spiking basket or axo-axonic cells.

Finally, we examined the peptidergic input to the central amygdala from the dorsal tegmentum. We found that a fraction of the neurons expressing vasoactive intestinal polypeptide (VIP) in the dorsal tegmentum is dopaminergic both in mice and humans. Using viral tracing in mice we showed that these VIP neurons terminate solely in the two nuclei of the extended amygdala: central amygdala and bed nucleus of stria terminalis.

Based on the connectivity, neurons expressing the neuropeptides somatostatin, neuropeptide Y, cholecystinin and VIP can contribute to controlling defensive behaviour by modifying the neuronal activity in amygdalar circuits.

9. Összefoglalás

A félelmi viselkedés és az érzelmi memória kialakításában a temporális lebenyben elhelyezkedő amygdala magok fontos szerepet játszanak. Az itt lévő sejttípusok és kapcsolatrendszerük felderítése hozzásegít minket az amygdalához kapcsolódó betegségek, például a szorongás és a poszttraumás stressz szindróma megértéséhez és kezeléséhez.

Az amygdala magok eltérő fejlődésük és funkciójuk alapján több almagra oszthatóak, ebben a disszertációban a bazális, laterális és a centrális amygdala magokat vizsgáltuk. Mindegyik mag bővelkedik neuropeptidet kifejező gátló idegsejtekben, amelyek posztzinaptikus sejtekre gyakorolt hatása időben elnyújtottabb, mint a klasszikus neurotranszmittert ürítő sejtek hatása. Mindemellett a neuropeptidet kifejező idegsejtek kapcsolatrendszere és morfológiai felépítésük még feltáratlan. Így azt tűztük ki célul, hogy megvizsgáljuk az itt elhelyezkedő szomatosztatint, neuropeptid Y-t vagy kolecisztokinint kifejező gátlósejteket. Kutatásaink során a szomatosztatint kifejező idegsejteknek két altípusát különítettük el morfológia és nitrogén-monoxid-szintáz tartalom alapján, habár a tüzelési mintázatuk hasonló volt. A neuropeptid Y⁺ sejtek három különböző alcsoportját különítettük el: legnagyobb arányban a neurogliaform sejttípus van jelen, lassabb tüzeléssel és sűrű axon felhővel, kisebb arányban fordultak elő gyorsan tüzelő, sima dendritű gátlósejtek és legkisebb arányban tüskés dendritű, szomatosztatint tartalmazó sejteket. A kolecisztokinin tartalmú gátlósejtek 40%-a volt jelölhető egyes típusú kannabinoid receptor elleni antitesttel. Meglepő módon a genetikailag jelölt kolecisztokinin gátlósejtek egy része neurogliaform sejt, gyorsan tüzelő kosár- vagy axo-axonikus sejt tulajdonságaival rendelkezett.

Végezetül a centrális amygdala peptiderg beidegzését vizsgáltuk, amely a dorzális tegmentumból ered. A dorzális tegmentumban található vazoaktív intesztinális polipeptidet (VIP) kifejező idegsejtek vizsgálatánál azt találtuk, hogy egy részük dopaminerg nem csak az egérben, hanem az emberben is. Egérben ezek a sejtek kizárólag a kiterjedt amygdala két magjába vetítenek.

Az általunk vizsgált neuropeptideket kifejező sejtek kapcsolati és morfológiai tulajdonságaik alapján az amygdala neuronális működésének módosításán keresztül hozzájárulhatnak a védekező viselkedés befolyásolásához.

10. References

- Abs, E., Poorthuis, R. B., Apelblat, D., Muhammad, K., Pardi, M. B., Enke, L., Kushinsky, D., Pu, D. L., Eizinger, M. F., Conzelmann, K. K., Spiegel, I., & Letzkus, J. J. (2018). Learning-Related Plasticity in Dendrite-Targeting Layer 1 Interneurons. *Neuron*, *100*(3), 684–699.e6. <https://doi.org/10.1016/j.neuron.2018.09.001>
- Acsády, L., Arabadzisz, D., & Freund, T. F. (1996). Correlated morphological and neurochemical features identify different subsets of vasoactive intestinal polypeptide-immunoreactive interneurons in rat hippocampus. *Neuroscience*, *73*(2), 299–315. [https://doi.org/10.1016/0306-4522\(95\)00610-9](https://doi.org/10.1016/0306-4522(95)00610-9)
- Adolphs, R., Tranel, D., & Damasio, A. R. (1998). The human amygdala in social judgment. *Nature*, *393*(6684), 470–474. <https://doi.org/10.1038/30982>
- Alheid, G. F. (2003). Extended amygdala and basal forebrain. *Annals New York Academy of Sciences*, *985*, 185–205. <https://doi.org/doi:10.1111/j.1749-6632.2003.tb07082.x>
- Alvarez-Bolado, G., Rosenfeld, M. G., Swanson, L. W., & Baer, V. (1995). Model of Forebrain Regionalization Based on Spatiotemporal Patterns of POU-I11 Homeobox Gene Expression, Birthdates, and Morphological Features. *The Journal of Comparative Neurology*, *355*, 237–295. <https://doi.org/10.1002/cne.903550207>
- Andero, R., Daniel, S., Guo, J. D., Bruner, R. C., Seth, S., Marvar, P. J., Rainnie, D., & Ressler, K. J. (2016). Amygdala-dependent molecular mechanisms of the Tac2 pathway in fear learning. *Neuropsychopharmacology*, *41*(11), 2714–2722. <https://doi.org/10.1038/npp.2016.77>
- Andrási, T., Veres, J. M., Rovira-Esteban, L., Kozma, R., Vikór, A., Gregori, E., & Hájos, N. (2017). Differential excitatory control of 2 parallel basket cell networks in amygdala microcircuits. *PLoS Biology*, *15*(5). <https://doi.org/10.1371/journal.pbio.2001421>
- Armstrong, C., Krook-Magnuson, E., & Soltesz, I. (2012). Neurogliaform and Ivy Cells: A Major Family of nNOS Expressing GABAergic Neurons. *Frontiers in Neural Circuits*, *6*. <https://doi.org/10.3389/fncir.2012.00023>
- Asede, D., Bosch, D., Lüthi, A., Ferraguti, F., & Ehrlich, I. (2015). Sensory inputs to

- intercalated cells provide fear-learning modulated inhibition to the basolateral amygdala. *Neuron*, 86(2), 541–554. <https://doi.org/10.1016/j.neuron.2015.03.008>
- Azad, S. C. (2004). Circuitry for Associative Plasticity in the Amygdala Involves Endocannabinoid Signaling. *Journal of Neuroscience*, 24(44), 9953–9961. <https://doi.org/10.1523/JNEUROSCI.2134-04.2004>
- Barsy, B., Kocsis, K., Magyar, A., Babiczky, Á., Szabó, M., Veres, J. M., Hillier, D., Ulbert, I., Yizhar, O., & Máttyás, F. (2020). Associative and plastic thalamic signaling to the lateral amygdala controls fear behavior. *Nature Neuroscience*, 23(5), 625–637. <https://doi.org/10.1038/s41593-020-0620-z>
- Barsy, B., Szabó, G. G., András, T., Vikór, A., & Hájos, N. (2017). Different output properties of perisomatic region-targeting interneurons in the basal amygdala. *European Journal of Neuroscience*, 45(4), 548–558. <https://doi.org/10.1111/ejn.13498>
- Baxter, M. G., & Crosson, P. L. (2012). Facing the role of the amygdala in emotional information processing. In *Proceedings of the National Academy of Sciences of the United States of America* (Vol. 109, Issue 52, pp. 21180–21181). <https://doi.org/10.1073/pnas.1219167110>
- Beinfeld, M. C., & Connolly, K. (2001). Activation of CB1 cannabinoid receptors in rat hippocampal slices inhibits potassium-evoked cholecystokinin release, a possible mechanism contributing to the spatial memory defects produced by cannabinoids. *Neuroscience Letters*, 301(1), 69–71. [https://doi.org/10.1016/S0304-3940\(01\)01591-9](https://doi.org/10.1016/S0304-3940(01)01591-9)
- Bezaire, M. J., & Soltesz, I. (2013). Quantitative assessment of CA1 local circuits: Knowledge base for interneuron-pyramidal cell connectivity. *Hippocampus*, 23(9), 751–785. <https://doi.org/10.1002/hipo.22141>
- Bienvenu, T. C. M., Busti, D., Magill, P. J., Ferraguti, F., & Capogna, M. (2012). Cell-Type-Specific Recruitment of Amygdala Interneurons to Hippocampal Theta Rhythm and Noxious Stimuli In Vivo. *Neuron*, 74(6), 1059–1074. <https://doi.org/10.1016/j.neuron.2012.04.022>
- Blythe, S. N., Wokosin, D., Atherton, J. F., & Bevan, M. D. (2009). Cellular mechanisms underlying burst firing in substantia nigra dopamine neurons. *Journal of Neuroscience*, 29(49), 15531–15541. <https://doi.org/10.1523/JNEUROSCI.2961->

09.2009

- Bowers, M. E., & Ressler, K. J. (2015). Interaction between the Cholecystinin and Endogenous Cannabinoid Systems in Cued Fear Expression and Extinction Retention. *Neuropsychopharmacology*, 40(3), 688–700. <https://doi.org/10.1038/npp.2014.225>
- Burdach, K. F. (1819). *Vom Baue und Leben des Gehirns*.
- Busti, D., Geracitano, R., Whittle, N., Dalezios, Y., Mańko, M., Kaufmann, W., Sätzler, K., Singewald, N., Capogna, M., & Ferraguti, F. (2011). Different fear states engage distinct networks within the intercalated cell clusters of the amygdala. *Journal of Neuroscience*, 31(13), 5131–5144. <https://doi.org/10.1523/JNEUROSCI.6100-10.2011>
- Carrive, P. (1993). The periaqueductal gray and defensive behavior: Functional representation and neuronal organization. *Behavioural Brain Research*, 58(1–2), 27–47. [https://doi.org/10.1016/0166-4328\(93\)90088-8](https://doi.org/10.1016/0166-4328(93)90088-8)
- Cassell, M. D., Gray, T. S., & Kiss, J. Z. (1986). Neuronal Architecture in the Rat Central Nucleus of the Amygdala: A Cytological, Hodological, and Immunocytochemical Study. *The Journal of Comparative Neurology*, 246, 478–499. <https://doi.org/10.1002/cne.902460406>.
- Chhatwal, J. P., Gutman, A. R., Maguschak, K. A., Bowser, M. E., Yang, Y., Davis, M., & Ressler, K. J. (2009). Functional Interactions between Endocannabinoid and CCK Neurotransmitter Systems May Be Critical for Extinction Learning. *Neuropsychopharmacology*, 34(2), 509–521. <https://doi.org/10.1038/npp.2008.97>
- Chieng, B. C. H., Christie, M. J., & Osborne, P. B. (2006). Characterization of neurons in the rat central nucleus of the amygdala: Cellular physiology, morphology, and opioid sensitivity. *Journal of Comparative Neurology*, 497(6), 910–927. <https://doi.org/10.1002/cne.21025>
- Cho, J. R., Treweek, J. B., Robinson, J. E., Xiao, C., Bremner, L. R., Greenbaum, A., & Gradinaru, V. (2017). Dorsal Raphe Dopamine Neurons Modulate Arousal and Promote Wakefulness by Salient Stimuli. *Neuron*, 94(6), 1205-1219.e8. <https://doi.org/10.1016/j.neuron.2017.05.020>
- Ciocchi, S., Herry, C., Grenier, F., Wolff, S. B. E., Letzkus, J. J., Vlachos, I., Ehrlich, I., Sprengel, R., Deisseroth, K., Stadler, M. B., Müller, C., & Lüthi, A. (2010).

- Encoding of conditioned fear in central amygdala inhibitory circuits. *Nature*, 468(7321), 277–282. <https://doi.org/10.1038/nature09559>
- Comeras, L. B., Herzog, H., & Tasan, R. O. (2019). Neuropeptides at the crossroad of fear and hunger: a special focus on neuropeptide Y. *Annals of the New York Academy of Sciences*, nyas.14179. <https://doi.org/10.1111/nyas.14179>
- De Olmos, J. S., & Heimer, L. (1999). The concepts of the ventral striatopallidal system and extended amygdala. *Annals of the New York Academy of Sciences*, 877, 1–32. <https://doi.org/10.1111/j.1749-6632.1999.tb09258.x>
- Defelipe, J., López-Cruz, P. L., Benavides-Piccione, R., Bielza, C., Larrañaga, P., Anderson, S., Burkhalter, A., Cauli, B., Fairén, A., Feldmeyer, D., Fishell, G., Fitzpatrick, D., Freund, T. F., González-Burgos, G., Hestrin, S., Hill, S., Hof, P. R., Huang, J., Jones, E. G., ... Ascoli, G. A. (2013). New insights into the classification and nomenclature of cortical GABAergic interneurons. *Nature Reviews Neuroscience*, 14(3), 202–216. <https://doi.org/10.1038/nrn3444>
- DeFeudis, F. V., Delgado, J. M. R., & Roth, R. H. (1969). Content, synthesis and collectability of amino acids in various structures of the brains of rhesus monkeys. *Brain Research*. [https://doi.org/10.1016/0006-8993\(70\)90453-1](https://doi.org/10.1016/0006-8993(70)90453-1).
- Del Boca, C., Lutz, P. E., Le Merrer, J., Koebel, P., & Kieffer, B. L. (2012). Cholecystokinin knock-down in the basolateral amygdala has anxiolytic and antidepressant-like effects in mice. *Neuroscience*, 218, 185–195. <https://doi.org/10.1016/j.neuroscience.2012.05.022>
- Dougalis, A. G., Matthews, G. A. C., Bishop, M. W., Brischoux, F., Kobayashi, K., & Ungless, M. A. (2012). Functional properties of dopamine neurons and co-expression of vasoactive intestinal polypeptide in the dorsal raphe nucleus and ventro-lateral periaqueductal grey. *European Journal of Neuroscience*, 36(10), 3322–3332. <https://doi.org/10.1111/j.1460-9568.2012.08255.x>
- Dougalis, A. G., Matthews, G. A. C., Liss, B., & Ungless, M. A. (2017). Ionic currents influencing spontaneous firing and pacemaker frequency in dopamine neurons of the ventrolateral periaqueductal gray and dorsal raphe nucleus (vlPAG/DRN): A voltage-clamp and computational modelling study. *Journal of Computational Neuroscience*, 42(3), 275–305. <https://doi.org/10.1007/s10827-017-0641-0>
- Dufour, M. A., Woodhouse, A., Amendola, J., & Goillard, J. M. (2014). Non-linear

- developmental trajectory of electrical phenotype in rat substantia nigra pars compacta dopaminergic neurons. *ELife*, 3. <https://doi.org/10.7554/eLife.04059>
- Duvarci, S., & Pare, D. (2014). Amygdala microcircuits controlling learned fear. *Neuron*, 82(5), 966–980. <https://doi.org/10.1016/J.NEURON.2014.04.042>
- Ehrlich, I., Humeau, Y., Grenier, F., Cioocchi, S., Herry, C., & Lüthi, A. (2009). Amygdala Inhibitory Circuits and the Control of Fear Memory. In *Neuron* (Vol. 62, Issue 6, pp. 757–771). <https://doi.org/10.1016/j.neuron.2009.05.026>
- Fadok, J. P., Krabbe, S., Markovic, M., Courtin, J., Xu, C., Massi, L., Botta, P., Bylund, K., Müller, C., Kovacevic, A., Tovote, P., & Lüthi, A. (2017). A competitive inhibitory circuit for selection of active and passive fear responses. *Nature*, 542(7639), 96–99. <https://doi.org/10.1038/nature21047>
- Fadok, J. P., Markovic, M., Tovote, P., & Lüthi, A. (2018). New perspectives on central amygdala function. In *Current Opinion in Neurobiology* (Vol. 49, pp. 141–147). Elsevier Ltd. <https://doi.org/10.1016/j.conb.2018.02.009>
- Fendt, M., & Fanselow, M. S. (1999). The neuroanatomical and neurochemical basis of conditioned fear. *Neuroscience and Behavioral Reviews*, 23, 743–760. [https://doi.org/10.1016/S0149-7634\(99\)00016-0](https://doi.org/10.1016/S0149-7634(99)00016-0)
- Frankland, P. W., Josselyn, S. A., Bradwejn, J., Vaccarino, F. J., & Yeomans, J. S. (1997). Activation of Amygdala Cholecystokinin_B Receptors Potentiates the Acoustic Startle Response in the Rat. *The Journal of Neuroscience*, 17(5), 1838–1847. <https://doi.org/10.1523/JNEUROSCI.17-05-01838.1997>
- Freund, T. F., & Katona, I. (2007). Perisomatic Inhibition. In *Neuron* (Vol. 56, Issue 1, pp. 33–42). <https://doi.org/10.1016/j.neuron.2007.09.012>
- Fryxell, J. M., Packer, C., McCann, K., Solberg, E. J., & Sæther, B. E. (2010). Resource management cycles and the sustainability of harvested wildlife populations. *Science*, 328(5980), 903–906. <https://doi.org/10.1126/science.1185802>
- Fu, W., Le Maitre, E., Fabre, V., Bernard, J.-F., David Xu, Z.-Q., & Hökfelt, T. (2010). Chemical Neuroanatomy of the Dorsal Raphe Nucleus and Adjacent Structures of the Mouse Brain. *The Journal of Comparative Neurology | Research in Systems Neuroscience*, 518, 3464–3494. <https://doi.org/10.1002/cne.22407>
- Fuentealba, P., Klausberger, T., Karayannis, T., Suen, W. Y., Huck, J., Tomioka, R., Rockland, K., Capogna, M., Studer, M., Morales, M., & Somogyi, P. (2010).

- Expression of COUP-TFII Nuclear Receptor in Restricted GABAergic Neuronal Populations in the Adult Rat Hippocampus. *Journal of Neuroscience*, 30(5), 1595–1609. <https://doi.org/10.1523/JNEUROSCI.4199-09.2010>
- Gray, T. S. (1983). The Morphology of Somatostatin-Immunoreactive Neurons in the Lateral Nucleus of the Rat Amygdala. *Peptides*, 4, 663–668. [https://doi.org/10.1016/0196-9781\(83\)90015-3](https://doi.org/10.1016/0196-9781(83)90015-3)
- Grössl, F., Munsch, T., Meis, S., Griessner, J., Kaczanowska, J., Pliota, P., Kargl, D., Badurek, S., Kraitsy, K., Rassoulpour, A., Zuber, J., Lessmann, V., & Haubensak, W. (2018). Dorsal tegmental dopamine neurons gate associative learning of fear. *Nat Neurosci*, 21(7), 952–962. <https://doi.org/10.1038/s41593-018-0174-5>
- Gulyás, A. I., Megias, M., Emri, Z., & Freund, T. F. (1999). Total Number and Ratio of Excitatory and Inhibitory Synapses Converging onto Single Interneurons of Different Types in the CA1 Area of the Rat Hippocampus. *The Journal of Neuroscience*, 19(22), 10082–10097. <http://rsb.info.nih.gov/nih-image/>
- Gungor, N. Z., & Paré, D. (2016). Functional heterogeneity in the bed nucleus of the stria terminalis. *Journal of Neuroscience*, 36(31), 8038–8049. <https://doi.org/10.1523/JNEUROSCI.0856-16.2016>
- Guthman, E. M., Garcia, J. D., Ma, M., Chu, P., Baca, S. M., Smith, K. R., Restrepo, D., & Huntsman, M. M. (2020). Cell-type-specific control of basolateral amygdala neuronal circuits via entorhinal cortex-driven feedforward inhibition. *ELife*, 9. <https://doi.org/10.7554/eLife.50601>
- Hagihara, K. M., Bukalo, O., Zeller, M., Aksoy-Aksel, A., Karalis, N., Limoges, A., Rigg, T., Campbell, T., Mendez, A., Weinholtz, C., Mahn, M., Zweifel, L. S., Palmiter, R. D., Ehrlich, I., Lüthi, A., & Holmes, A. (2021). Intercalated amygdala clusters orchestrate a switch in fear state. *Nature*, 594(7863), 403–407. <https://doi.org/10.1038/s41586-021-03593-1>
- Hájos, N. (2021). Interneuron Types and Their Circuits in the Basolateral Amygdala. *Frontiers in Neural Circuits*, 15. <https://doi.org/10.3389/fncir.2021.687257>
- Hájos, N., Acsády, L., & Freund, T. F. (1996). Target Selectivity and Neurochemical Characteristics of VIP-immunoreactive Interneurons in the Rat Dentate Gyrus. *European Journal of Neuroscience*, 8, 1415–1431. <https://doi.org/10.1111/j.1460-9568.1996.tb01604.x>

- Harris, K. D., Hochgerner, H., Skene, N. G., Magno, L., Katona, L., Bengtsson Gonzales, C., Somogyi, P., Kessaris, N., Linnarsson, S., & Hjerling-Leffler, J. (2018). Classes and continua of hippocampal CA1 inhibitory neurons revealed by single-cell transcriptomics. *PLOS Biology*, *16*(6), e2006387. <https://doi.org/10.1371/journal.pbio.2006387>
- Harro, J. (2006). CCK and NPY as anti-anxiety treatment targets: promises, pitfalls, and strategies. *Amino Acids*, *31*(3), 215–230. <https://doi.org/10.1007/s00726-006-0334-x>
- Hasue, R. H., & Shammah-Lagnado, S. J. (2002a). Origin of the dopaminergic innervation of the central extended amygdala and accumbens shell: A combined retrograde tracing and immunohistochemical study in the rat. *Journal of Comparative Neurology*, *454*(1), 15–33. <https://doi.org/10.1002/cne.10420>
- Hasue, R. H., & Shammah-Lagnado, S. J. (2002b). Origin of the dopaminergic innervation of the central extended amygdala and accumbens shell: A combined retrograde tracing and immunohistochemical study in the rat. *The Journal of Comparative Neurology*, *454*(1), 15–33. <https://doi.org/10.1002/cne.10420>
- He, M., Tucciarone, J., Lee, S., Nigro, M. J., Kim, Y., Levine, J. M., Kelly, S. M., Krugikov, I., Wu, P., Chen, Y., Gong, L., Hou, Y., Osten, P., Rudy, B., & Huang, Z. J. (2016). Strategies and Tools for Combinatorial Targeting of GABAergic Neurons in Mouse Cerebral Cortex. *Neuron*, *91*(6), 1228–1243. <https://doi.org/10.1016/j.neuron.2016.08.021>
- Herry, C., Ferraguti, F., Singewald, N., Letzkus, J. J., Ehrlich, I., & Lüthi, A. (2010). Neuronal circuits of fear extinction. In *European Journal of Neuroscience* (Vol. 31, Issue 4, pp. 599–612). <https://doi.org/10.1111/j.1460-9568.2010.07101.x>
- Hintiryan, H., Bowman, I., Johnson, D. L., Korobkova, L., Zhu, M., Khanjani, N., Gou, L., Gao, L., Yamashita, S., Bienkowski, M. S., Garcia, L., Foster, N. N., Benavidez, N. L., Song, M. Y., Lo, D., Cotter, K. R., Becerra, M., Aquino, S., Cao, C., ... Dong, H. W. (2021). Connectivity characterization of the mouse basolateral amygdalar complex. *Nature Communications*, *12*(1). <https://doi.org/10.1038/s41467-021-22915-5>
- Hou, W. H., Kuo, N., Fang, G. W., Huang, H. S., Wu, K. P., Zimmer, A., Cheng, J. K., & Lien, C. C. (2016). Wiring specificity and synaptic diversity in the mouse lateral

- central amygdala. *Journal of Neuroscience*, 36(16), 4549–4563.
<https://doi.org/10.1523/JNEUROSCI.3309-15.2016>
- Huber, D., Veinante, P., & Stoop, R. (2005). Vasopressin and Oxytocin Excite Distinct Neuronal Populations in the Central Amygdala. *Science*, 308(5719), 245–248.
<https://doi.org/10.1126/science.1105636>
- Hunt, S., Sun, Y., Kucukdereli, H., Klein, R., & Sah, P. (2017). Intrinsic circuits in the lateral central amygdala. *ENeuro*, 4(1). <https://doi.org/10.1523/ENEURO.0367-16.2017>
- Janak, P. H., & Tye, K. M. (2015). From circuits to behaviour in the amygdala. In *Nature* (Vol. 517, Issue 7534, pp. 284–292). Nature Publishing Group.
<https://doi.org/10.1038/nature14188>
- Jasnow, A. M., Ressler, K. J., Hammack, S. E., Chhatwal, J. P., & Rainnie, D. G. (2009). Distinct Subtypes of Cholecystikinin (CCK)-Containing Interneurons of the Basolateral Amygdala Identified Using a CCK Promoter-Specific Lentivirus. *Journal of Neurophysiology*, 101(3), 1494–1506.
<https://doi.org/10.1152/jn.91149.2008>
- Kannan, M., Vasan, G., Haziza, S., Huang, C., Chrapkiewicz, R., Luo, J., Cardin, J. A., Schnitzer, M. J., & Pieribone, V. A. (2022). Dual-polarity voltage imaging of the concurrent dynamics of multiple neuron types. *Science*, 378(6619).
<https://doi.org/10.1126/science.abm8797>
- Katona, I., Acsády, L., & Freund, T. . (1999). Postsynaptic targets of somatostatin-immunoreactive interneurons in the rat hippocampus. *Neuroscience*, 88(1), 37–55.
[https://doi.org/10.1016/S0306-4522\(98\)00302-9](https://doi.org/10.1016/S0306-4522(98)00302-9)
- Katona, I., Rancz, E. A., Acsády, L., Ledent, C., Mackie, K., Hájos, N., & Freund, T. F. (2001). Distribution of CB1 Cannabinoid Receptors in the Amygdala and their Role in the Control of GABAergic Transmission. *The Journal of Neuroscience*, 21(23), 9506–9518. <https://doi.org/10.1523/JNEUROSCI.21-23-09506.2001>
- Kepecs, A., & Fishell, G. (2014). Interneuron cell types are fit to function. In *Nature* (Vol. 505, Issue 7483, pp. 318–326). <https://doi.org/10.1038/nature12983>
- Kim, J., Zhang, X., Muralidhar, S., LeBlanc, S. A., & Tonegawa, S. (2017). Basolateral to Central Amygdala Neural Circuits for Appetitive Behaviors. *Neuron*, 93(6), 1464–1479.e5. <https://doi.org/10.1016/j.neuron.2017.02.034>

- Klausberger, T., Márton, L. F., Baude, A., Roberts, J. D. B., Magill, P. J., & Somogyi, P. (2004). Spike timing of dendrite-targeting bistratified cells during hippocampal network oscillations in vivo. *Nature Neuroscience*, 7(1), 41–47. <https://doi.org/10.1038/nn1159>
- Kozicz, T., Vigh, S., & Arimurá, A. (1997). Axon terminals containing PACAP-and VIP-immunoreactivity form synapses with CRF-immunoreactive neurons in the dorsolateral division of the bed nucleus of the stria terminalis in the rat. *Brain Research*, 767, 109–119.
- Kozicz, T., Vigh, S., & Arimurá, A. (1998). The source of origin of PACAP-and VIP-immunoreactive fibers in the laterodorsal division of the bed nucleus of the stria terminalis in the rat. *Brain Research*, 810, 211–219. [https://doi.org/10.1016/s0006-8993\(98\)00692-1](https://doi.org/10.1016/s0006-8993(98)00692-1)
- Krabbe, S., Paradiso, E., d’Aquin, S., Bitterman, Y., Courtin, J., Xu, C., Yonehara, K., Markovic, M., Müller, C., Eichlisberger, T., Gründemann, J., Ferraguti, F., & Lüthi, A. (2019). Adaptive disinhibitory gating by VIP interneurons permits associative learning. *Nature Neuroscience*, 22(11), 1834–1843. <https://doi.org/10.1038/s41593-019-0508-y>
- Larry W. Swanson, & Gorica D. Petrovich. (1998). What is the amygdala? *Trends in Neuroscience*, 21, 323–331. [https://doi.org/https://doi.org/10.1016/S0166-2236\(98\)01265-X](https://doi.org/https://doi.org/10.1016/S0166-2236(98)01265-X)
- Li, H., Penzo, M. A., Taniguchi, H., Kopec, C. D., Huang, Z. J., & Li, B. (2013). Experience-dependent modification of a central amygdala fear circuit. *Nature Neuroscience*, 16(3), 332–339. <https://doi.org/10.1038/nn.3322>
- Lim, L., Mi, D., Llorca, A., & Marín, O. (2018). Development and Functional Diversification of Cortical Interneurons. *Neuron*, 100(2), 294–313. <https://doi.org/10.1016/J.NEURON.2018.10.009>
- Lin, R., Liang, J., Wang, R., Li, A., Gong, H., Yan, T., Zhou, Y., Liu, Y., Feng, Q., Sun, F., Luo, M., & Li, Y. (2020). The Raphe Dopamine System Controls the Expression of Incentive Memory. *Neuron*, 106, 498–514. <https://doi.org/10.1016/j.neuron.2020.02.009>
- Lorincz, A., & Nusser, Z. (2010). Molecular identity of dendritic voltage-gated sodium channels. *Science*, 328(5980), 906–909. <https://doi.org/10.1126/science.1187958>

- Lucas, E. K., Jegarl, A. M., Morishita, H., & Clem, R. L. (2016). Multimodal and Site-Specific Plasticity of Amygdala Parvalbumin Interneurons after Fear Learning. *Neuron*, *91*(3), 629–643. <https://doi.org/10.1016/j.neuron.2016.06.032>
- Manassero, E., Renna, A., Milano, L., & Sacchetti, B. (2018). Lateral and Basal Amygdala Account for Opposite Behavioral Responses during the Long-Term Expression of Fearful Memories. *Scientific Reports*, *8*(1), 518. <https://doi.org/10.1038/s41598-017-19074-3>
- Mańko, M., Bienvenu, T. C. M., Dalezios, Y., & Capogna, M. (2012). Neurogliaform cells of amygdala: A source of slow phasic inhibition in the basolateral complex. *Journal of Physiology*, *590*(22), 5611–5627. <https://doi.org/10.1113/jphysiol.2012.236745>
- Margolis, E. B., Lock, H., Hjelmstad, G. O., & Fields, H. L. (2006). The ventral tegmental area revisited: Is there an electrophysiological marker for dopaminergic neurons? *Journal of Physiology*, *577*(3), 907–924. <https://doi.org/10.1113/jphysiol.2006.117069>
- Martina, M., Royer, S., & Paré, D. (1999). Physiological Properties of Central Medial and Central Lateral Amygdala Neurons. *Journal of Neurophysiology*, *82*(4), 1843–1854. <https://doi.org/10.1152/jn.1999.82.4.1843>
- Matthews, G. A., Nieh, E. H., Vander, C. M., Wildes, C. P., Ungless, M. A., & Tye, K. M. (2016). Dorsal Raphe Dopamine Neurons Represent the Experience of Social Isolation. *Cell*, *164*, 617–631. <https://doi.org/10.1016/j.cell.2015.12.040>
- Mátyás, F., Freund, T. F., & Gulyás, A. I. (2004). Convergence of excitatory and inhibitory inputs onto CCK-containing basket cells in the CA1 area of the rat hippocampus. *European Journal of Neuroscience*, *19*(5), 1243–1256. <https://doi.org/10.1111/j.1460-9568.2004.03225.x>
- McCullough, K. M., Morrison, F. G., Hartmann, J., Carlezon, W. A., & Ressler, K. J. (2018). Quantified coexpression analysis of central amygdala subpopulations. *ENeuro*, *5*(1). <https://doi.org/10.1523/ENEURO.0010-18.2018>
- McDonald, A. ., & Mascagni, F. (2001a). Colocalization of calcium-binding proteins and GABA in neurons of the rat basolateral amygdala. *Neuroscience*, *105*(3), 681–693. [https://doi.org/10.1016/S0306-4522\(01\)00214-7](https://doi.org/10.1016/S0306-4522(01)00214-7)
- McDonald, A. ., & Mascagni, F. (2001b). Localization of the CB1 type cannabinoid

- receptor in the rat basolateral amygdala: high concentrations in a subpopulation of cholecystinin-containing interneurons. *Neuroscience*, 107(4), 641–652. [https://doi.org/10.1016/S0306-4522\(01\)00380-3](https://doi.org/10.1016/S0306-4522(01)00380-3)
- Mcdonald, A. J. (1982a). Cytoarchitecture of the Central Amygdaloid Nucleus of the Rat. *The Journal of Comparative Neurology*, 208, 401–418. <https://doi.org/10.1002/cne.902080409>.
- Mcdonald, A. J. (1982b). Neurons of the Lateral and Basolateral Amygdaloid Nuclei: A Golgi Study in the Rat. *The Journal of Comparative Neurology*, 212, 293–312. <https://doi.org/10.1002/cne.902120307>.
- Mcdonald, A. J. (1989). Coexistence of somatostatin with neuropeptide Y, but not with cholecystinin or vasoactive intestinal peptide, in neurons of the rat amygdala. In *Brain Research* (Vol. 500).
- McDonald, A. J. (1984). Neuronal organization of the lateral and basolateral amygdaloid nuclei in the rat. *The Journal of Comparative Neurology*, 222(4), 589–606. <https://doi.org/10.1002/cne.902220410>
- Mcdonald, A. J., & Augustine, J. R. (1993). Localization of GABA-like immunoreactivity in the monkey amygdala. *Neuroscience*, 52(2), 281–294. [https://doi.org/10.1016/0306-4522\(93\)90156-a](https://doi.org/10.1016/0306-4522(93)90156-a).
- McDonald, A. J., & Betette, R. L. (2001). Parvalbumin-containing neurons in the rat basolateral amygdala: morphology and co-localization of Calbindin-D28k. *Neuroscience*, 102(2), 413–425. [https://doi.org/10.1016/S0306-4522\(00\)00481-4](https://doi.org/10.1016/S0306-4522(00)00481-4)
- McDonald, A. J., Mascagni, F., & Zaric, V. (2012). Subpopulations of somatostatin-immunoreactive non-pyramidal neurons in the amygdala and adjacent external capsule project to the basal forebrain: evidence for the existence of GABAergic projection neurons in the cortical nuclei and basolateral nuclear complex. *Frontiers in Neural Circuits*, 6. <https://doi.org/10.3389/fncir.2012.00046>
- Mcdonald, A. J., Payne, D. R., & Mascagni, F. (1993). Identification of putative nitric oxide producing neurons in the rat amygdala using nadph-diaphorase histochemistry. *Neuroscience*, 52(1), 97–106.
- Mcdonald, A. J., & Pearson, J. C. (1989). Coexistence of GABA and peptide immunoreactivity in non-pyramidal neurons of the basolateral amygdala. *Neuroscience Letters*, 100, 53–58. [https://doi.org/10.1016/0304-3940\(89\)90659-9](https://doi.org/10.1016/0304-3940(89)90659-9).

- McDonald, A. J., & Zaric, V. (2015). Gabaergic somatostatin-immunoreactive neurons in the amygdala project to the entorhinal cortex. *Neuroscience*, *290*, 227–242. <https://doi.org/10.1016/j.neuroscience.2015.01.028>
- McDonald A J. (1991). Topographical organization of amygdaloid projections to the caudatoputamen, nucleus accumbens, and related striatal-like areas of the rat brain. *Neuroscience*, *44*(I), 15–33. [https://doi.org/10.1016/0306-4522\(91\)90248-m](https://doi.org/10.1016/0306-4522(91)90248-m).
- McKernan, M. G., & Shinnick-Gallagher, P. (1997). Fear conditioning induces a lasting potentiation of synaptic currents in vitro. *Nature*, *390*(6660), 607–611. <https://doi.org/10.1038/37605>
- McNally, G. P., & Cole, S. (2006). Opioid receptors in the midbrain periaqueductal gray regulate prediction errors during Pavlovian fear conditioning. *Behavioral Neuroscience*, *120*(2), 313–323. <https://doi.org/10.1037/0735-7044.120.2.313>
- McNally, G. P., Johansen, J. P., & Blair, H. T. (2011). Placing prediction into the fear circuit. *Trends in Neurosciences*, *34*(6), 283–292. <https://doi.org/10.1016/j.tins.2011.03.005>
- Miles, R., Tóth, K., Attila, G., Norbert, H., & Tamás, F. (1996). Differences between somatic and dendritic inhibition in the hippocampus. *Neuron*, *16*, 815–823. [https://doi.org/10.1016/s0896-6273\(00\)80101-4](https://doi.org/10.1016/s0896-6273(00)80101-4).
- Millhouse, O. E. (1986). The intercalated cells of the amygdala. *Journal of Comparative Neurology*, *247*(2), 246–271. <https://doi.org/10.1002/cne.902470209>
- Miyoshi, G., & Fishell, G. (2011). GABAergic Interneuron Lineages Selectively Sort into Specific Cortical Layers during Early Postnatal Development. *Cerebral Cortex*, *21*(4), 845–852. <https://doi.org/10.1093/cercor/bhq155>
- Muller, J. F., Mascagni, F., & McDonald, A. J. (2007). Postsynaptic targets of somatostatin-containing interneurons in the rat basolateral amygdala. *Journal of Comparative Neurology*, *500*(3), 513–529. <https://doi.org/10.1002/cne.21185>
- Oláh, S., Füle, M., Komlósi, G., Varga, C., Báldi, R., Barzó, P., & Tamás, G. (2009). Regulation of cortical microcircuits by unitary GABA-mediated volume transmission. *Nature*, *461*(7268), 1278–1281. <https://doi.org/10.1038/nature08503>
- Pape, H.-C., & Pare, D. (2010). Plastic Synaptic Networks of the Amygdala for the Acquisition, Expression, and Extinction of Conditioned Fear. *Physiol. Rev.*, *90*, 419–463. <https://doi.org/10.1152/physrev.00037.2009>

- Paré, D. (2003). Role of the basolateral amygdala in memory consolidation. In *Progress in Neurobiology* (Vol. 70, Issue 5, pp. 409–420). Elsevier Ltd. [https://doi.org/10.1016/S0301-0082\(03\)00104-7](https://doi.org/10.1016/S0301-0082(03)00104-7)
- Paspalas, C., Geric, B., Halasy, K., Papadopoulos, G., & Hajós, F. (2000). Distribution and synaptology of vasoactive intestinal polypeptide (VIP) immunoreactive structures in the rat periaqueductal grey. *Journal of Neurocytology*, 29(8), 541–549. <https://doi.org/10.1023/A:1011081432697>
- Patel, S., Hill, M. N., Cheer, J. F., Wotjak, C. T., & Holmes, A. (2017). The endocannabinoid system as a target for novel anxiolytic drugs. *Neuroscience & Biobehavioral Reviews*, 76, 56–66. <https://doi.org/10.1016/j.neubiorev.2016.12.033>
- Paul, A., Crow, M., Raudales, R., He, M., Gillis, J., & Huang, Z. J. (2017). Transcriptional Architecture of Synaptic Communication Delineates GABAergic Neuron Identity. *Cell*, 171(3), 522–539.e20. <https://doi.org/10.1016/j.cell.2017.08.032>
- Paxinos, G., & Franklin, K. B. (2004). *The mouse brain in stereotaxic coordinates*. Boston: Elsevier Academic Press.
- Perrenoud, Q., Rossier, J., Geoffroy, H., Vitalis, T., & Gallopin, T. (2013). Diversity of GABAergic Interneurons in Layer VIa and VIb of Mouse Barrel Cortex. *Cerebral Cortex*, 23(2), 423–441. <https://doi.org/10.1093/cercor/bhs032>
- Phillips, R. G., & LeDoux, J. E. (1992). Differential contribution of amygdala and hippocampus to cued and contextual fear conditioning. *Behavioral Neuroscience*, 106(2), 274–285. <https://doi.org/10.1037/0735-7044.106.2.274>
- Pitkänen, A., Savander, V., & LeDoux, J. E. (1997). Organization of intra-amygdaloid circuitries in the rat: an emerging framework for understanding functions of the amygdala. *Trends in Neuroscience*, 20, 517–523. [https://doi.org/10.1016/s0166-2236\(97\)01125-9](https://doi.org/10.1016/s0166-2236(97)01125-9)
- Polepalli, J. S., Gooch, H., & Sah, P. (2020). Diversity of interneurons in the lateral and basal amygdala. *Npj Science of Learning*, 5(1). <https://doi.org/10.1038/s41539-020-0071-z>
- Poulin, J. F., Caronia, G., Hofer, C., Cui, Q., Helm, B., Ramakrishnan, C., Chan, C. S., Dombeck, D. A., Deisseroth, K., & Awatramani, R. (2018). Mapping projections of molecularly defined dopamine neuron subtypes using intersectional genetic approaches. *Nature Neuroscience*, 21(9), 1260–1271.

- <https://doi.org/10.1038/s41593-018-0203-4>
- Poulin, J. F., Gaertner, Z., Moreno-Ramos, O. A., & Awatramani, R. (2020). Classification of Midbrain Dopamine Neurons Using Single-Cell Gene Expression Profiling Approaches. In *Trends in Neurosciences* (Vol. 43, Issue 3, pp. 155–169). Elsevier Ltd. <https://doi.org/10.1016/j.tins.2020.01.004>
- Poulin, J. F., Zou, J., Drouin-Ouellet, J., Kim, K. Y. A., Cicchetti, F., & Awatramani, R. B. (2014). Defining midbrain dopaminergic neuron diversity by single-cell gene expression profiling. *Cell Reports*, 9(3), 930–943. <https://doi.org/10.1016/j.celrep.2014.10.008>
- Prager, E. M., Bergstrom, H. C., Wynn, G. H., & Braga, M. F. M. (2016). The basolateral amygdala γ -aminobutyric acidergic system in health and disease. *Journal of Neuroscience Research*, 94(6), 548–567. <https://doi.org/10.1002/jnr.23690>
- Price, D. D. (2000). Psychological and Neural Mechanisms of the Affective Dimension of Pain. *Science*, 288(5472), 1769–1772. <https://doi.org/10.1126/science.288.5472.1769>
- Rhomberg, T., Rovira-Esteban, L., Vikór, A., Paradiso, E., Kremser, C., Nagy-Pál, P., Papp, O. I., Tasan, R., Erdélyi, F., Szabó, G., Ferraguti, F., & Hájos, N. (2018). Vasoactive intestinal polypeptide-immunoreactive interneurons within circuits of the mouse basolateral amygdala. *Journal of Neuroscience*, 38(31), 6983–7003. <https://doi.org/10.1523/JNEUROSCI.2063-17.2018>
- Rogan, M. T., Stäubli, U. V., & LeDoux, J. E. (1997). Fear conditioning induces associative long-term potentiation in the amygdala. *Nature*, 390(6660), 604–607. <https://doi.org/10.1038/37601>
- Rosen, J. B., & Schulkin, J. (1998). From normal fear to pathological anxiety. *Psychological Review*, 105(2), 325–350. <https://doi.org/10.1037/0033-295X.105.2.325>
- Rosenkranz, J. A., Venheim, E. R., & Padival, M. (2010). Chronic Stress Causes Amygdala Hyperexcitability in Rodents. *Biological Psychiatry*, 67(12), 1128–1136. <https://doi.org/10.1016/j.biopsych.2010.02.008>
- Rovira-Esteban, L., Péterfi, Z., Attila Vikór, ·, Máté, Z., Szabó, · Gábor, & Hájos, N. (2017). Morphological and physiological properties of CCK/CB1R-expressing interneurons in the basal amygdala. *Brain Structure and Function*, 222, 3543–3565.

- <https://doi.org/10.1007/s00429-017-1417-z>
- Sah, P., Faber, E. S. L., Lopez De Armentia, M., & Power, J. (2003). The Amygdaloid Complex: Anatomy and Physiology. *Physiol Rev*, 83, 803–834. <https://doi.org/10.1152/physrev.00002.2003.-A>
- Schnell, S. A., Staines, W. A., & Wessendorf, M. W. (1999). Reduction of Lipofuscin-like Autofluorescence in Fluorescently Labeled Tissue. *Journal of Histochemistry & Cytochemistry*, 47, 719–730. <http://www.jhc.org>
- Shalev, A., Liberzon, I., & Marmar, C. (2017). Post-Traumatic Stress Disorder. *New England Journal of Medicine*, 376(25), 2459–2469. <https://doi.org/10.1056/NEJMra1612499>
- Sharp, B. M. (2017). Basolateral amygdala and stress-induced hyperexcitability affect motivated behaviors and addiction. *Translational Psychiatry*, 7(8), e1194–e1194. <https://doi.org/10.1038/tp.2017.161>
- Sik, A., Ylinen, A., Penttonen, M., & Buzsáki, G. (1994). Inhibitory CA1-CA3-Hilar Region Feedback in the Hippocampus. *Science*, 265(5179), 1722–1724. <https://doi.org/10.1126/science.8085161>
- Sun, N., & Cassell, M. D. (1993). Intrinsic GABAergic Neurons in the Rat Central Extended Amygdala. *The Journal of Comparative Neurology*, 330(1), 381–404.
- Takács, V. T., Szőnyi, A., Freund, T. F., Nyiri, G., & Gulyás, A. I. (2015). Quantitative ultrastructural analysis of basket and axo-axonic cell terminals in the mouse hippocampus. *Brain Structure and Function*, 220(2), 919–940. <https://doi.org/10.1007/s00429-013-0692-6>
- Takarae, Y., & Sweeney, J. (2017). Neural Hyperexcitability in Autism Spectrum Disorders. *Brain Sciences*, 7(12), 129. <https://doi.org/10.3390/brainsci7100129>
- Tamás, G., Lőrincz, A., Simon, A., & Szabadics, J. (2003). Identified Sources and Targets of Slow Inhibition in the Neocortex. *Science*, 299.
- Taylor, N. E., Pei, J., Zhang, J., Vlasov, K. Y., Davis, T., Taylor, E., Wengvan Dort, F. J. J., Solt, K., & Brown, E. N. (2019). The role of glutamatergic and dopaminergic neurons in the periaqueductal Gray/Dorsal Raphe: Separating analgesia and anxiety. *ENeuro*, 6(1). <https://doi.org/10.1523/ENEURO.0018-18.2019>
- Tovote, P., Fadok, J. P., & Lüthi, A. (2015). Neuronal circuits for fear and anxiety. In *Nature Reviews Neuroscience* (Vol. 16, Issue 6, pp. 317–331). Nature Publishing

- Group. <https://doi.org/10.1038/nrn3945>
- Tricoire, L., Pelkey, K. A., Daw, M. I., Sousa, V. H., Miyoshi, G., Jeffries, B., Cauli, B., Fishell, G., & McBain, C. J. (2010). Common Origins of Hippocampal Ivy and Nitric Oxide Synthase Expressing Neurogliaform Cells. *Journal of Neuroscience*, *30*(6), 2165–2176. <https://doi.org/10.1523/JNEUROSCI.5123-09.2010>
- Veening, J. G., Swanson, L. W., & Sawchenko, P. E. (1984). The Organization of Projections from the Central Nucleus of the Amygdala to Brainstem Sites involved in Central Autonomic Regulation: A Combined Retrograde Transport-Immunohistochemical Study. In *Brain Research* (Vol. 303).
- Vereczki, V. K., Müller, K., Krizsán, É., Máté, Z., Fekete, Z., Rovira-Esteban, L., Veres, J. M., Erdélyi, F., & Hájos, N. (2021). Total Number and Ratio of GABAergic Neuron Types in the Mouse Lateral and Basal Amygdala. *The Journal of Neuroscience*, *41*(21), 4575–4595. <https://doi.org/10.1523/jneurosci.2700-20.2021>
- Vereczki, V. K., Veres, J. M., Müller, K., Nagy, G. A., Rácz, B., Barsy, B., & Hájos, N. (2016). Synaptic organization of perisomatic gabaergic inputs onto the principal cells of the mouse basolateral amygdala. *Frontiers in Neuroanatomy*, *10*(MAR). <https://doi.org/10.3389/fnana.2016.00020>
- Veres, J. M., Nagy, G. A., & Hájos, N. (2017). Perisomatic GABAergic synapses of basket cells effectively control principal neuron activity in amygdala networks. *ELife*. <https://doi.org/10.7554/eLife.20721.001>
- Veres, J. M., Nagy, G. A., Vereczki, V. K., Andrási, T., & Hájos, N. (2014). Strategically positioned inhibitory synapses of axo-axonic cells potently control principal neuron spiking in the basolateral amygdala. *Journal of Neuroscience*, *34*(49), 16194–16206. <https://doi.org/10.1523/JNEUROSCI.2232-14.2014>
- Verma, D., Tasan, R. O., Herzog, H., & Sperk, G. (2012). NPY controls fear conditioning and fear extinction by combined action on Y 1 and Y 2 receptors. *British Journal of Pharmacology*, *166*(4), 1461–1473. <https://doi.org/10.1111/j.1476-5381.2012.01872.x>
- Vogel, E., Krabbe, S., Gründemann, J., Wamsteeker Cusulin, J. I., & Lüthi, A. (2016). Projection-Specific Dynamic Regulation of Inhibition in Amygdala Micro-Circuits. *Neuron*, *91*(3), 644–651. <https://doi.org/10.1016/j.neuron.2016.06.036>
- Wang, Y., Toledo-Rodriguez, M., Gupta, A., Wu, C., Silberberg, G., Luo, J., & Markram,

- H. (2004). Anatomical, physiological and molecular properties of Martinotti cells in the somatosensory cortex of the juvenile rat. *The Journal of Physiology*, *561*(1), 65–90. <https://doi.org/10.1113/jphysiol.2004.073353>
- Washburn, M. S., & Moises, H. C. (1992). Electrophysiological and Morphological Properties of Rat Basolateral Amygdaloid Neurons in vitro. *The Journal of Neuroscience*, *12*(10), 4066–4079.
- Watson, R. E., Wiegand, S. J., Clough, R. W., & Hoffman, G. E. (1986). Use of cryoprotectant to maintain long-term peptide immunoreactivity and tissue morphology. *Peptides*, *7*(1), 155–159. [https://doi.org/10.1016/0196-9781\(86\)90076-8](https://doi.org/10.1016/0196-9781(86)90076-8)
- Wolff, S. B. E., Gründemann, J., Tovote, P., Krabbe, S., Jacobson, G. A., Müller, C., Herry, C., Ehrlich, I., Friedrich, R. W., Letzkus, J. J., & Lüthi, A. (2014). Amygdala interneuron subtypes control fear learning through disinhibition. *Nature*, *509*(7501), 453–458. <https://doi.org/10.1038/nature13258>
- Xu, X., Roby, K. D., & Callaway, E. M. (2010). Immunochemical characterization of inhibitory mouse cortical neurons: Three chemically distinct classes of inhibitory cells. *The Journal of Comparative Neurology*, *518*(3), 389–404. <https://doi.org/10.1002/cne.22229>
- Yu, W., Pati, D., Pina, M. M., Schmidt, K. T., Boyt, K. M., Hunker, A. C., Zweifel, L. S., McElligott, Z. A., & Kash, T. L. (2021). Periaqueductal gray/dorsal raphe dopamine neurons contribute to sex differences in pain-related behaviors. *Neuron*. <https://doi.org/10.1016/j.neuron.2021.03.001>
- Zhao, Q., Ito, T., Soko, C., Hori, Y., Furuyama, T., Hioki, H., Konno, K., Yamasaki, M., Watanabe, M., Ohtsuka, S., Ono, M., Kato, N., & Yamamoto, R. (2022). Histochemical Characterization of the Dorsal Raphe-Periaqueductal Grey Dopamine Transporter Neurons Projecting to the Extended Amygdala. *Eneuro*, *9*(3), ENEURO.0121-22.2022. <https://doi.org/10.1523/ENEURO.0121-22.2022>

11. Bibliography of the candidate's publications

Publications related to this thesis

Viktória K. Vereczki¹, Kinga Müller¹, Éva Krizsán, Zoltán Máté, Zsuzsanna Fekete, Laura Rovira-Esteban, Judit M. Veres, Ferenc Erdélyi, Norbert Hájos

Total Number and Ratio of GABAergic Neuron Types in the Mouse Lateral and Basal Amygdala

Journal of Neuroscience 26 May 2021, 41 (21) 4575-4595; DOI: 10.1523/JNEUROSCI.2700-20.2021

¹equal contribution

Laura Rovira-Esteban, Ozge Gunduz-Cinar, Olena Bukalo, Aaron Limoges, Emma Brockway, Kinga Müller, Lief Fenno, Yoon Seok Kim, Charu Ramakrishnan, Tibor Andrási, Karl Deisseroth, Andrew Holmes, Norbert Hájos

Excitation of Diverse Classes of Cholecystokinin Interneurons in the Basal Amygdala Facilitates Fear Extinction

eNeuro 21 October 2019, 6 (6) ENEURO.0220-19.2019; DOI: 10.1523/ENEURO.0220-19.2019

Other publications

Vereczki VK¹, Veres JM¹, Müller K, Nagy GA, Rácz B, Barsy B and Hájos N

Synaptic organization of perisomatic GABAergic inputs onto the principal cells of the mouse basolateral amygdala

Frontiers in Neuroanatomy, 2016, Volume 10 Article 20, doi:10.3389/fnana.2016.00020

¹equal contribution

12. Acknowledgements

Completing a doctoral dissertation was a long and arduous journey, and I would not have made it without the support and guidance of many people. I am particularly grateful to my mentors, who have been instrumental in shaping me into the researcher and person I am today.

First and foremost, I would like to express my deep appreciation to Norbert Hájos my supervisor, his patient guidance and unwavering support have been invaluable throughout my doctoral studies. Judit Veres my first mentor has been an exemplary role model, always exhibiting a positive attitude and a deep commitment to scientific rigor and excellence. I have learned so much from my following mentor Laura Rovira-Esteban, not only in terms of technical skills but also in terms of the values and ethics that underlie scientific research. Thank you for challenging me to think critically, for inspiring me to pursue my research interests, for being a constant source of encouragement and motivation, and for always being available to answer my questions and provide guidance.

I would also like to thank Zsuzsanna Fekete, whose insights and feedback have been critical to the success of this dissertation.

Finally, I would like to express my gratitude to every old and recent member of Hájos's lab, whose support and friendship have sustained me through the ups and downs of my life and my research career. I have been fortunate to work alongside so many talented and dedicated researchers, and I am proud to have been a part of this community in the past eight years. Thank you for your encouragement, your friendship, and your shared passion for scientific discovery.

13. Tables

Table 1. To investigate the different neuronal types in BLA, PAG and extended amygdala nuclei in the following mouse lines, AAVs and combinations of antibodies to visualize the given antigens were used in this study.

Cell types	Mouse lines	Mixture of primary and secondary antibodies
SST ⁺ GABAergic neurons sampled in acute BLA slices	Sst-IRES-Cre (Ssttm2.1(cre)Zjh, Jax stock # 013044) + AAV5-DIO-EYFP OR AAVretro-mCherry-Flpo and AAVdj-Con/Fon-EYFP	goat anti-nNOS, mouse anti-Kv2.1, rabbit anti-PV DyL405-conjugated anti-goat and anti-rabbit, Cy3-conjugated anti- mouse
SST ⁺ GABAergic neurons in BLA	Sst-IRES-Cre + AAV5-DIO-EYFP	chicken anti-NeuN, mouse anti-GFP, goat anti-nNOS DyL405-conjugated anti-chicken, A488-conjugated anti-mouse, Cy3- conjugated anti-goat
NPY ⁺ neurons sampled in acute BLA slices	BAC-Npy-Cre mice (strain # RRID:MMRRC_034810-UCD) x Ai14 reporter (Gt(ROSA)26Sor_tm14(CAG/ LSL_tdTomato)Hze)	
NPY ⁺ GABAergic neurons in BLA	Npy ^{Cre} ;Dlx5/6 ^{Flp} offspring of BAC-Npy-Cre mice x	chicken anti-NeuN, mouse anti-GFP, goat anti-PV, rabbit anti-SST DyL405-conjugated anti-chicken, A488-conjugated anti-mouse, Cy3-

	Dlx5/6-Flpe (Tg(mI56i-flpe)39Fsh, JAX stock # 010815) + AAVdj-Con/Fon-EYFP	conjugated anti-goat, A647-conjugated anti-rabbit OR chicken anti-NeuN, mouse anti-GFP, rabbit anti-PV, rabbit anti-SST, rabbit anti-calbindin DyL405-conjugated anti-chicken, A488-conjugated anti-mouse, Cy3-conjugated anti-rabbit
CCK ⁺ GABAergic neurons sampled in acute BLA slice	CckCre;Dlx5/6Flp (CCK IN) Offspring of CCK-IRES-Cre (Ccktm1.1(cre)Zjh/J, JAX stock #012706) x Dlx5/6-Flpe	goat anti-CB ₁ R DyL405-conjugated donkey anti-goat OR rabbit anti-PV, chicken anti-Calb, mouse anti-ankyrin G A647-conjugated donkey anti-rabbit, DyL405-conjugated donkey anti-chicken, Alexa Fluor 488-conjugated donkey anti-mouse
CCK ⁺ GABAergic neurons in BLA	CckCre;Dlx5/6Flp (CCK IN) Offspring of CCK-IRES-Cre (Ccktm1.1(cre)Zjh/J, JAX stock #012706) x Dlx5/6-Flpe	rabbit anti-CaMKII and guinea pig anti-PV, rabbit anti-NPY and guinea pig anti-nNOS, rabbit anti-NPY and guinea pig anti-PV, or rabbit anti-PV and guinea pig anti-Calb Cy3-conjugated anti-rabbit, Cy5-conjugated anti-guinea pig,

		OR rat anti-SOM, rabbit anti-CB ₁ R Cy3-conjugated anti-rat, DyL405-conjugated anti-rabbit
VIP ⁺ neurons sampled in acute CeA or BNST slices	Vip-IRES-Cre (VIPtm1(cre)Zjh, JAX stock # 010908) +AAV5-EF1a-DIO-ChR2-mCherry or	rabbit anti-SST, rat anti-RFP, mouse anti-PKCδ DyL405-conjugated anti-rabbit, Cy3-conjugated anti-rat, A647-conjugated anti-mouse, OR rat anti-SST, mouse anti-PKCδ, Cy3-conjugated anti-rat, DyL405-conjugated anti-mouse,
VIP ⁺ neurons sampled in PAG	Vip-IRES-Cre (VIPtm1(cre)Zjh, JAX stock # 010908) + AAV1/2-Cre(on)-GFP + AAV1-CAG-FLEX-tdTomato + AAV1-Cre(on)-GFP	rabbit anti-VIP, mouse anti-TH, Cy3-conjugate anti-rabbit, A647-conjugated anti-mouse, OR goat anti-CTB, guinea pig anti-FG, Cy3-conjugated anti-goat, A488-conjugated anti-guinea pig
VIP ⁺ and VGAT ⁺ neurons in PAG	Vip/IRES_Cre//Gt(ROSA)26Sor_CAG/LSL_ZsGreen1 (Vip-IRES-Cre_ZsGreen1), VGAT/IRES-Cre//Gt(ROSA)26Sor_CAG/LS	Biocytin Cy3-conj. SA

	L_ ZsGreen1 (Vgat-IRES-Cre_ZsGreen1)	
VIP ⁺ neurons in PAG	Vip-Cre::tdTomato Offspring of Vip-IRES-Cre x Ai14 (Gt(ROSA)26Sor_tm14(CAG/ LSL_tdTomato)Hze; RRID:IMSR_JAX:007914)	

Table 2. Primary antibodies used in this study

Antigen	Source	Catalog #	Lot #	Host	Dilution	RRID
AnkyrinG	Santa Cruz Biotechnology	sc-28561	E2512	Rabbit	1:500	AB_633909
AnkyrinG	NeuroMab	75-146	441-4BK-91B	Mouse	1:100	AB_10673030
Calbindin	Synaptic Systems	214 004	214004/5	Guinea pig	1:3000	AB_10550535
Calbindin	Swant	CB-38a	9.03	Rabbit	1:5000	AB_10000340
Calbindin	Synaptic Systems	214 006	214 006/2	Chicken	1:1000	AB_2619903
Calretinin	Synaptic Systems	214 104	214 104/3	Guinea pig	1:1000	AB_10635160
Calretinin	Swant	7699/3H	18299	Rabbit	1:1000	AB_10000321
CamKII	Abcam	ab52476	GR312537-13	Rabbit	1:1000	AB_868641
CB1 cannabinoid receptor	Cayman Chemicals	10006590	4574771	Rabbit	1:1000	AB_409026
CB1 cannabinoid receptor	Frontier Institute Co.Ltd	CB1-Go-Af450	-	Goat	1:1000	AB_2571530
Choleratoxin B subunit	List Biological Laboratories	703	7032A9	Goat	1:20000	AB_10013220
FluoroGold	Protos Biotech	NM-101 FluGgp	-	Guinea pig	1:5000	AB_2314409
Gephyrin	Synaptic Systems	147 021	-	Mouse	1:1000	AB_2232546
GFP	Frontier Institute Co.Ltd	GFP-Go-Af1480	-	Goat	1:1000	AB_2571574
GFP	Millipore	MAB1083	3143158	Mouse	1:5000	AB_1587098
GFP	Synaptic Systems	132 006	1-2	Chicken	1:1000	AB_2713983
NeuN	Millipore	ABN91	3189200	Chicken	1:1000	AB_11205760
Neuroigin2	Synaptic Systems	129 511	-	Mouse	1:1000	AB_2619813
nNOS (neuronal)	Abcam	ab1376	GR3195323-6	Goat	1:5000	AB_300614
nNOS (neuronal)	Frontier Institute Co.Ltd	nNOS-GP-Af740	-	Guinea pig	1:1000	AB_2571733
NPY	ImmunoStar	22940	1112001	Rabbit	1:5000	AB_2307354
Kv2.1	Neuromab	75-014	449-3AK-78D	Mouse	1:1000	AB_10673392
pro CCK	Frontier Institute Co.Ltd	CCK-pro-Rb-Af350	-	Rabbit	1:5000	AB_2571674
Parvalbumin	Swant	PVG-214	-	Goat	1:5000	AB_2313848
Parvalbumin	Synaptic Systems	195004	195004/9	Guinea pig	1:1000	AB_2156476
Parvalbumin	Synaptic Systems	195 002	195002/7	Rabbit	1:500	AB_2156474
PKCd	Biosciences	610397	5357681	Mouse	1:1000	AB_397780
RFP	Chromotek	5F8	90228002AB-14	Rat	1:1000	AB_2336064
Somatostatin	Synaptic Systems	366 004	366 004/1-3	Guinea pig	1:500	AB_2620126
Somatostatin	Peninsula Laboratories	T-4103.0050	A15819	Rabbit	1:10000	AB_518614
Somatostatin	Millipore	MAB354	2984147	Rat	1:500	AB_2255365
Tyrosine hydroxylase	Synaptic Systems	213106	1-2	Chicken	1:1000	AB_2782977
Tyrosine hydroxylase	ImmunoStar	22941	1602001	Mouse	1:2000	AB_1624244

VAchT	Frontier Institute Co.Ltd	VAchT-Rb-Af1000	-	Rabbit	1:2000	AB_2571850
VGAT	Frontier Institute Co.Ltd	VGAT-GP-Af1000	-	Guinea pig	1:1000	AB_2571624
VGLUT1	Synaptic Systems	135 302	-	Rabbit	1:1000	AB_887875
VIP	ImmunoStar	20077	1513001	Rabbit	1:1000	AB_572270

Table 3. Secondary antibodies used in this study

Antigen	Source	Catalog #	Lot #	Host	Dilution	RRID
Alexa Fluor 488 anti-chicken	Jackson ImmunoResearch	703-545-155	146581	Donkey	1:500	AB_2340375
Alexa Fluor 488 anti-goat	Jackson ImmunoResearch	705-545-147	143223	Donkey	1:500	AB_2336933
Alexa Fluor 488 anti-guinea pig	Jackson ImmunoResearch	706-545-148	118980	Donkey	1:500	AB_2340472
Alexa Fluor 488 anti-mouse	Molecular Probes / Thermo Fisher Scientific	A21202	2090565	Donkey	1:500	AB_141607
Alexa Fluor 647 anti-mouse	Jackson ImmunoResearch	715-605-151	98871	Donkey	1:500	AB_2340863
Alexa Fluor 647 anti-rabbit	Jackson ImmunoResearch	711-605-152	99912	Donkey	1:500	AB_2492288
Cy3 anti-chicken	Jackson ImmunoResearch	703-165-155	124400	Donkey	1:500	AB_2340363
Cy3 anti-goat	Jackson ImmunoResearch	705-165-147	111783	Donkey	1:500	AB_2307351
Cy3 anti-mouse	Jackson ImmunoResearch	715-165-151	45374	Donkey	1:400	AB_2315777
Cy3 anti-rabbit	Jackson ImmunoResearch	711-166-152	111785	Donkey	1:500	AB_2313568
Cy3 anti-rat	Jackson ImmunoResearch	712-165-153	149608	Donkey	1:500	AB_2340667
Cy5 anti-goat	Jackson ImmunoResearch	705-175-147	111314	Donkey	1:200	AB_2340415
Cy5 anti-guinea pig	Jackson ImmunoResearch	706-175-148	113929	Donkey	1:400	AB_2340462
DyL405 anti-chicken	Jackson ImmunoResearch	703-475-155	140264	Donkey	1:500	AB_2340373
DyL405 anti-goat	Jackson ImmunoResearch	705-475-003	-	Donkey	1:500	AB_2340426
DyL405 anti-guinea pig	Jackson ImmunoResearch	706-475-148	129848	Donkey	1:500	AB_2340470
DyL405 anti-mouse	Jackson ImmunoResearch	715-475-151	98883	Donkey	1:500	AB_2340840
DyL405 anti-rabbit	Jackson ImmunoResearch	711-475-152	98072	Donkey	1:500	AB_2340616
Streptavidin, Alexa Fluor 488	Molecular Probes / Thermo Fisher Scientific	S11223	93B2		1:10000	AB_2315383
Streptavidin, Alexa Fluoro 647	Molecular Probes/ Thermo Fisher Scientific	S21374	1990312		1:10000	AB_2336066
Streptavidin, Cy3	Sigma-Aldrich	S6402	SLBB1903 V		1:10000	

Table 4. Fraction of distinct types of GABAergic cells in the LA and BA. In each case, the counting was performed in sections prepared from three mice. # of NeuN⁺ cells refer to the total number of neurons counted in the given number of sections (# of sec.) indicated. Significant difference is shown in bold and in italic.

Neuron types	LA % of inh. neurons	# of NeuN + cells	# of sec.	BA % of inh. neurons	# of NeuN + cells	# of sect.	t-test <i>p value</i>
All SST ⁺ INs (n = 3 mice)	2.3 ± 0.3	6,031	10	5.4 ± 0.8	10,406	13	<i>0.0018</i>
SST ⁺ nNOS ⁺	41.6 ± 5.4% of all SST ⁺ neurons			25 ± 5.4% of all SST ⁺ neurons			<i>0.043</i>
All NPY ⁺ GABAergic cells (n = 6 mice)	3.8 ± 0.3	10,458	12	8.1 ± 0.7	6,931	11	<i>< 0.001</i>
NPY ⁺ PV ⁺	23.7 ± 1.9% of all NPY ⁺ GABAergic cells			29.7 ± 2.7% of all NPY ⁺ GABAergic cells			0.085
NPY ⁺ SST ⁺	30.9 ± 3.6% of all NPY ⁺ GABAergic cells			25.5 ± 3.0% of all NPY ⁺ GABAergic cells			0.26
NGF cells	46.6 ± 4.7 % of all NPY ⁺ GABAergic cells			42.9 ± 2.8 % of all NPY ⁺ GABAergic cells			0.51

Table 5. Single-cell properties of SST-expressing GABAergic cell types in the LA and BA recorded from 8 mice. Data are presented as the median with the first and third quartiles in parentheses. P values obtained by Mann-Whitney (MW) U test are indicated. Significant difference is shown in bold and in italic. AP, action potential; AHP, after hyperpolarization, ISI, inter-spike interval.

Parameters	SST⁺ interneurons (n=17-24)	SST⁺ GABAergic proj. cells (n=15-20)	MW test p
AP half-width (ms)	0.7 (0.6, 0.8)	0.8 (0.7, 0.8)	0.16
Spike rate (Hz)	45 (37.5, 51.3)	55 (32.5, 72.5)	0.37
AHP 50% decay (ms)	34.6 (9.2, 65.8)	27.6 (13.5, 42.7)	0.72
ISI between the first two spikes	9.2 (7.9, 11.85)	7.6 (6.35, 10.3)	0.17
ISI between the last two spikes	28.2 (21.55, 33.35)	26.75 (16.3, 34.1)	0.65
Accommodation ratio	2.98 (1.91, 4.29)	2.86 (2.16, 4.48)	0.93
Input resistance (M Ω)	252.8 (219.9, 362.6)	279.3 (196.6, 388.3)	0.97
Membrane time constant (ms)	24.75 (20.81, 33.4)	20.8 (15.23, 25.7)	0.053
Membrane capacitance (pF)	93.3 (76.7, 121.2)	71.5 (55.5, 93.8)	<i>0.014</i>
Relative sag amplitude	0.28 (0.134, 0.427)	0.177 (0.125, 0.399)	0.4
Sag delay (ms)	84.6 (62.3, 99.5)	62.8 (49.4, 99.4)	0.45

Table 6. Single-cell properties of the three NPY-expressing GABAergic cell types in the LA and BA recorded from 5 mice. Data are presented as the median with the first and third quartiles in parentheses. P values obtained by statistical tests are indicated. Significant differences shown in bold and in italic were determined by Kruskal-Wallis ANOVA and Mann-Whitney (MW) U test, respectively. NGF, neurogliaform cell; Fast-spiking, fast-spiking PV⁺ interneurons; SST⁺, SST-immunoreactive interneurons. AP, action potential; AHP, after hyperpolarization, ISI, inter-spike interval.

Parameters	NGF (n=26-28)	Fast-spiking (n=14-17)	SST ⁺ (n=8)	Kruskal - Wallis ANOVA	NGF vs FS MW test	NGF vs SST ⁺ MW test	FS vs SST ⁺ MW test
AP half-width (ms)	0.9 (0.8, 1)	0.5 (0.4, 0.5)	0.7 (0.6, 0.7)	<0.001	<i><0.001</i>	0.007	<i><0.001</i>
Spike rate (Hz)	50 (31.3, 58.8)	70 (61.6, 114.1)	37.55 (27.5, 58.75)	<0.001	<i><0.001</i>	0.38	0.0029
AHP 50% decay (ms)	58.8 (38.7, 114.7)	14.4 (10.1, 29.5)	24.1 (9.62, 75.3)	<0.001	<i><0.001</i>	0.09	0.37
ISI between the first two spikes	9.65 (5.57, 18.17)	8.2 (5.8, 11.17)	9.8 (5.35, 13.37)	0.56			
ISI between the last two spikes	25.25 (19.9, 34.3)	15.3 (5.9, 17.8)	29 (17.62, 39.65)	<0.001	<i><0.001</i>	0.97	0.009
Accommodation ratio	2.25 (1.72, 3.8)	1.51 (1.35, 1.76)	3.125 (2.42, 3.81)	<0.001	0.003	0.16	<i><0.001</i>
Input resistance (MΩ)	177.55 (154.45, 234.7)	133.4 (109.1, 205.5)	233.3 (136.6, 302.8)	0.033	0.011	0.57	0.11
Membrane time constant (ms)	9.71 (8.89, 11.54)	9.64 (8.52, 12.34)	18.18 (12.52, 24.6)	0.004	0.81	0.002	0.0037
Membrane capacitance (pF)	53 (43, 62.7)	68.4 (58.3, 84.8)	76.7 (56.5, 137.1)	0.004	0.007	0.014	0.56
Relative sag amplitude	0.123 (0.096, 0.168)	0.1 (0.068, 0.14)	0.196 (0.112, 0.235)	0.046	0.44	0.029	0.029

Table 7. Single-cell properties of VIP⁺ glutamatergic or VGAT-expressing GABAergic cell types in the dorsal tegmentum. Data are presented as the median with the first and third quartiles in parentheses. P values obtained by Mann-Whitney (MW) U test are indicated. Significant difference is shown in bold and in italic. AP, action potential

Parameters	VIP⁺ neurons (n=14-18)	VGAT⁺ neurons (n=11)	MW test p
AP half-width (ms)	0.85 (0.8, 1)	0.50 (0.4, 0.5)	<i>0.00039</i>
AP threshold	-34.1 (-35.3, -30.9)	-37.6 (-44.9, -35.9)	<i>0.01472</i>
AP amplitude	76 (68.1, 82.4)	80.7 (76.4, 86.4)	0.16888
Input resistance (MΩ)	327.45 (280.4, 411.4)	634 (418.2, 780)	<i>0.0028</i>
Membrane time constant (ms)	8.963 (6.87, 12.38)	26.07 (15.16, 28.14)	<i>0.00010</i>
Membrane capacitance (pF)	27.02 (23.43, 33.4)	40.47 (22.46, 64.23)	0.09189
Relative sag amplitude	0.14 (0.07, 0.28)	0.08 (0.04, 0.18)	0.12098
Sag delay (ms)	162.9 (150.8, 176.4)	251.9 (190.5, 288.1)	<i>0.00112</i>